Study of Mechanical Behavior of Additive Manufactured Lattice Structures to achieve Optimal Product Design.

Nikolaos Kladovasilakis

SCHOOL OF SCIENCE AND TECHNOLOGY

A thesis submitted for the degree of

Master of Science (MSc) in Strategic Product Design

January, 2020

Thessaloniki – Greece

Student Name: Nikolaos Kladovasilakis

SID: 1106180009
Supervisors: Asst. Prof. Dimitrios Tzetzis
Dr. Konstantinos Tsongas

I hereby declare that the work submitted is mine and that where I have made use of another's work; I have attributed the source(s) according to the Regulations set in the Student's Handbook.

January, 2020
Thessaloniki - Greece

Abstract

Recent developments in additive manufacturing have led to fabrication of geometries with great complexity. Such are the three classes of lattice geometries (e.g. honeycombs, strut geometries and triply periodic minimal surfaces). In this research is studied the mechanical behavior of third-class lattice structures. In particular, this paper investigated the following structures with triply periodic minimal surfaces (TPMS): Gyroid, Schwarz Diamond and Schwarz Primitive. Fusion Deposition Modeling (FDM) technique is used in order to fabricate specimens in different relative densities, using Polylactic acid (PLA) as a construction material. Furthermore, the specimens tested through compressive experiments to deduct the mechanical properties of the third-class lattice structures. Also, a finite element analysis was performed in the 3D CAD models of the specimens to verify experimental results. Results showed that each geometry influences the mechanical properties of the structure through the size effect that affects all lattice structures. However, the way the geometries were designed and fabricated resulted in smaller effect of size effect on construction, especially at increased relative densities. More specifically, the Schwarz Diamond structure had the most advanced mechanical properties of the structures that were studied, with the Gyroid structure being very close. The Schwarz Primitive structure showed very good performance in energy absorption especially during plastic deformation of the specimens. Finally, the integrity of the mechanical properties of geometries deteriorates greatly as the relative density of structures decrease. Finally, a case study of an additive manufactured scaffold was studied. The scaffold had as internal structure the Schwarz Diamond geometries and the results was very promising in order to the scaffold complete its mission successfully.

Keywords: Additive Manufacture, Lattice structures, Finite Element Analysis, Tissue Engineering.

Nikolaos Kladovasilakis

24/01/2020

Acknowledgment

Without the presence, support and tolerance of some people, this thesis would not have been possible.

First of all, I would like to thank my supervisor Dr. Dimitrios Tzetzis, Assistant Professor of School of Science and Technology at International Hellenic University, for the scientific, spiritual, and moral support he provided me. His advices and guidance have played a key role both in my scientific training and in developing my dissertation thesis.

A big thank you to the co-supervisor Dr. Konstantinos Tsongas, for the generous help he gave me, the excellent cooperation between us and the patience he showed in the obstacles that appeared.

Moreover, thanks to Mr. Manolis Jimjimis technical laboratory associate at International Hellenic University, who played a key role in the 3D printing procedures but also in the conduction of the experiments.

Finally, I would like to thank my family for supporting me in this postgraduate study and in the preparation of this dissertation.

Contents

Topology Optimization

1.1. Introduction

In the 21st century, all scientific disciplines aim to optimize and make sustainable results and outcomes. That is, using the most advanced materials in the best possible way to achieve the best possible result. In the same context is the design of structures and objects through structural optimization.

Structural optimization deals with optimizing the design of a structure so that it can handle the loads it receives. There are three ways to do this: sizing optimization, shape optimization, and topology optimization. In recent years, topology optimization has seen the most growth due to the development of better design programs (3D CAD), the increment of computing power and the development of 3D printing technologies. Topology optimization has a wide range of applications. The first steps in the development of this procedure of design, appeared in the aeronautical industry (for weight reduction) and in medicine (through lattice design). Increasingly, topology optimization has also been developed in other areas such as automotive industry, industrial design and civil engineering.

1.2. Historical view

The interest in optimal design of a structure is not new. From the 16th century, Galileo Galilei (1564 - 1642) began to search for the optimal structural shapes to handle mechanical loads. His research concerned the process of fracturing brittle materials depending on the shapes and the loads applied to them. Subsequently, the contribution of Leonard Euler (1707-1783), Gottfried Wilhelm Leibniz (1646-1716) and Joseph-Louis Lagrange (1736-1813) to the analytical and numerical methods of solutions and the development of calculus gave the mathematical tools needed to further develop structural optimization.

Thus, in 1904 Anthony George Maldon Michell (1870-1959) published a book on structural optimization with the title: 'The limits of the economy of material in frame-structures'. In this book, Michell used the already existing mathematical tools and advanced geometry in order to create two-dimensional models, with optimal shape and topology depending on the loads that applied on the models (Figure 1) [1].

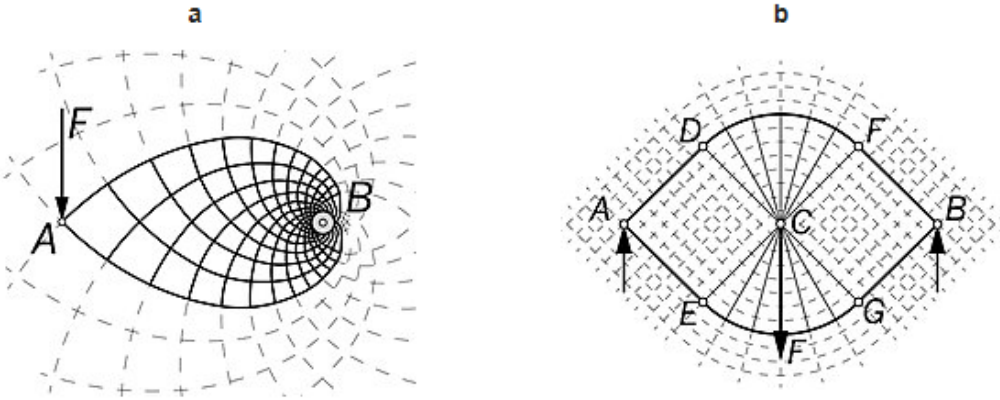

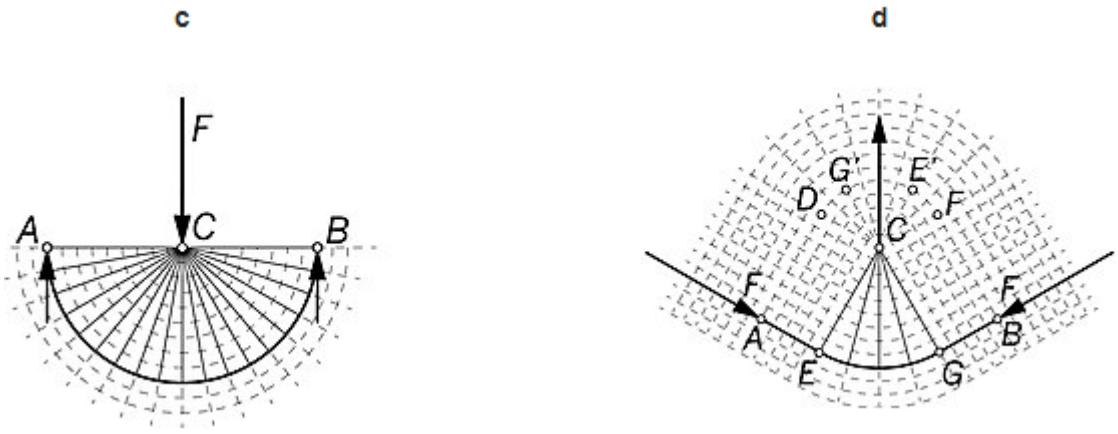

Fig. 1. Michell provided several examples of optimum frames: a) force F applied at A with support on B; b) force F applied at C between supports at points A and B; c) force F applied at C between supports at A and B; d) Centrally-loaded beam with force away from the straight line between supports.

In the last decades, with the development of design software (3D CAD) and engineering analysis software (CAE), significant progress has been made in structural optimization in both the macrostructure and the microstructure of a part. Particularly in the microstructure, the contribution of lattice structures is big. Lattice structures are created by copying the microstructure of some materials (Crystalline structures) or by using advanced geometries and mathematical formulations for optimal topology design (Triply Periodic Minimal Surfaces-TPMS).

1.3. Procedure of Structural Optimization

However, before delving into the structural optimization of a structure and microstructure, it is necessary to formulate the questions that the designers have to answer by doing this process and the procedure that have to follow. These questions are the following [2]:

- What is the purpose/use of the designed product?
- Which quantities of the product must remain unchanged?
- What is the goal of the product (loads that must handle etc.)?
- Which are the constraints to be respected?
- How do I optimize the product?

Once the above questions have been answered by the designer, the process of structural optimization begins. The designer is required to find the optimal shape and topology of the product so that the product can handle mechanical loads with the least possible mass. To achieve the minimum mass with their designer constraints (loads, remain regions etc.), an optimization problem algorithm must be implemented. The

mathematical description of the algorithm, adapted in structural optimization, is present below and the following steps are described in Figure 2.

Assuming that an object consists of a finite number of elements, which have a certain number of degrees of freedom and assuming that there is linear flexibility in the object; the mathematical algorithm for this structural optimization problem is formed as follows [3]:

$$\begin{cases} Minimize \quad f(x) \\ s.t. \quad g(x) \le 0 \\ \qquad x_{\min} \le x \le x_{\max} \\ \qquad K(x)u = F(x) \end{cases} \tag{1.1}$$

Where

- x: is the design variable, a parameter that describe the design and can change during the optimization process,
- f: is the objective function, a function that returns values, which shows the goodness of the design (mass, cost, stress etc.),
- $g(x) \le 0$: is the constrain functions,
- K(x): is the stiffness matrix of the structure,
- u: is the displacement vector,
- F(x): is the force vector,
- K(x)u = F(x): this equation represents the equilibriums, that occur in a static load.

The above mathematical formulation is as simplified as possible, as it minimizes only the quantity *f*. Therefore, it is the simplest form for structural optimization of an object. The figure, below, represents the steps that a designer has to follow when uses an algorithm like that, in order to obtain structural optimization [4].

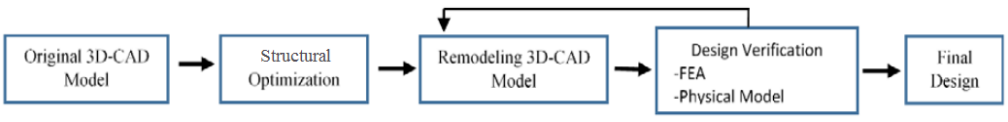

Fig. 2. Structural Optimization process

1.4. Classification of Structural Optimization

Structural optimization in object design is done in three different ways. These are presented and analysed below [5]:

- Sizing Optimization

Sizing optimization of an object is a study done by the engineer who designs the object and is intended solely for the calculation of crucial dimensions of the designed part, to be as much as it should, in order to, the object, can handle the load received during use. Crucial dimensions are usually cross-sectional, diameters, lengths, thicknesses, etc. Usually, through sizing optimization, the final external dimensions of the object are determined.

- Shape Optimization

Shape optimization is intended to optimize the shape or reshape an object in order to manage in the best way the loads that it's received, that is, to make the loads more uniformly distributed over the object. However, the shape changes within the domain of the material, that is, within the outer dimensions of the object.

- Topology Optimization

Topology optimization is the most general way of structural optimization. In topology optimization of an object, the engineer / designer is required to calculate the optimum mass distribution within the object's volume which is already defined, in external dimensions terms in order to can handle the loads it receives. Topology optimization can have much in common with shape optimization and can be both done simultaneously. However, sizing optimization always precedes topology optimization.

The following figure (Fig. 3) illustrates three different way of structural optimization in a two-dimensional model, that are mentioned above

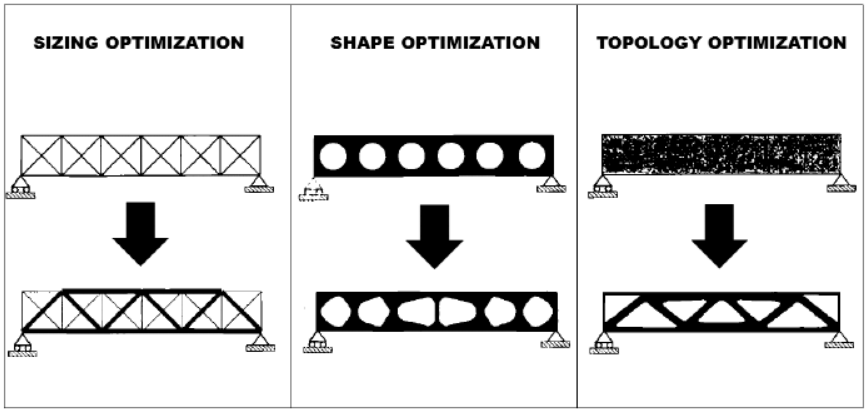

Fig. 3. Sizing, Shape and Topology Optimization.

1.5. Topology Optimization Process

As mentioned above, topology optimization (TO) is the mathematical method (algorithms) that optimizes the distribution of the material within an already defined domain, with certain loads that the object receives and already constraints and boundary conditions. The goal is usually to minimize the mass of the object.

Topology optimization determines the overall distribution of the elemental masses (elements) through the object's design domain. Typically, topology optimization has as input data the results of sizing optimization and shape optimization. There are two different approaches (types of algorithms) for topology optimization: the discrete approach (truss-based) and the continuous approach (density-based).

The discrete topology optimization approach (truss-based approach) starts with an initial dense mesh of nodes and bars in the already given volume of the object. This mesh, may be diffuse into the domain volume (ground -truss) or be consisted of repeating cells of the same structure (lattice design). In the first case, the purpose of topology optimization is to calculate which nodes and bars contribute the most in order to maintain them and which nodes and bars have the smallest or insignificant contribution and can be removed. The original mesh, in this case, plays a very important role. In the case of lattice design, topology optimization determines the size of the cells (length, radius and thickness) in order to minimize the mass with the existing constraints.

The continuous approach of topology optimization (density-based approach) starts with the division of the given volume of the object to small elements, which named voxels. Each voxel has its own initial density value, which will also be a design variable. Then, the topology optimization algorithm adjusts density values for each voxel depending on the loads the object receives. These values can range from 0 to 1. A value of 1 means that at this voxel the material is fully dense, so the material has to be maintained, and a value of 0 means that at this voxel, the material can be removed. All the voxels that having intermediate values, they do not have to be full of material to handle the loads, so they can be replaced by lattice structures. This approach of topology optimization is also the one you find in many commercial software and more specifically through the SIMP algorithm (Solid Isotropic Material with Penalization).

The following figures (Fig. 4, Fig. 5), illustrate the topology optimization of two different cases using the truss-based approach in the first figure and the density-based approach in the second [6].

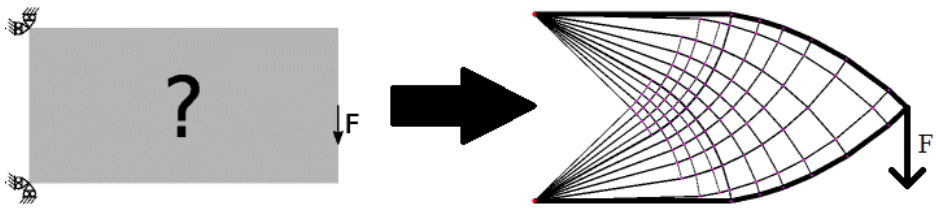

Fig. 4. Truss-based approach.

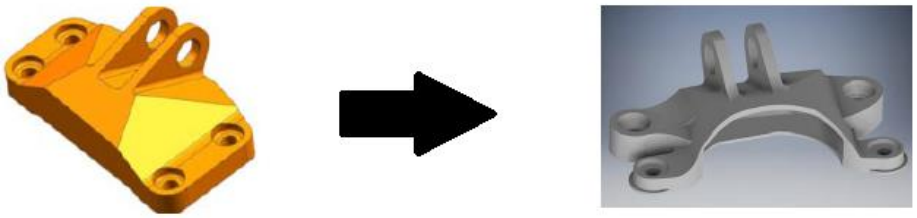

Fig. 5. Density-based approach.

In addition to background methodologies and algorithms, a typical example of topology optimization is presented as well as a diagram of it, in order to understand how an object is practically topologically optimized [7].

A predetermined geometry is given (either two-dimensional or three-dimensional), the supports of this geometry, the loads it receives, and the material of which the geometry is constituted are also given. The goal is to design the optimal structure that can handle the given loads. This is happened by finding the internal geometry that must be filled with material. This can be done after having several iterations of finite elements analyses (FEA), where a piece of material is removed from the geometry domain each time until the optimal geometry is found. The rate of material removal, the way and the efficiency of the process depend on the original design of the object and the methodology / algorithm that the engineer will use for topology optimization.

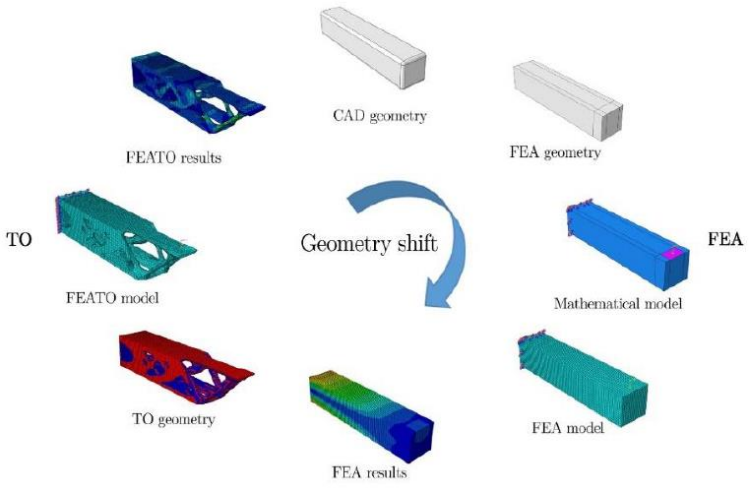

Fig. 6. Procedure of Topology Optimization

Lattice Design

2.1. Introduction

As mentioned in the previous chapter, lattice structures play a very important role in the topology optimization process of an object. As both approaches, truss-based and density based, have the design element of a lattice structure. The first approach has as a key element of it, as the lattice structures are the sum of nodes and bars which are exported as a result of topology optimization. The second one introduces lattice structures to the regions of geometry that do not need to be filled with object's material.

However, lattice structures are not something new that was discovered while researching the structural optimization of an object. Lots of lattice structures are scattered in nature and it is there where first-time scientists observed and studied them. Scientists, initially, referred to these materials as cellular materials because of the repetition of their structures. For example, such materials are bones, sponges, corals, etc. Early studies of these materials showed very promising mechanical properties, but there was lack of technology for the artificial manufacturing of these materials.

After many years, these studies went deeper into theoretical and mathematical levels. The discovery of crystalline metal structures (BCC, FCC, etc.) has shown the importance and the need for further study of lattice structures. Moreover, the studies of Joseph-Louis Lagrange (1736-1813) and Karl Hermann Amandus Schwarz (1843-1921) on topology and advanced geometries have led to the discovery of more complex lattice structures (TPMS). And then, the superiority of these structures was understood, but the important problem of the artificially manufacture of this structure remained unsolved.

The solution of artificial manufacturing lattice structures inside geometries was provided by modern 3D printers. Modern 3D printers are capable of producing these complex geometries so that experimental studies can be carried out to determine the detailed mechanical properties of the lattice structures. The 3D printing methods, which are used to manufacture lattice structures, are: fused deposition modeling (FDM), stereolithography (SLA), selective laser sintering (SLS) and direct metal laser sintering (DMLS).

Nowadays, thanks to the latest piece of the puzzle, the 3D printers, topology optimization through lattice designs, has been studied experimentally and has found many applications in various industries (aerospace, automotive, biomechanical engineering etc.) [8].

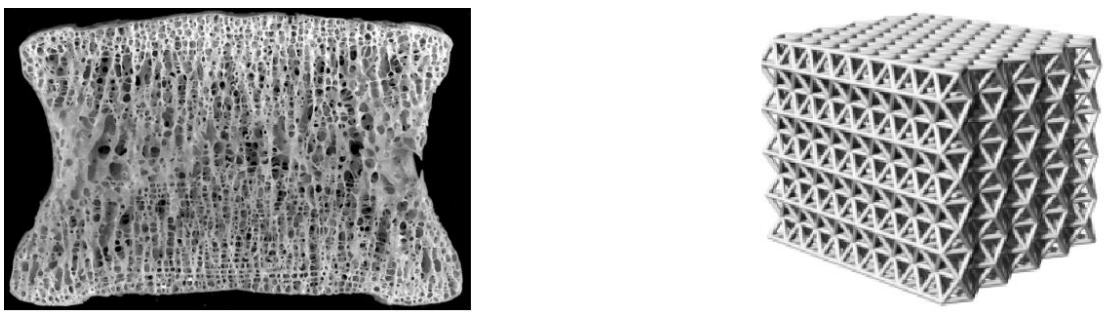

Fig. 7. a) Natural lattice structure (bone); b) Artificial lattice structure.

2.2. Classification of Cellular materials

2.2.1. General about Cellular materials

There is a plethora of objects consisting of lattice structures. The lattice structures of these objects have been created either naturally or artificially. The wide variety of lattice structures creates the need for their classification and evaluation. Below, the major categories of lattice structures are presented.

- Stochastic cellular materials

In these materials the position, size, and shape of the unit cell are stochastic. Each unit cells resemble each other, but they differ in size and shape. Most of such structures are produced by nature, although they may be artificially produced. They are divided into two categories: open-cell structure and closed-cell structure. The open-cell structure consists of beams and nodes while the closed-cell structure consists of material pockets (Figure 8). Examples of materials that contain such structures are bones, sponges, corals etc.

Fig. 8. a) Open-cell stochastic lattice structure; b) Closed-cell stochastic lattice structure.

- Ordered (Periodic) cellular materials – Lattice materials (structures)

This term is meant materials consisting of lattice structures which are repeated periodically within the geometry of the material. Also, the unit cells of the lattice structure have precise geometry and are similar to each other, in terms of shape. Usually these materials are artificial, but they can also be found in nature (honeycombs). Below is an in-depth analysis at the lattice structures.

2.2.2. Lattice Structures

Periodic cellular materials are materials consisting of lattice structures. Their internal structures are specific and defined in terms of shape, size and geometry (i.e., they are non-stochastic). This section will list and analyze all the types of lattice structures known to date.

The first and foremost separation of these structures relates to whether the structure grows in three dimensions or only in two. As such, there are 2D lattice structures and 3D lattice structures.

- 2D lattice structures

These are lattice structures, which have a specific geometry in two of the three dimensions and in the third dimension they simply extrude the 2D geometry. Examples of structures are honeycomb structures (hexagonal, square, etc.), which are developed with orientation from layer to layer, and prismatic structures that are similar to honeycomb structures but their orientation ids rotated 90 degrees (Figure 9) [9].

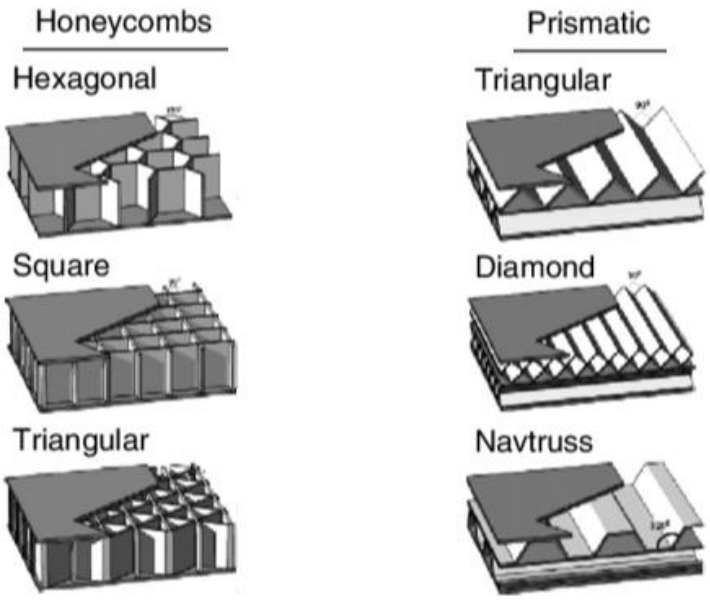

Fig. 9. Illustrates the honeycombs structures (right) and the prismatic structures (left).

- 3D lattice structures

The 3D lattice structures are more complicated than all the other lattice structures that mentioned above. It is extremely rare to be found in macro-geometries in nature and therefore almost all structures of these geometries are artificial. Although, it was extremely difficult to manufacture these geometries until recently, this changed with the development of 3D printers. But what are these structures and why are they so complicated?

The 3D lattice structures were derived from the study of the crystalline structures of metals (BCC, FCC, etc.). Therefore, just as the metal atoms formed the nodes of the structure and the forces between them, formed the trusses, so in the 3D lattice geometry there are areas of high material density (nodes) and areas where the material accumulates in the distance between the nodes (trusses). In this way, nodes and trusses are created in a specific way so that their periodic repetition creates the 3D lattice structure. Examples of these structures are the octet-truss, Kelvin structure, Gibson-Ashby structure, diamond structure, etc. and are shown below in Figure 10 [10].

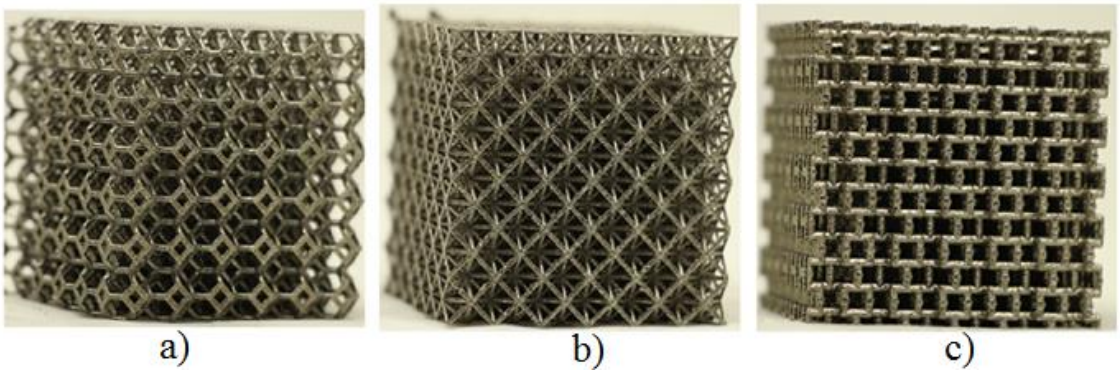

Fig. 10. a) Kelvin lattice structure; b) Octet-truss lattice structure; c) Gibson-Ashby lattice structure.

In addition to the 3D lattice structures that having nodes and trusses as structural elements, there are also 3D lattice structures consisting only of surfaces intertwined in such a way as to create structural elements. These 3D lattice structures are called triply periodic minimal surfaces (TPMS). The discovery of these surfaces was made, on a theoretical and mathematical level, by the German mathematician Karl Hermann Amandus Schwarz. But, until recently, due to the difficulty of their manufacture they had no practical applications in structural optimization. TPMS are subject to very precise mathematical formulas. The most well-known and promising TPMS lattice geometries are: Gyroid, Schwarz Diamond and Schwarz Primitive [11-12].

Gyroid:

It is a geometry that was discovered by NASA scientist Alan Schoen, in 1970. It belongs to the associate family or Bonnet family of a minimal surface in differential geometry.

Mathematic equation for Gyroid:

$$\sin x \cdot \cos y + \sin y \cdot \cos z + \sin z \cdot \cos x = 0$$

Fig.11. a) Unit cell of Gyroid; b) Solid model of Gyroid.

Schwarz Diamond:

This particular geometry was described by Hermann Schwarz but analyzed by Alan Schoen. The reason why this particular geometry was named diamond is that it has the shape of an inflated tubular of the diamond bond structure.

Mathematic equation for Schwarz Diamond:

$$\sin x \cdot \sin y \cdot \sin z + \sin x \cdot \cos y \cdot \cos z + \cos x \cdot \sin y \cdot \cos z + \cos x \cdot \cos y \cdot \cos z = 0$$

Fig.12. a) Unit cell of Schwarz Diamond; b) Solid model of Schwarz Diamond.

Schwarz Primitive:

Like Schwarz Diamond, this lattice geometry was described by Hermann Schwarz and analyzed by Alan Schoen. The great specialty of the Schwarz Primitive structure is the fact that it has a high surface-to-volume ratio which makes it suitable for applications where high porosity is required (tissue scaffolds) [13].

Mathematic equation for Schwarz Primitive:

$$\cos x + \cos y + \cos z = 0$$

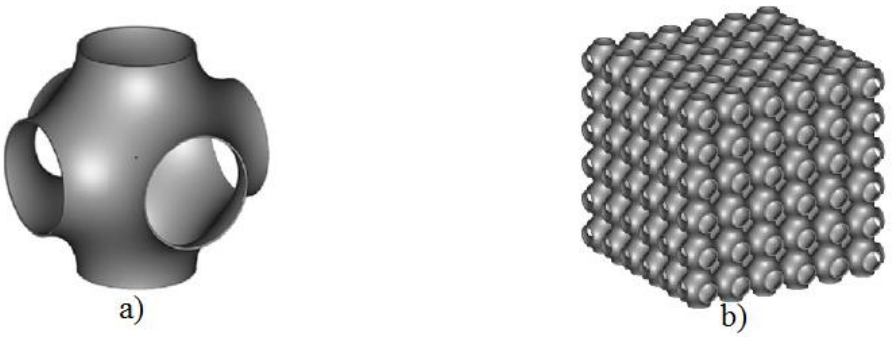

Fig.13. a) Unit cell of Schwarz Primitive; b) Solid model of Schwarz Primitive.

All 3D lattice structures (truss and TPMS) until recently have been very difficult to study and manufacture. The study was difficult because these structures have great complexity in their geometry and finite element analysis was impossible. Likewise, the construction of these structures was impossible due to the lack of suitable manufacture tools (3D printers). However, all these have changed over the last decade and now there are tools for both studying and constructing these structures. Therefore, this study aims to contribute to the research of these structures and present possible applications.

2.3. Current use of Lattice Structure

In the previous section, cellular materials were presented and analyzed, as well as various lattice structures developed within them. In this section it is presented the current uses and potential uses of these materials in the future. Cellular materials, as it is shown below, have been used in many industries for years and years, but due to the development of 3D printers, it has begun to suggest the use of lattice structures in applications that have been impossible up to the present. Below, it is reported some of these uses:

- Packaging:

The main role of the packaging of an item is to protect it from any damage it may cause during transportation or storage. Consequently, the most suitable materials for this application are materials that can absorb large amounts of kinetic energy into their structure without transmitting it to the item. Cellular materials, and hence the lattice structures, can absorb much more energy than traditional materials (Figure 14). This is why cellular materials such as foams (stochastic lattice structures) or cardboards packaging (honeycomb structures) have been used in packaging for decades.

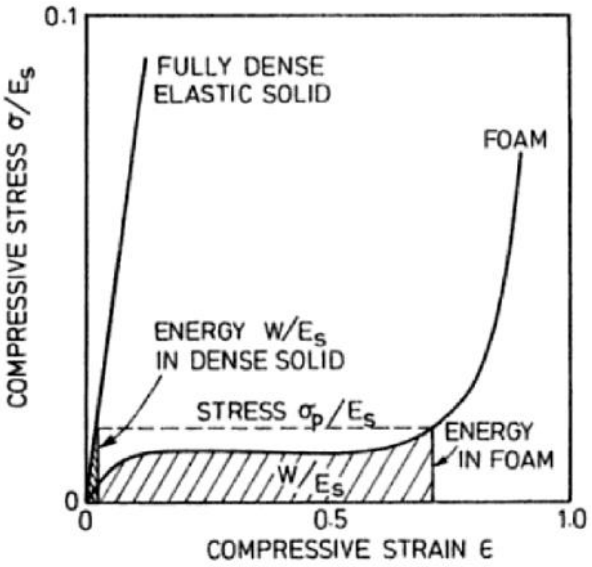

Fig. 14. Comparison of dense solid and foam of the same material in energy absorption terms.

- Stability and seismic isolation:

When a construction is built, the most essential property it must have, are seismic isolation and structural stability. Lattice structures can offer both in the construction. As mentioned above, lattice structures can absorb large amounts of energy which makes them suitable for seismic isolation. For example, the pentamode structure is probably the most promising lattice structure for seismic isolation. Also, through the lattice structures, a construction could lead to topology optimization and therefore have a light-weight construction with maximum structural stability. This is the reason why trusses have been used for many years in order to replicate lattice structures and achieve topology optimization [14].

- Thermal insulation:

Another classic use of cellular materials for decades is thermal insulation. The factors of cellular materials that contribute to better thermal insulation are three:

i. The small fraction of the solid phase,

ii. The presence of many cells which make difficult the thermal convection and transmission of thermal radiation as they are absorbed by the many walls,

iii. And the gas trapped inside the cells, has usually low thermal conductivity.

For these reasons, the best cellular materials for thermal insulation are of closed-cells. Therefore, such materials are used where thermal insulation is required or thermal shock must be avoided. For example, insulation of oxygen tanks in rockets (Figure 15), thermal insulation of houses, etc. [15]

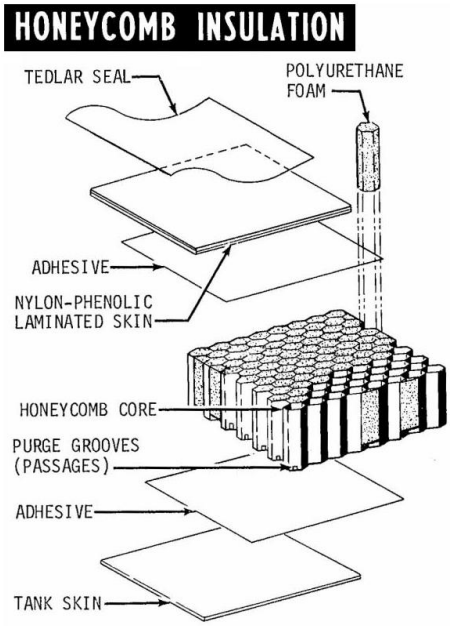

Fig. 15. Lay-out of LH_2 tank of rocket Saturn V.

- Acoustic insulation:

Another old application of lattice structures through cellular materials is acoustic insulation. The internal structure of these materials with multiple unit cells is capable of absorbing and neutralizing a wide range of acoustic waves resulting in very good acoustic performance. A very good example of this application of lattice structures is in building materials where very good performance is achieved in both thermal and acoustic insulation (Figure 16).

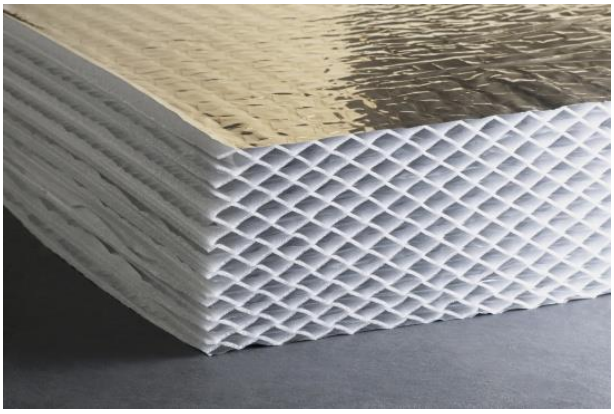

Fig. 16. Example of building material HYBRIS suitable for thermal and acoustic insulation (Internal structure: polyethylene foam).

In the figures above, the applications of cellular are presented and analyzed that have been taking place since the last century and mainly concerned simple lattice structures. But below are presented applications that have been developed over the last ten years as they are related to more complex lattice structures. Some of these applications are:

- Mechanical engineering:

In recent years, lattice structures have been introduced in many areas of mechanical engineering (such as automotive, aerospace industry, etc.) at a rapid rate and in many applications due to the development of 3D printers. The first application of cellular materials with lattice geometry ready to be produced is in catalysts and filters. This is because lattice structures, such as TPMS, have high surface area to volume ratio and thus bind a larger number of foreign particles. At the same rationale, lattice structures have been tried to integrate into heat exchangers as again the large surface area relative to the volume increases their efficiency. Furthermore, the most important application of lattice structures in mechanical engineering is the manufacture of lightweight part, topologically optimized through lattice structures. However, this application is still very limited mainly due to the cost and lack of mechanical properties of 3D printed metal part [16].

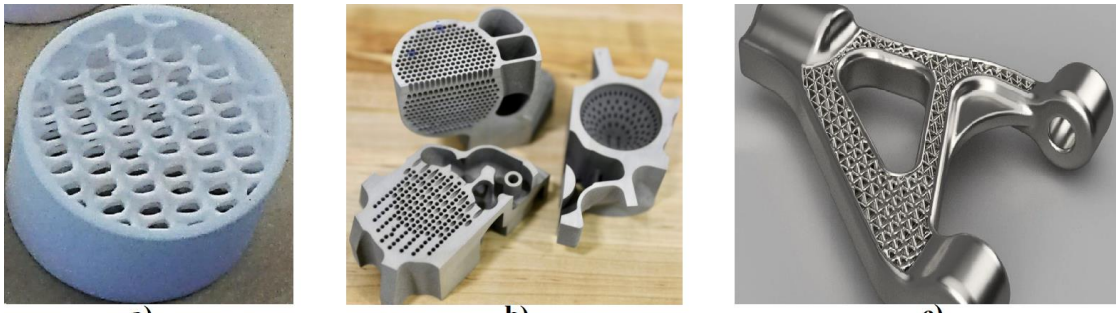

a) b) c)

Fig. 17. a) Complex lattice structure in catalyst (experimental); b) 3D printed heat exchanger from GE; c) 3D printed lightweight part.

- Biomechanical engineering:

As in mechanical engineering, as well as in biomechanical engineering, lattice structures have found very promising applications in recent years. In addition to the very good mechanical properties (energy absorption, mechanical strength etc), they also appear to have a number of other properties that allow the lattice structures to perform well within the human body. As an artificial structure that mimics natural bones is the appropriate implant for recuperate and regenerate damaged tissue cells. Thus, the basic applications of lattice structures in biomechanical engineering are biomedical implants and scaffolds for tissue engineering. Also, one of great interest application is the application of using lattice structures and 4D engineering to develop better medical implants, such as stents, heart valves or even vascular grafts.

a) b) c)

Fig. 18. a) Dental implant with partial lattice structure; b) Scaffolds for tissue engineering; c) Stent of 4D manufacturing process.

These are the most important applications of cellular materials and lattice structures. There are several others that are either still in a very experimental stage, such as batteries with lattice internal geometry (Figure 19a) [17], or have simpler uses, such as soles of sneakers (Figure 19b). The source of this rapid development of applications for lattice structures are the new ways of manufacturing these structures through 3D printers as will be shown in the next section.

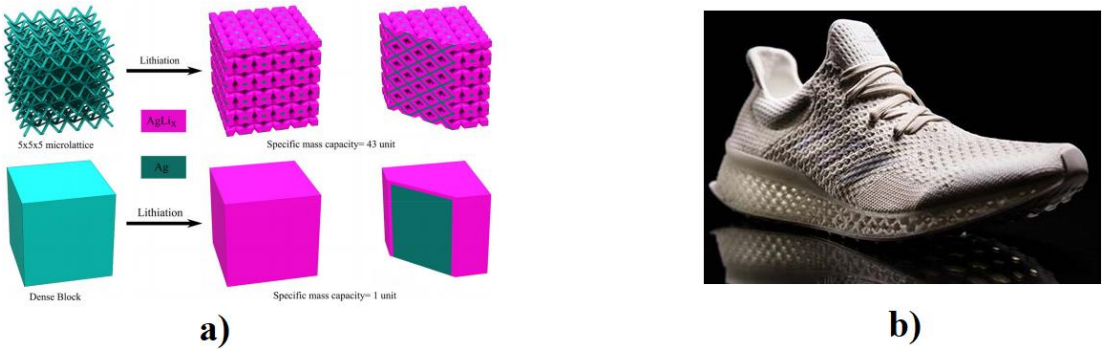

Fig. 19. a) Replacement of battery's solid elements batteries with lattice elements; b) Example of 3D printed lattice sneakers sole.

2.4. Manufacturing of Lattice Structures

2.4.1. General about 3D-Printing

As, it has already been presented above, the technology that has helped most the development of lattice structures is 3D-Printing or otherwise Additive Manufacturing (AM). But what is 3D-Printing? Why does it make easier to manufacture lattice structures? And what are the techniques that made 3D printing possible for a wide variety of materials?

Additive manufacturing, or else 3D-Printing, is the process by which a digital 3D model is converted into a real solid 3D object. The produced object is made layer by layer in one direction until the final object is manufactured. Each layer is a thin cross-section of the object. The thinner these layers are, the better the resolution of the item is. 3D printing is a very new process; the first solid steps were made 30 years ago (late 1980s) by Scott Crump (who founded Stratasys) and Charles Hull (who founded 3D Systems). In order to 3D print an object the following steps must be followed:

i. Model Configuration:
In this step, the internal and external geometries of the object are configured. These geometries either are designed in CAD software or are the result of reverse engineering (CMM, laser scanning etc).

ii. Create STL file:
Special software converts geometry (internal and external) into a point cloud and then into a polygons mesh.

iii. Transfer the STL file to the 3D printer:
The file is transferred to the printer's software and finalized before printing (size, orientation, supports, etc.). Digital geometry is also sliced in order to identify precisely the layers of print.

iv. Set-up of 3D printer:
It sets up various factors of the printer, such as the materials and other constrains that may exist depending on the printing technique.

v. Printing:

3D printing of an object is an automated process and does not require any intervention from user. However, user should oversight the process in order to avoid any failures of the process.

vi. Removal and post-processing:

The printed object should be carefully removed as it may have a high temperature or a brittle geometry. After removing the object, the procedures for finishing follow. This step removes any printing imperfections and supports that may have been used. Also, if possible, a further processing (finishing) of the object is performed to optimize its surface finish and accuracy of the object.

2.4.2. Techniques of 3D Printing and Additive Manufacturing

The basic principle of 3D printing is to make the produced object, layer by layer. However, not all 3D printers use the same layer coating technique and it is a characteristic that separates different techniques. According to the American Society for Testing and Materials (ASTM) there are 7 different 3D printing techniques that will be presented and analyzed below in this section. Therefore, the current 3D printing techniques are [18-19]:

- Vat Photopolymerization technique

Vat Photopolymerization is a 3D printing technique where UV light and curable materials (resins) are used as raw materials and in the process of printing certain areas (layers) of material are cured and the result is to solidify and produce (layer by layer) the desired geometry. This technique was discovered in the mid-1980s by engineer Charles Hull (who also discovered the STL. file format). There are four different approaches to this technique that have been explored in recent years: Stereolithography (SLA - the most widespread), Digital light processing (DLP), Continuous liquid interface production (CLIP) and Two-photon (2 PP) and multiphoton polymerization (MPP). Depending on the chosen approach for this particular technique, the printing speed and the thickness of the layers can be varied, the layers thickness, in some cases, can reach to a few micrometers.

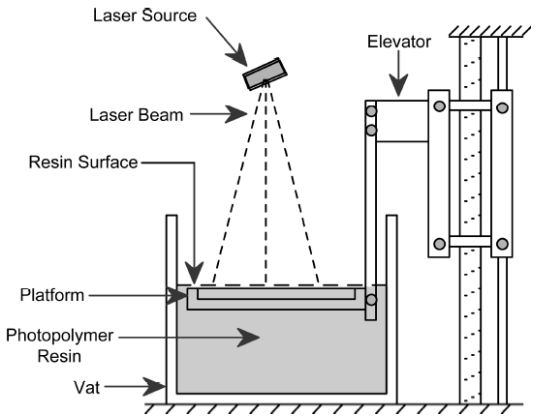

Fig. 20. Schematic set-up of Vat Photopolymerization technique.

- Material Jetting

In this 3D printing technique, droplets of material (such as photopolymer or thermoplastic materials) are positioned to form the pattern of the printed object, such as in 2D ink jet printing only where the drops of material from the layers, that creates the 3D object (layer by layer). Then, with the use of UV light the printed object hardens in order to produce the solid model. The Figure 19 shows a graphical representation of the process.

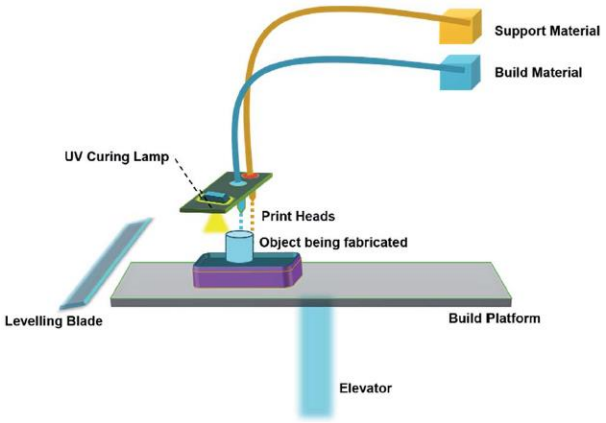

Fig. 21. Schematic set-up of Material Jetting technique.

- Binder Jetting

In this method of additive manufacturing, the raw material is in powder form in a tank. Then, there is a part of the printer that contains the glue in liquid form and depending on the printed object it sticks the powder at specific points. Again, the process is done layer by layer and the tank with the powder in each layer is lowered. The materials that can be used are metals, polymers, and ceramics. There is a schematic illustration in Figure 20.

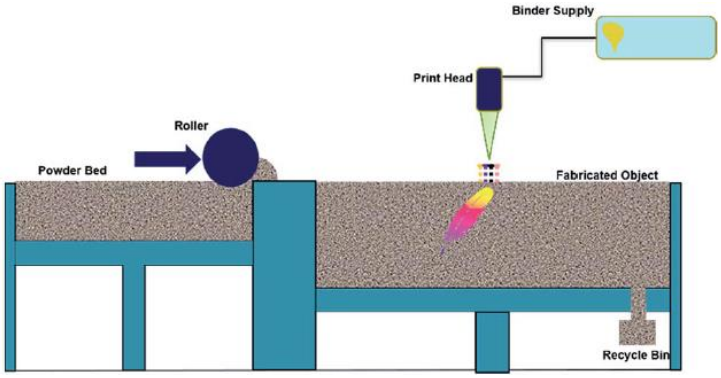

Fig. 22. Schematic set-up of Bitter Jetting technique.

- Sheet lamination

The Sheet lamination technique is a 3D printing process where the raw material is separated into sheets which are cut in the printed object's pattern and then they are bonded together either by glue or by other methods (such as ultrasonic welding). Below is a graphical illustration of the process.

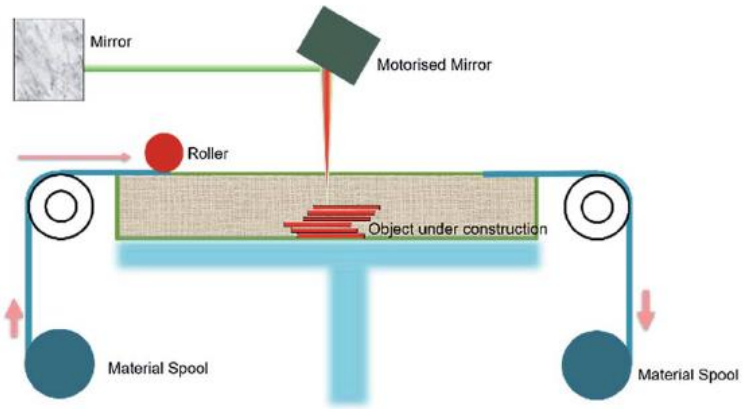

Fig. 23. Schematic set-up of Sheet lamination technique.

- Material Extrusion

This technique has a commercially named as Fused Deposition Modeling (FDM) or Fused Filament Fabrication (FFF) and is probably the most widely used 3D printing technique in the world right now. In this technique the raw material (usually thermoplastic) is wrapped in a spool and has the form of a filament. The material filament passes through a nozzle where it melts and is positioned in the correct position. The nozzle has the ability to move horizontally and vertically with the help of computer-aided manufacturing (CAM) software and G-code. The material is then positioned in such a way that the layers and finally the object are created.

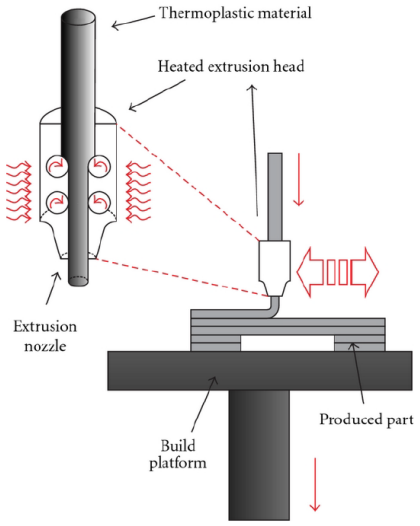

Fig. 24. Schematic set-up of FDM technique.

- Powder Bed Fusion

Powder Bed Fusion is a 3D printing technique that uses either a laser or an electron beam to sinter or melt or both the raw material in order to form the desired geometry. The process is as follows the raw material is in powder and spreads on a powder bed then a laser beam melts or sinters the powder particles according to the geometry's cross-section of the object creating a thin cross section (layer) of overall geometry. Immediately afterwards, the powder bed goes down for a layer thickness and the process is repeated until the entire object is created, layer by layer. This 3D printing technique has many advantages over the others techniques as it does not require supports, has very good mechanical properties of the produced object and the unused powder of raw material can be used again in other printing. There are five variants of the Powder Bed Fusion technique and these are the following:

a. Selective Laser Sintering (SLS)

b. Selective Laser Melting (SLM)

c. Direct Metal Laser Sintering (DMLS)

d. Electron Beam Melting (EBM)

e. Selective Heat Sintering (SHS).

From the above ways of applying Powder Bed Fusion the Selective Laser Sintering (SLS) is the most widespread for plastics while Direct Metal Laser Sintering (DMLS) is the most widespread for metals. The differences of these techniques with the rest are minimal and mainly focus on whether they sinter or melt the powder particles of the raw material and with which way (laser beam or electron beam). The following figure shows a typical Powder Bed Fusion layout.

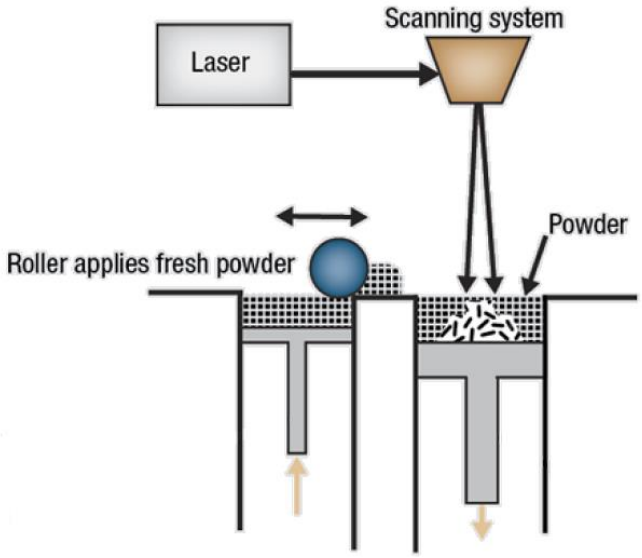

Fig. 25. Schematic set-up of Powder Bed Fusion technique.

- Directed Energy Deposition

The Directional Energy Deposition (DED) 3D printing technique is a combination of FDM and Powder Bed Fusion techniques, mainly made with metals. The process is as follows: the raw material is either powder or filaments and spreads them to the desired path by nozzles in order to form a layer. At the exit of the nozzles, the raw material is completely melted by either a laser or an electron beam or a plasma arc. The nozzles follow the path to form the cross section of the geometry. Again, layer by layer the final geometry is formed.

This technique is usually applied to high-tech metal components aimed at the rapid manufacturing applications. Below is a schematic illustration of the direct energy deposition (DED) device.

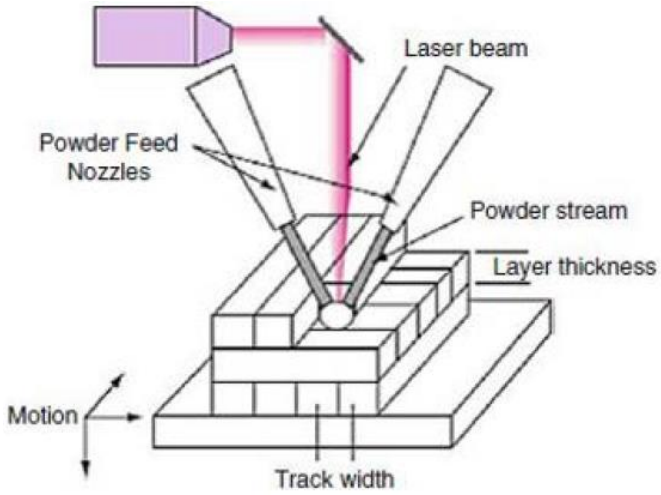

Fig. 26. Schematic set-up of Directional Energy Deposition (DED) technique.

These are the hitherto known 3D printing techniques. 3D printing is still very young as a process, is being studied all over the world and is developed constantly. One of the most interesting and new aspects of 3D printing (as it was first mentioned in 2013) is its transformation into 4D printing. In this process (Figure 25), a smart material is selected for the construction of an object, and through a smart design, which usually includes lattice structures; 3D printing of the static structure of the object is made. Subsequently, the static structure of the object is introduced into a field of operation where receives a stimulus (i.e. heat, light, etc.), thus the geometry of the object is changed to better serve its purpose. A classic example of such application is the 4D medical stent where due to the temperature of the human body it expands so as to inflate the artery.

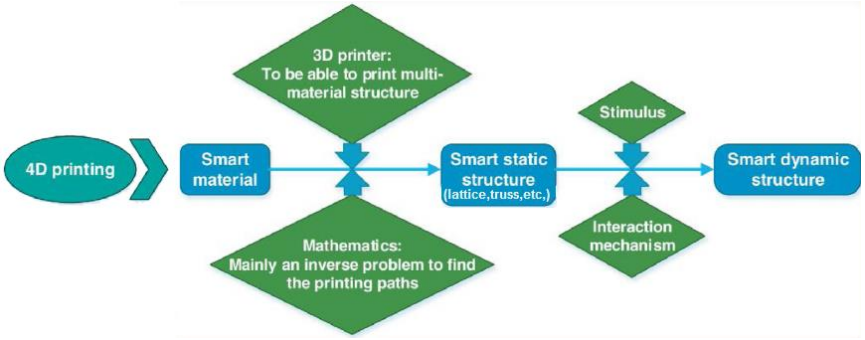

Fig. 27. Schematic presentation of 4D printing process.

Investigation of Mechanical Properties for Lattice Structures

3.1. Introduction

The previous chapters have analyzed the needs and the ways to topologically optimize the design of an object. It was also emphasized that through lattice structures and with the help of 3D printing, topology optimization of the design of an object can be achieved in various applications. However, as it mentioned above, complex lattice structures (that is, those containing trusses and TMPS structures) can only be manufactured with 3D printing. As a result, because 3D printing technology is so new, as well as the software that can handle such complex geometries, there is lack of enough experimental and theoretical models for the mechanical properties of these structures.

However, though the existing literature seems the lattice structures affect the mechanical properties of the whole structure. According to these studies, the decrease in the mechanical behavior of lattice structures is due to the size effect. The size effect is mainly influenced by the relative density (foam structure) and the geometric parameters of each lattice structure. In particular, the mechanical properties of the structure, such as Young Modulus and yield strength, appear to be different from the solid material, which is why other terms different from that of solid (i.e. effective young modulus) are used. The majority of research on this topic has focused on structures consisting of trusses, due to its ease of design and computation. These studies have shown that Young modulus is affected as follows $E_{lattice}/E_{solid}=C_n\rho^n_{relative}$ and yield strength as follows: $\sigma_{lattice}/\sigma_{solid}=C_m\rho^m_{relative}$. The variables C_n, C_m, n and m are variables influenced by geometry, that is, by each lattice structure applied. The variables C_n and C_m range from 0.1 to 4. While the variables n and m are from 1 to 2. The larger the exponential indices (n & m), the more intense the size effect with decreasing relative density [20-21-22-23]. The few studies on lattice TPMS structures are showing that the same phenomenon appears on TPMS lattice structures. However, it seems that TPMS geometries have smaller exponential coefficients than lattice structures with trusses. Indicatively, n and m can be less than one, which means that the size effect on these structures is significantly smaller [24-25-26-27-28-29]. In summary, the values of mechanical properties of Young Modulus and yield strength are reduced in lattice structures due to the size effect. This decrease, in proportion to the relative density, causes a significant reduction in mechanical properties values up to 70% -80% for relative densities of less than 30%.

In order to improve the existing literature, in this chapter the research is focused on the calculation of the mechanical properties of these complex TPMS geometries. More specific, this study is focused on lattice structures which consisting TPMS elements especially the most common ones: Gyroid, Schwarz Diamond and Schwarz Primitive.

The mechanical properties of TPMS structures, which are studied, are the elasticity modulus (Young Modulus) and how this is affected by the relative density and changing geometry. The aim is minimizing the size effect and also to identify the compressive yield strength of each geometry and observed a pattern for each geometry that can predict the mechanical behavior of each TPMS geometry. In order to reduce the phenomenon of size effect, the TPMS structures are required to have parameters (length and thickness) of their unit cells comparatively large to the whole structure and to be combined with solid pieces of material (plates) also plays an important role.

Thus, in the context of this research was selected Polylactic acid or polylactide as structure material (PLA) which can be printed with FDM technique (large and solid

unit cells), low cost and may have applications with TPMS geometries (scaffolds for tissue engineering). Subsequently, experiments were carried out with compressive loads on the 3D printed specimens to study the mechanical properties. Finally, the experimental data are compared with the results of finite element analysis in order to derive predictive patterns of the mechanical behavior of the each TPMS geometries for PLA material.

3.2. Procedure of Design & 3D Printing

3.2.1. Design of Specimens with Lattice Structure

Designing lattice structures, even with modern design methods, before 2-3 years was not an easy case and took long time for both proper calculation and design. Today, there is a plethora of software that have filled this gap with specialized algorithms. Thus, in this software the designer inserts the geometry that wants to have an internal lattice structure, and then by adjusting some input variables the software automatically extracts the desired geometry (internal - external). However, this extracted geometry is a surface model that makes more difficult further modifications of the geometry. Some software, that can design lattice structures, are:

- *SpaceClaim (ANSYS)*
- *3DXpert (3D Systems)*
- *nTopology*
- *Autodesk Within*

For the needs of this research, SpaceClaim software of the ANSYS software platform was used. The first reason that this software was chosen is that it is compatible with ANSYS's overall platform, so there will be no geometry compatibility problems with the software that performs finite element analysis. The second reason is that it contains all the major lattice structures such as honeycomb, truss and TPMS structures. Also, this software is quite easy to use with simple and comprehensible input variables when creating lattice geometry. Finally, SpaceClaim is accessible to everyone as it is included in the student version of ANSYS 19 R2.

After selecting the design software, the next step is the exact geometry of the specimens. Knowing that for compressive loads, the geometry selected in the literature is usually cubic, hence cubes were selected as general geometry of specimens in this study. Also, in this study, there is an increased interest in the use of lattice structures in medical applications. Therefore, PLA was chosen as a structural material of the specimens. The reasons that led to this plastic material are its bio-compatibility with human body and the ease of 3D printing this material with FDM technology. Given the construction material, the general geometry and the way the specimens are manufactured, the next step is to determine the dimensions.

Determining the dimensions of the specimens is a very important step and it directly affects the experiments as well as the actions that need to be taken to extract the experimental data. The outer dimensions selected for all the specimens were 50mm x 50mm x 50mm. The main reason for this option was to reduce as much as possible the size effect. Other important factors were: the inability of FDM technology to 3D print smaller pieces with very high accuracy, and the possible inability of the experiment to be performed in the event of a larger specimen due to exceeding the maximum load limit of the press.

Finally, the last parameter, that must be taken into consideration when designing the specimens, was that due to their geometry in the upper and lower surface (lattice structures ending) there was a high probability that the specimens were sliding on the table of the press during the experiments. Therefore, in order to ensure the stability of the specimens and minimize size effect, it was decided to add two straight plates at the top and bottom of the structure with 2mm thickness. These plates will form a unique body with the lattice structures of the specimens, so the final dimensions of the specimens will be 50mm length, 50mm width and 54mm height. Below, the procedure for designing the above specimens will be presented in the SpaceClaim software.

The first step, in designing the specimens, is to design the lattice structure. As mentioned above, the outer dimension of the structure is 50mm x 50mm x 50mm. Therefore, a plane of design is selected and the cross section of the specimen is drawn, that is, a 50mm x 50mm square (Figure 28). Immediately afterwards, the cross section is extruded to the third dimension (with the pull command) to create a 50x50x50 cube (Figure 29), inside that cube the lattice structure is going to be created.

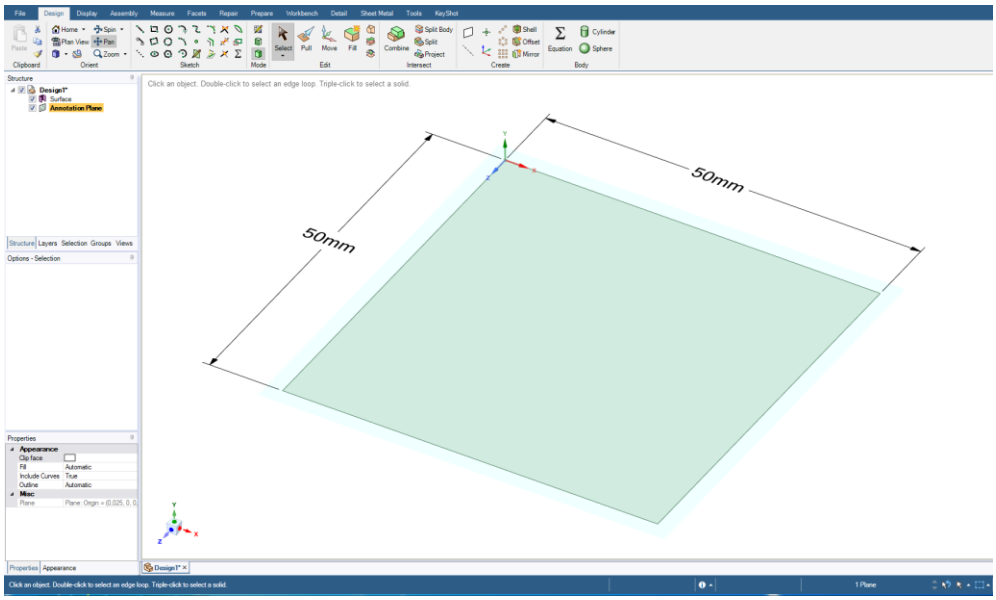

Fig. 28. SpaceClaim design panel and designing the specimens.

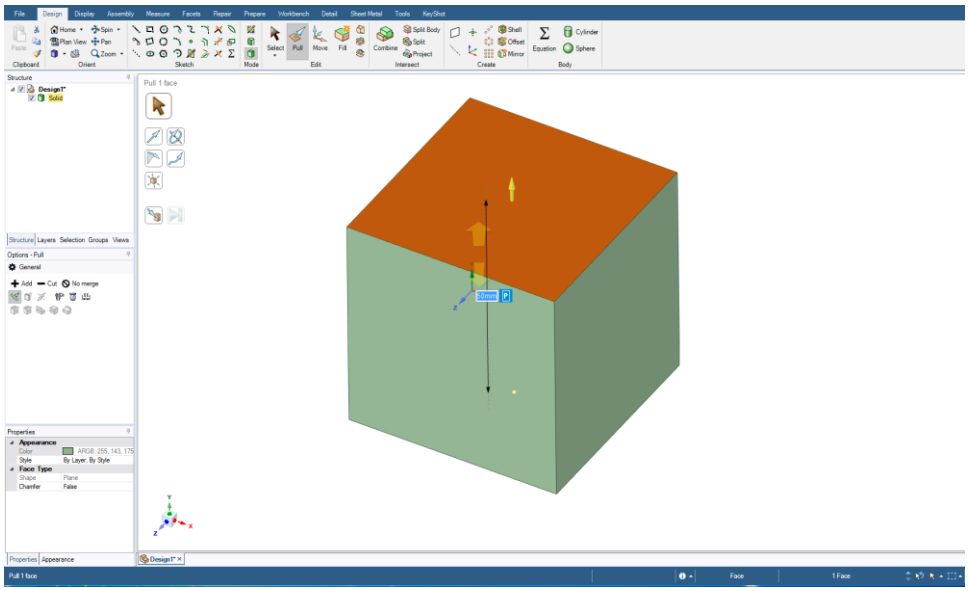

Fig. 29. The cube where the lattice structure is going to be made.

Then, the volume of this cube is used to develop the lattice geometries. But in this software as in many others, because all the lattice structures are geometrically very complex, they are exported as surface models. Therefore, the already designed cube must be transformed into a surface model. This is done as follows: on the toolbar there is the facets tab which has the convert command that converts a solid model into a surface model (Figure 30). After the model is converted, the creation of the lattice structures is followed with the shell command (found on the Facets tab). Once this command is selected, a pop-up window opens. In this window, in the infill section there are all available lattice structures provided by the software as well as the ability to customize lattice structures. The lattice structures that the software provides are:

- *Extrusions (Honeycombs & prismatic structures)*
- *Lattices (truss lattice structures)*
- *Minimal Surfaces (TPMS structures)*

Still, in the same section the designer can enter three parameters for the desired geometry he wants: length, thickness and relative density of the overall lattice structure. Of course, these input variables are interdependent. Figure 31 illustrates the options the software provides.

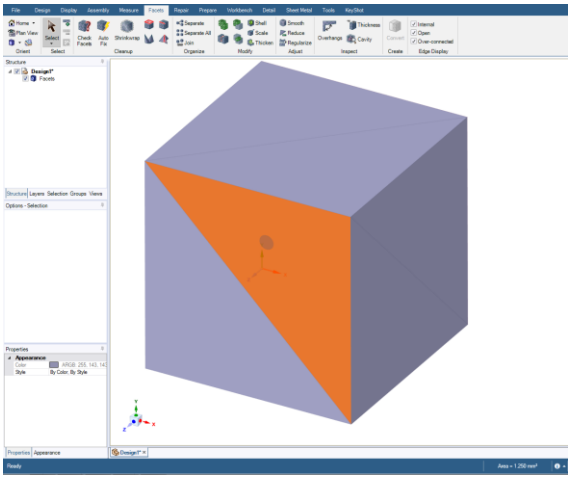

Fig. 30. Converting a cube to a surface model.

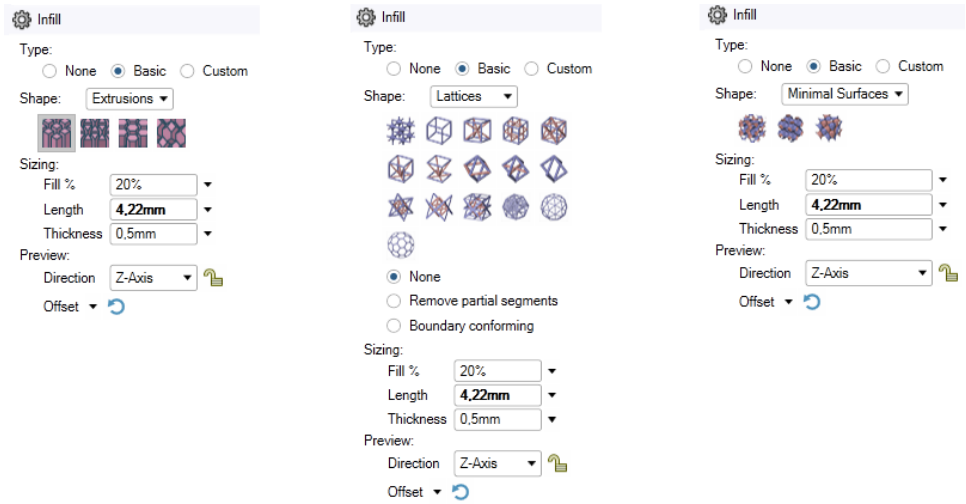

Fig. 31. Options of lattice geometries: honeycombs (right), trusses (center), TPMS (left) and input parameters.

Having chosen the desired lattice structure and having introduced the geometry parameters, the whole lattice geometry is extracted into a surface model (Figure 32). In order to complete the design of the specimens, two solid plates have to be designed on the bottom and top surface of the adorable structures (Figure 32).

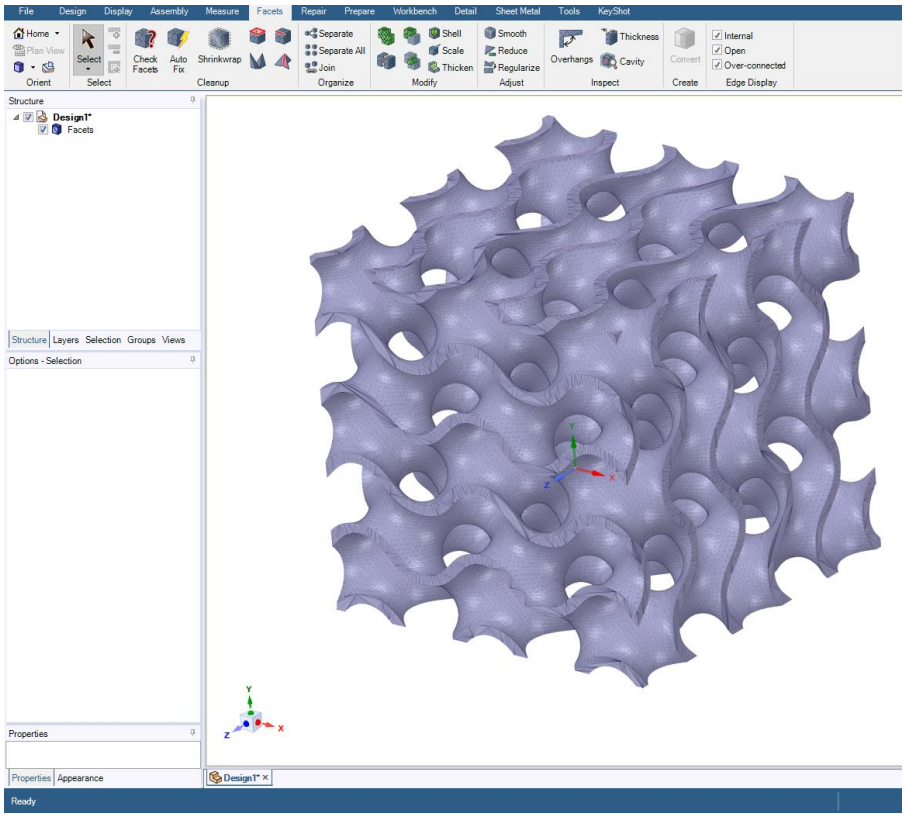

Fig. 32. Surface model of Gyroid lattice structure.

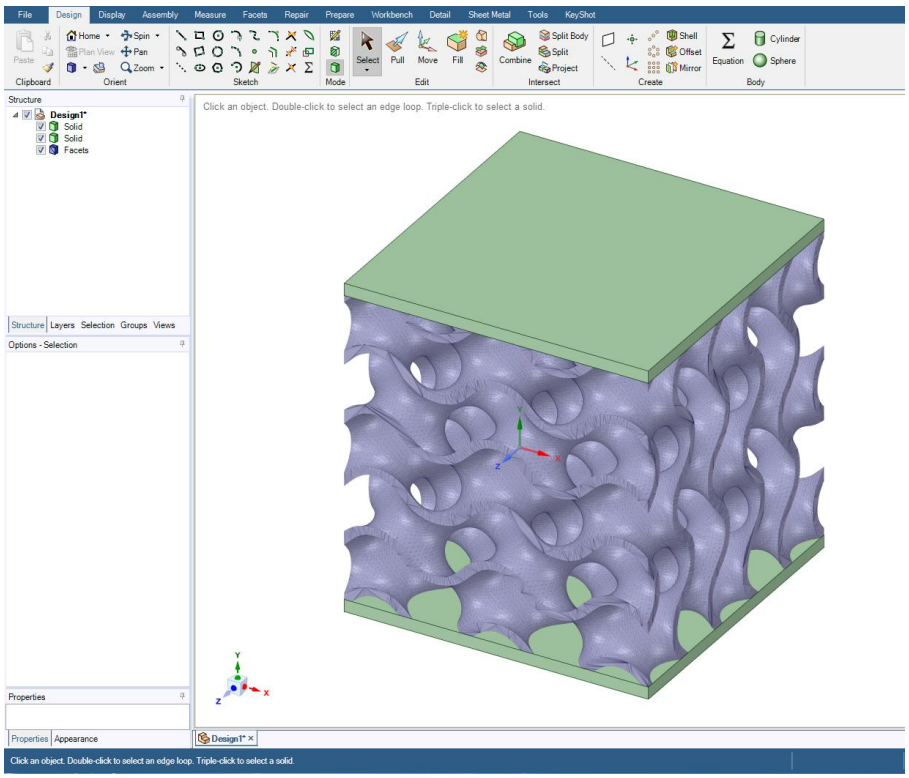

Fig. 33. Design of final specimen with Gyroid structure.

The purpose of this research is to study TPMS structures as they are considered to be superior in their mechanical properties in comparison to other lattice structures. More specifically, the most important TPMS structures are studied: Gyroid, Schwarz Diamond and Schwarz Primitive. Still, the lattice structures within the specimens should be as symmetrical as possible to avoid any failures in the experiments. Therefore, because of the needs of the experiments, samples of various relative densities had to be manufactured, the length of the elements of each specimen remained constant (for symmetry reasons) and only the thickness of the elements was changed. Table 1 presents the design parameters for all the specimens that are designed and used in this study.

Table 1. Design Parameters of each specimen.

TPMS Structure	Relative Density of Lattice region	Actual Relative Density of specimens	Element Length (mm)	Element Thickness (mm)
Gyroid	10%	16,7%	4	0,65
	20%	26,1%		1,3
	30%	35%		1,95
Schwarz Diamond	10%	16,7%	5,1	0,67
	20%	26,1%		1,33
	30%	35%		2
Schwarz Primitive	10%	16,7%	3,75	0,54
	20%	26,1%		1,07
	30%	35%		1,61

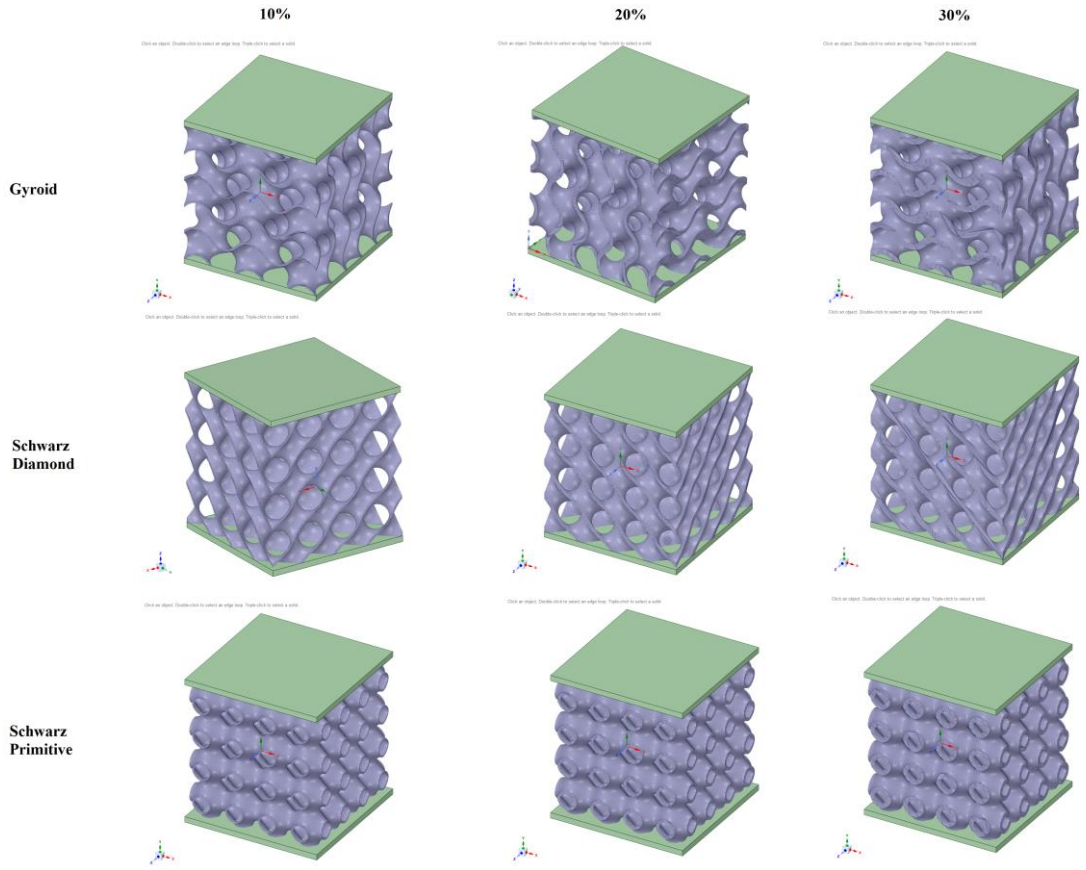

Fig. 34. Designed specimens.

3.2.2. 3D Printing of Specimens

After the design procedure of the specimens, that contains the lattice structures, is completed, the next step is to 3D print them with a 3D FDM printer; hence the experiments of this study could be carried out.

The specimen's drawing files are converted to STL. format to allow slicing and 3D-printing of their geometries. Next, the Cura BCN3D software is used to determine the print parameters as well as the slicing of the specimen's geometries. The printer used for 3D printing of the specimens is the BCN3D Sigma R17 (FDM - Appendix I). The following table shows the parameters for printing all specimens.

Table 2. General Printing Parameters of all specimens

Parameters of 3D Printing

Material	*PLA (filament)*
Layer Height	*0,2mm*
Wall Thickness	*0,8mm*
Infill	*100%*
Printing Temperature	*200^0C*
Printing Speed	*60 mm/s*

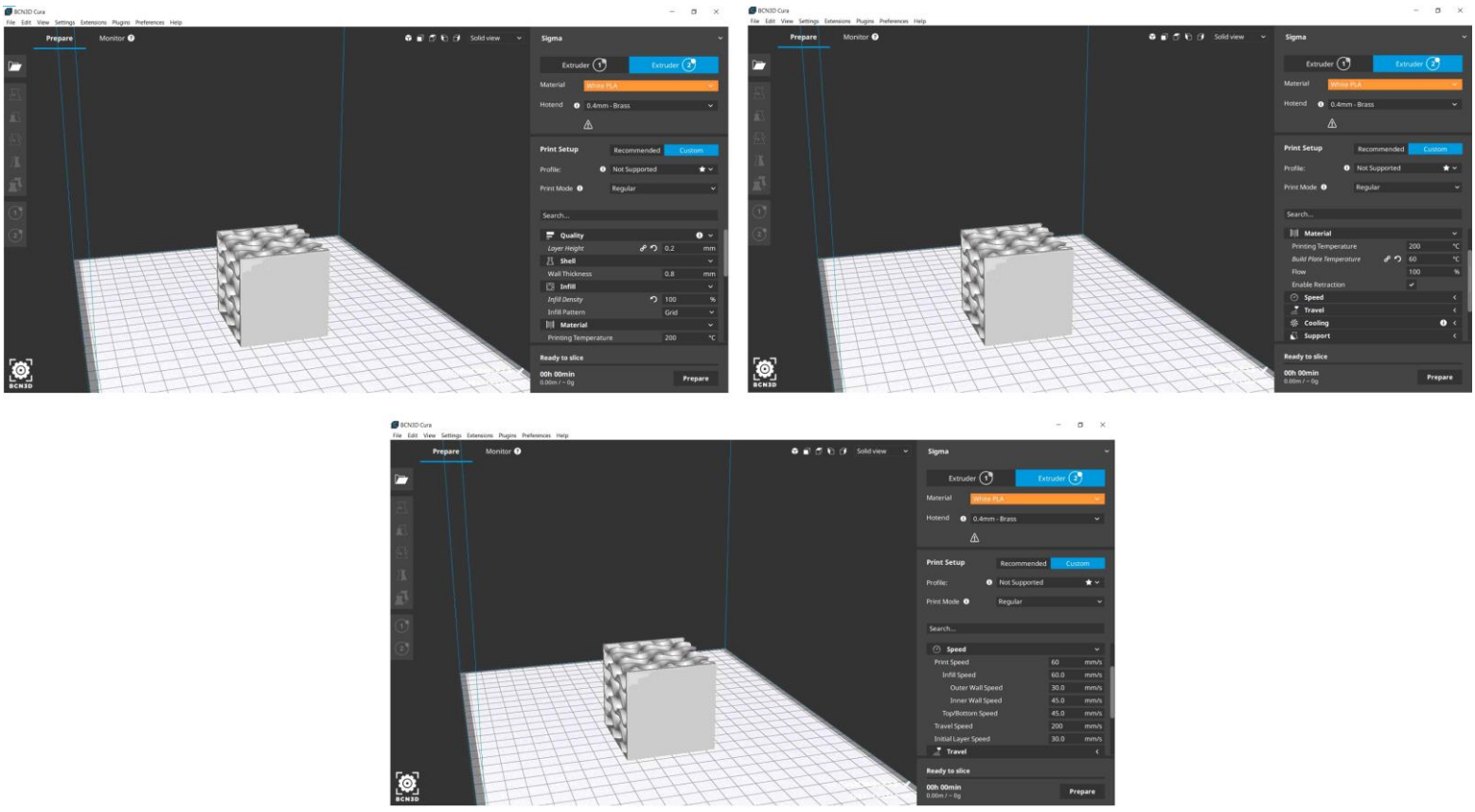

Fig. 35. Detailed Figures of 3D-Printing Software.

Figure 35 shows more details of 3D - printing (orientation, individual speeds, etc.) as well as the environment of the CURA software.

The printing material as mentioned above is Polylactic Acid (PLA), due to its biocompatibility with the human body. The raw material of the PLA is a black filament with 2.85mm diameter.

The mechanical properties of the raw material are calculated by the nano - indentation process. The SHIMADZU DUH-211S (Dynamic Ultra Micro Hardness Tester - Appendix II) equipment was used for this procedure. It is a machine that calculates the mechanical properties of a material (Young Modulus, Hardness, etc.) through dynamic nano - indentation. That is to say, with the aid of a microscope, an area of material, which is fairly smooth, is selected and then the machine penetrates into that area through a force chosen by the user. The force of indentation, in this procedure, is 200mN. This procedure is necessary in order to verify the precise mechanical properties of the raw material before conducting the experiments. More than three measurements were performed to obtain safe and reliable results. Below are the results of the indentation's measurements.

Fig. 36. Equipment of SHIMADZU DUH-211S.

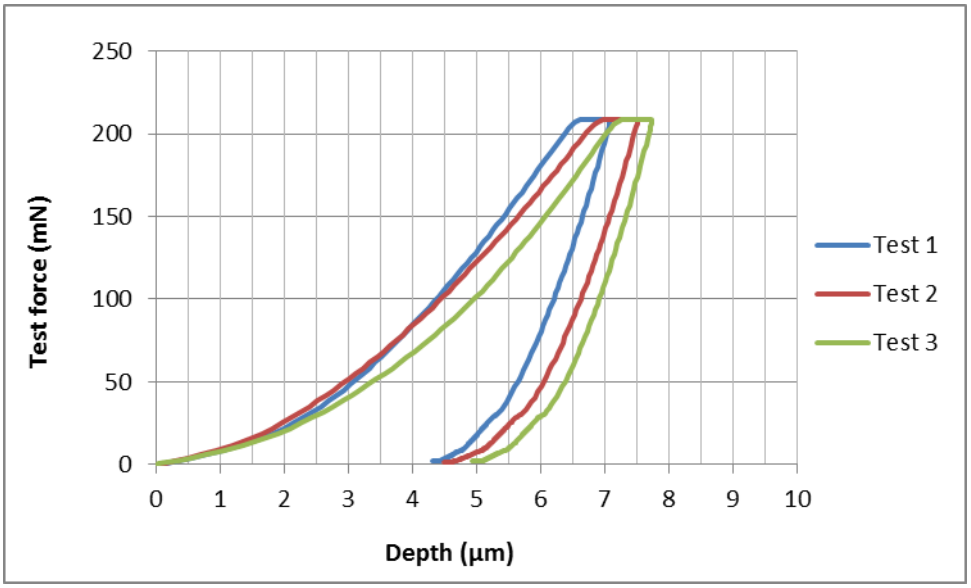

Fig. 37. Graph of the nano – indentation measurements.

Table 3. Properties of Raw material.

PLA Properties	
Density	1,25g/cm^3
Young Modulus	3400MPa
Poisson Ratio	0,4
Compressive Yield Strength	92MPa

Figure 38 shows the 9 separate types of 3D-printed specimens. In particular, 9 different types of specimens were printed with internal lattice structures Gyroid, Schwarz Diamond and Schwarz Primitive, at relative densities for lattice structure at 10%, 20% and 30%.

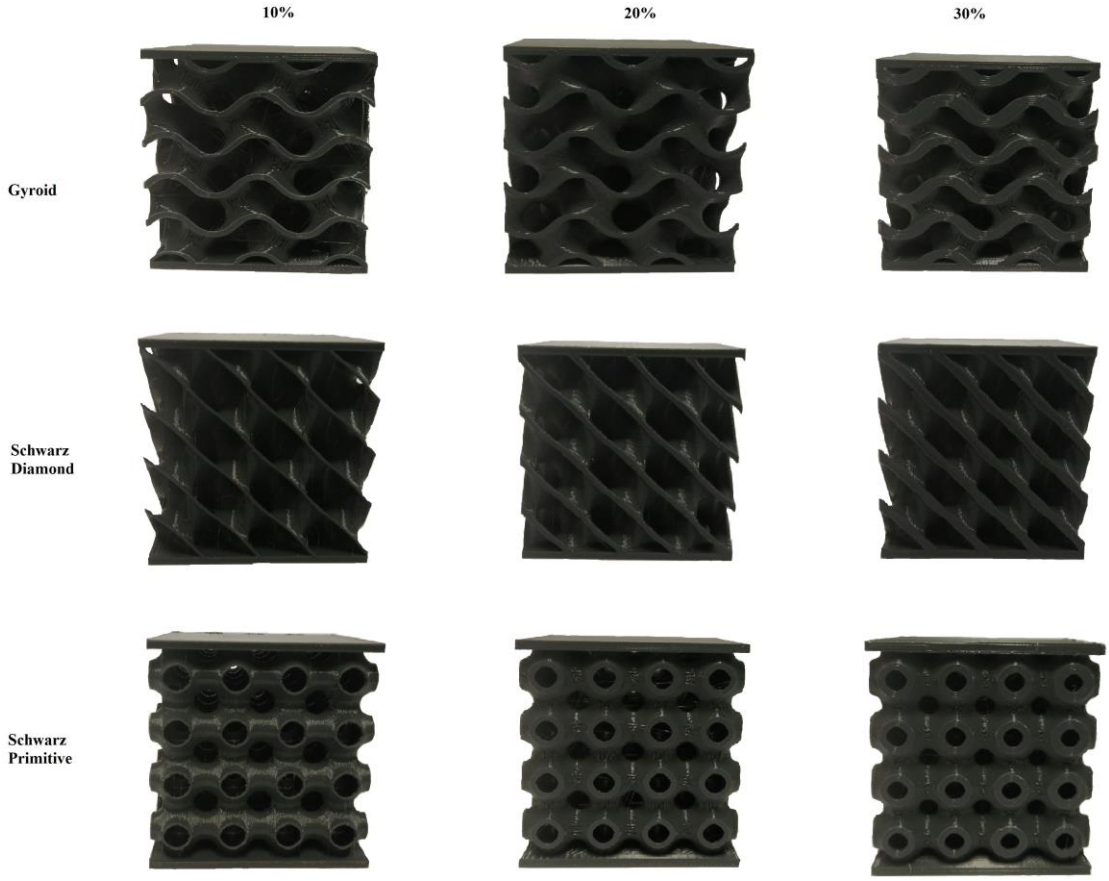

Fig. 38. 3D-Printed specimens.

Table 4. Properties of 3D Printed Specimens.

TPMS	Relative Density	Weight of specimen (gr.)	Time of Printing
Gyroid	16,7%	28,18	~ 4h
	26,1%	44,04	~5h and 30min.
	35%	59,06	~7h and 30min.
Schwarz Diamond	16,7%	28,18	~ 4h
	26,1%	44,04	~5h and 30min.
	35%	59,06	~7h and 30min.
Schwarz Primitive	16,7%	28,18	~ 4h
	26,1%	44,04	~5h and 30min.
	35%	59,06	~7h and 30min.

3.3. Compression Testing & F. E. Analysis

3.3.1. Description of the Experiment

In the previous section, the design and manufacture of specimens, through which the mechanical properties of lattice structures will be examined, were presented. This section presents the experiment's setup and the experimental results.

Initially, all experiments in this study were conducted at the Digital Manufacturing and Materials Characterization Laboratory (DMMC Lab) of the International Hellenic University. The experiments that were carried out are compression loading of the specimens. The equipment used for these experiments is Testometric - M500-50AT (Appendix III). The Testometric -M500-50AT is considered a very reliable measuring machine for tensile, compressive, bending and circular load experiments. The maximum capacity of this machine is 50kN.

Fig. 39. Testometric-M500-50AT machine.

All experiments that were carried out in this study have the same set up. Firstly, the compression plates of the machine are positioned up and down and then marked, so that cubic specimens to be positioned as close as possible to the center of the plates. Then, the speed at which the top plate would move and crush the specimens is selected at 5mm / min. The speed of the experiments was chosen after extensive research in the existing literature and various tests. The main reason for choosing this speed was the reliability of the output results.

3.3.2. Results of the Experiments

In the preceding sections, the design and manufacturing of the specimens, which are used in the experiments, were described. Also, the laboratorial equipment, which used for the experiments as well as the way the experiments were carried out, was also presented.

In this section, the results of these experiments are presented and analyzed. The same speed of application for compressive loads (~ 5mm / min.) was applied to all specimens regardless of their density. Moreover, all specimens handled compressive loads of up to 15% of their strain, that is, displacement from the nominal length of approximately 8mm.

Below, the experimental results for each lattice structure are presented.

Schwarz Primitive:

This lattice structure is considered to be the least strong of all three TPMS geometries, as shown in the results below is the structure that has the least force and least load for the same deformation (strain). However, the results for the energy absorption of this TPMS structure are very promising. Below, there are figures of the compressive loading of Schwarz Primitive specimens for all its densities.

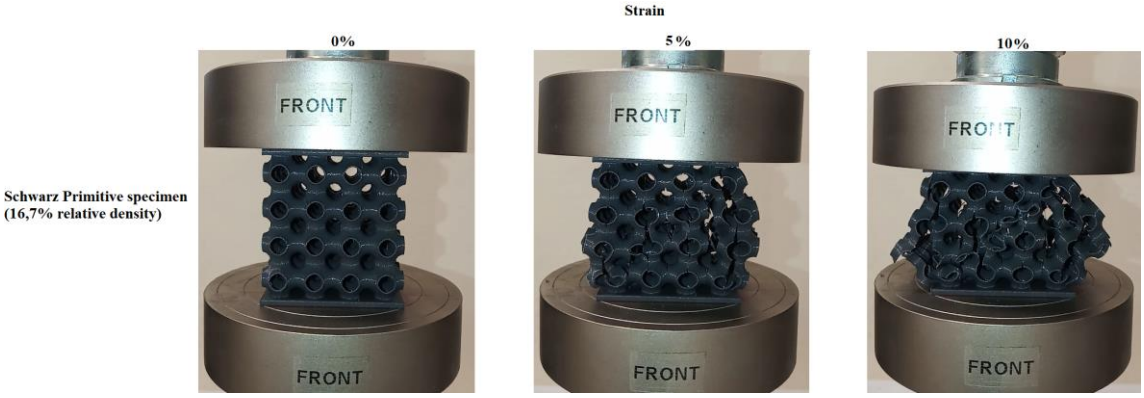

Fig. 40. Deformation of Schwarz Primitive specimen with 16,7% relative density.

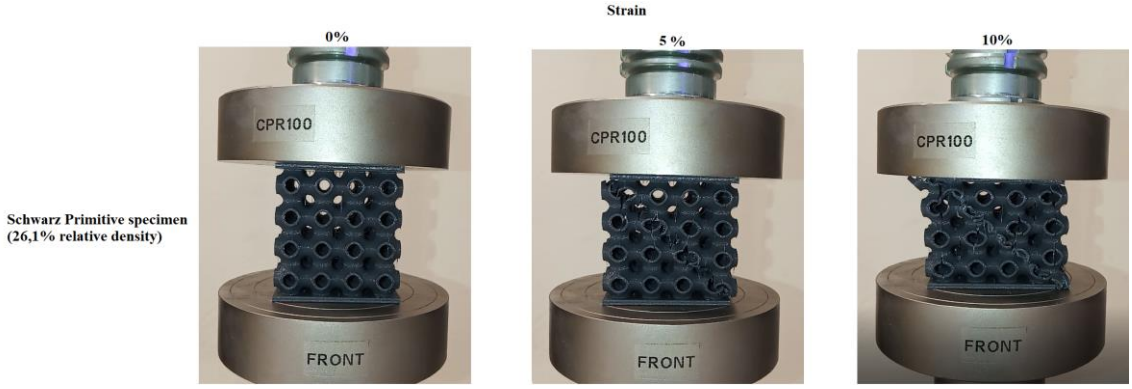

Fig. 41. Deformation of Schwarz Primitive specimen with 26,1% relative density.

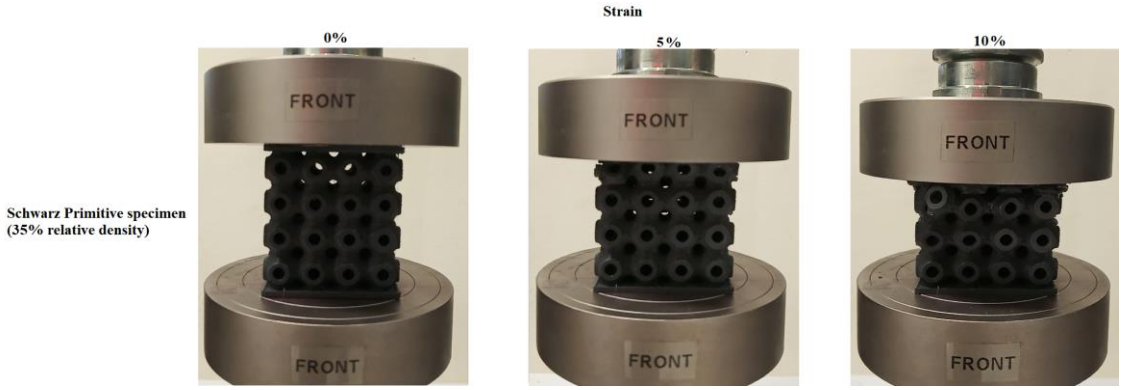

Fig. 42. Deformation of Schwarz Primitive specimen with 35% relative density.

As shown in the above figures from the experiments, the specimens with Schwarz Primitive structure are crushed. The images also show intense shears stress events which result in the material breaking in the diagonal of the specimen. Furthermore, each unit cell brakes in the region with the maximum curvature. Still, it is worth noting that this structure accumulates loads on the unit cells layer closest to the point of application of force. This is why the upper layer breaks first and the rest do not seem to be so affected. Below is the final force-to-displacement diagram for examined Schwarz Primitive specimens with different densities.

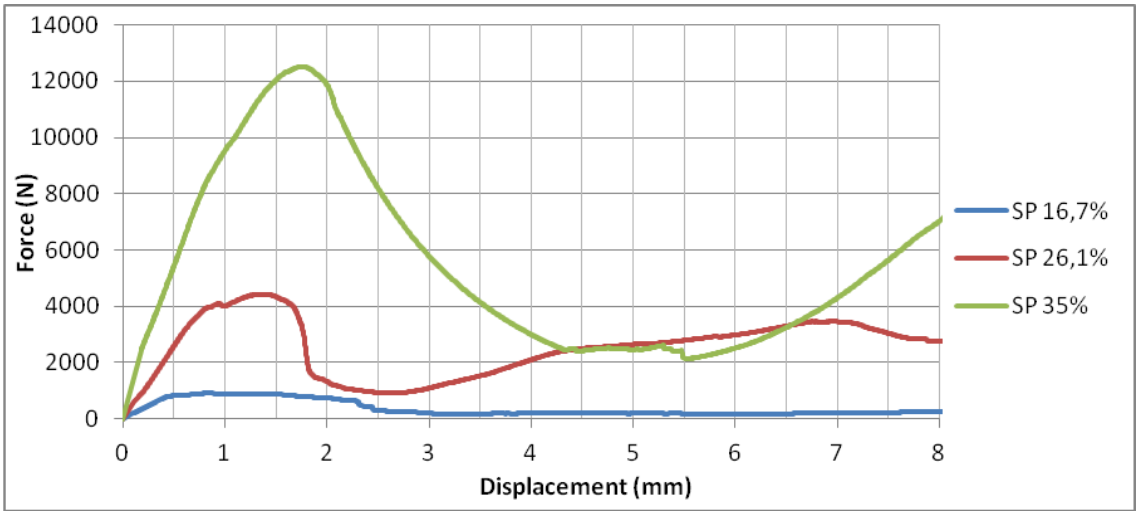

Fig. 43. Force to Displacement diagram for Schwarz Primitive specimens.

As expected, the specimens with the highest relative density withstood the greatest compressive forces for the same rate of displacement. Examined the above diagram, the mechanical properties of the Schwarz Primitive lattice specimens (Table 5) as well as the stress to strain diagrams are extracted (Figure 44).

Table 5. Experimental Mechanical Properties of Schwarz Primitive specimens.

Experimental Results	*Relative Density*		
	16,7%	26,1%	35%
Effective Young Modulus	2250 MPa	2334 MPa	2713 MPa
Compressive Yield Strength	18,82 MPa	34,01 MPa	57,66 MPa
Max. Force	847,5 N	3981 N	12520 N

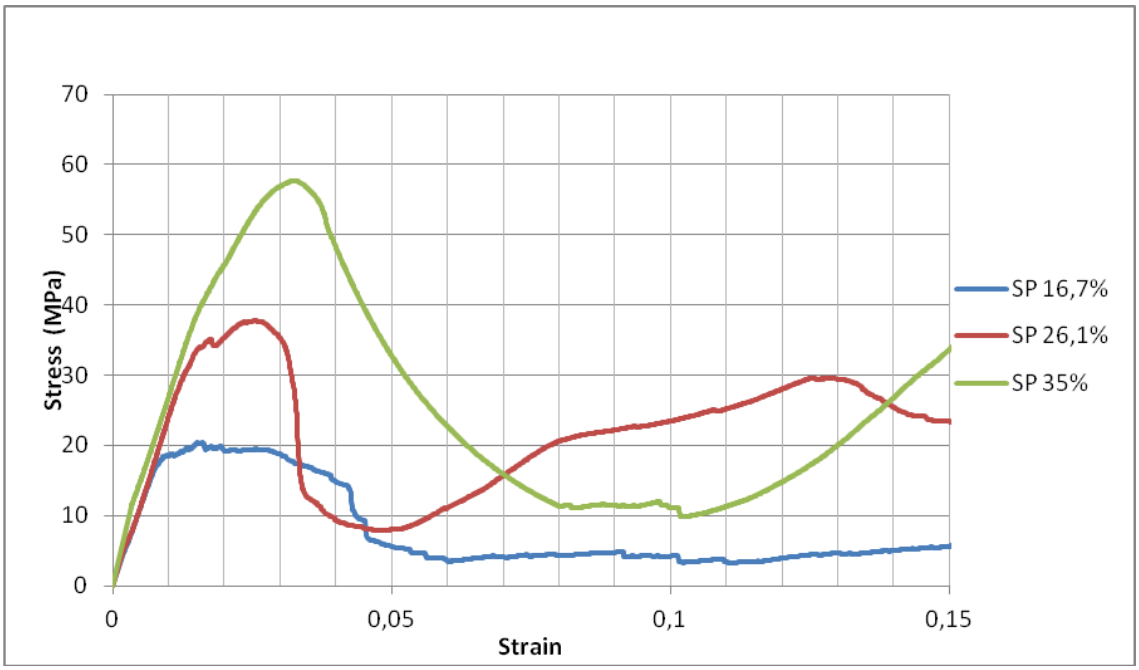

Fig. 44. Stress to Strain diagram for Schwarz Primitive specimens.

Experimental results for the specimens with the Schwarz Primitive lattice structure show that in compressive loading after the elastic branch a small plateau is created which means that the integrity of the unit cells of the specimens, for a short period of time, is compact, despite the fact that the structure has passed the yield strength point.

Furthermore, during plastic deformation of the specimens the unit cells of the structure fail individually from top to bottom. This means that the unit cells at the top of the specimen are broken without breaking the unit cells in the bottom layer, so this property of this structure holds the plastic deformation branch at high stresses. This lead, as will be shown in the next chapter, to potential high energy absorption.

Gyroid:

The Gyroid structure is the most widespread TPMS geometry and as shown in the experimental results below it has a very good performance in both strength and energy absorption terms. However, it is not the strongest lattice structure that is studied in this dissertation.

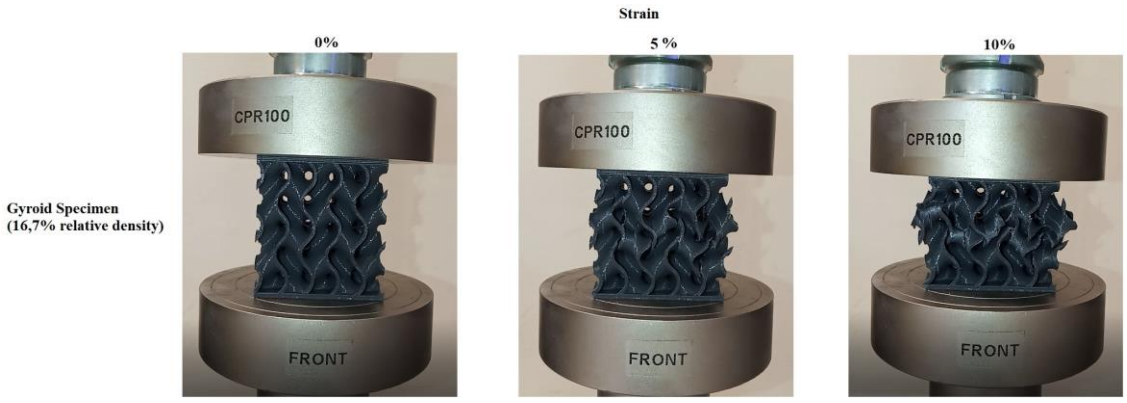

Fig. 45. Deformation of Gyroid specimen with 16,7% relative density.

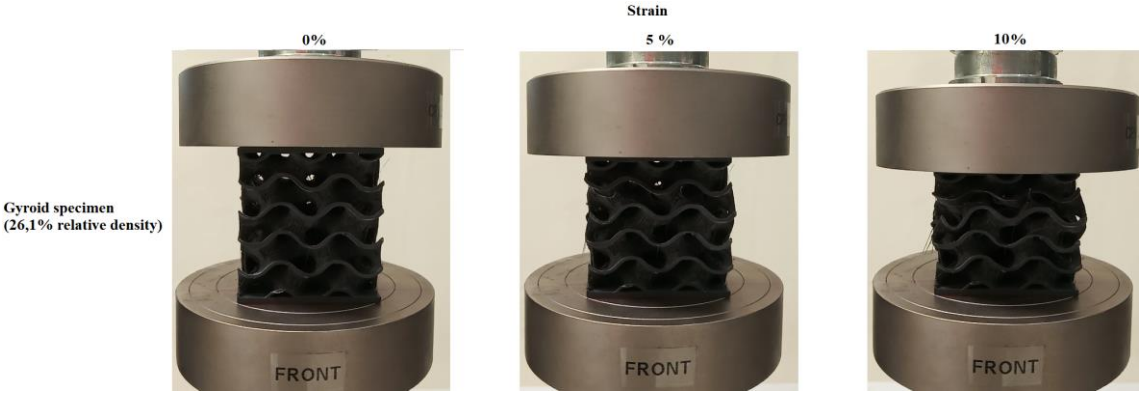

Fig. 46. Deformation of Gyroid specimen with 26,1% relative density.

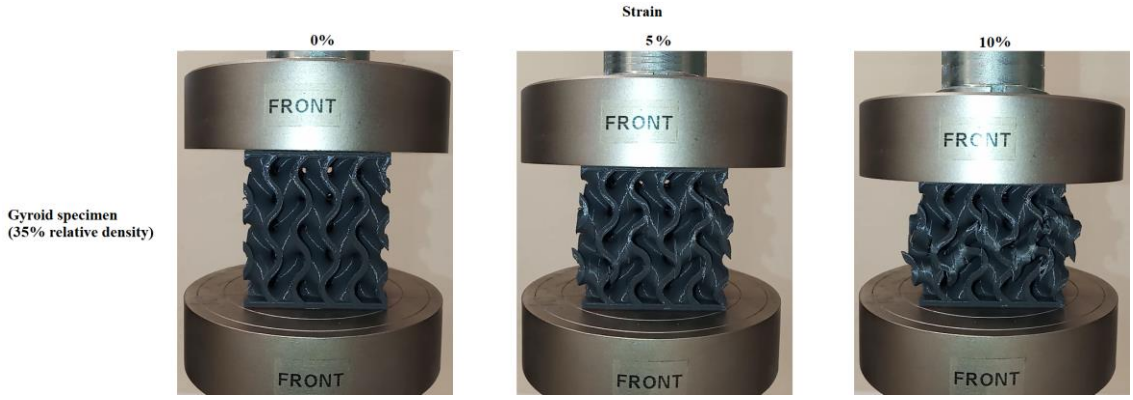

Fig. 47. Deformation of Gyroid specimen with 35% relative density.

Above are illustrated images of conducting experiments for different relative specimen's densities and different deformations (strains). In contrast to other structures in the specimen with Gyroid structure, no strong shear effects are observed. However, it appears that this particular structure accumulates the stresses at the center of the specimens, thereby leading to their failure. Below is the final force-to-displacement diagram for examined Gyroid specimens with different densities.

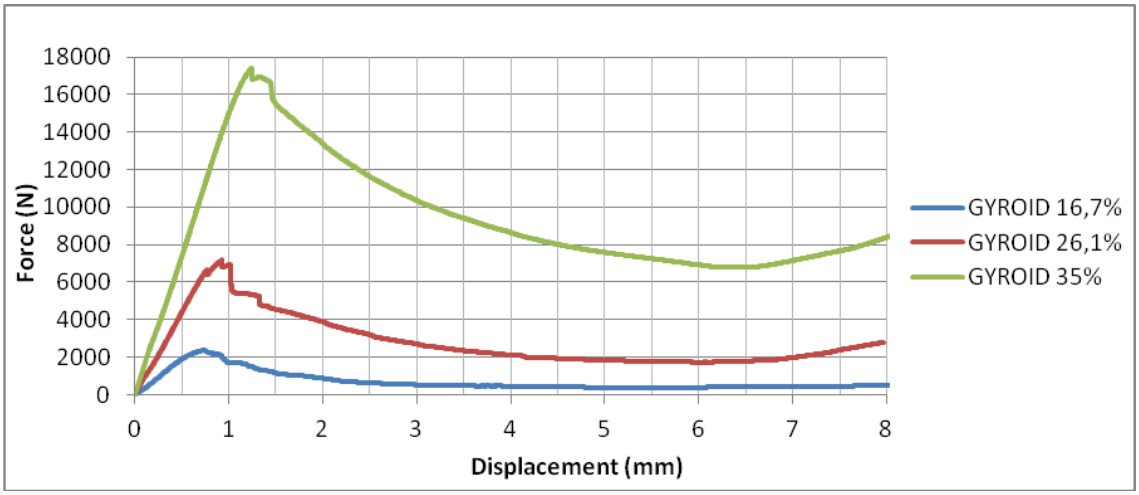

Fig. 48. Force to Displacement diagram for Gyroid specimens.

Table 6. Experimental Mechanical Properties of Gyroid specimens.

Experimental Results	*Relative Density*		
	16,7%	26,1%	35%
Effective Young Modulus	2708 MPa	2804 MPa	2928 MPa
Compressive Yield Strength	30,08 MPa	43,17 MPa	63,49 MPa
Max. Force	2305 N	7177 N	17415 N

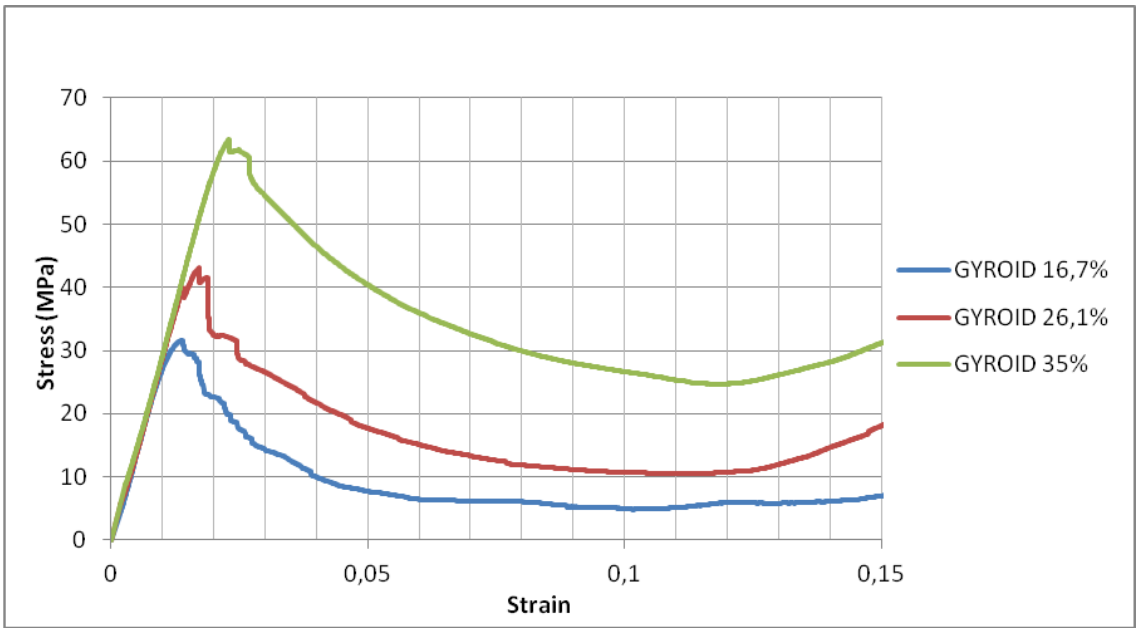

Fig. 49. Stress to Strain diagram for Gyroid specimens.

Gyroid-shaped specimens exhibit a very smooth elastic branch (straight line) and reach the yield point of the structure, irrespective of their relative density. At the same time, their maximum strength is large enough for their size and relative density.

In the plastic deformation branch, beyond the yield point of the structure, the behavior of the specimens is the expected from the literature for this type of structure. That is, after the yield point of the structure the material softens (post-softening) and then withstands much smaller loads. Finally, after a deformation point, the densification of the material begins.

Schwarz Diamond:

The Schwarz Diamond structure is characterized by many studies in the literature the strongest structure between lattice and TPMS structures. A validated conclusion, that can be drawn from this study as well as from the experimental results presented below.

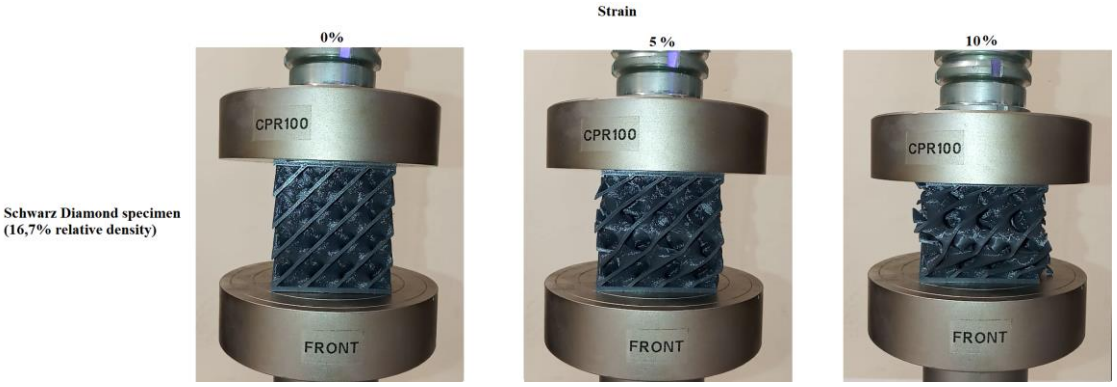

Fig. 50. Deformation of Schwarz Diamond specimen with 16,7% relative density.

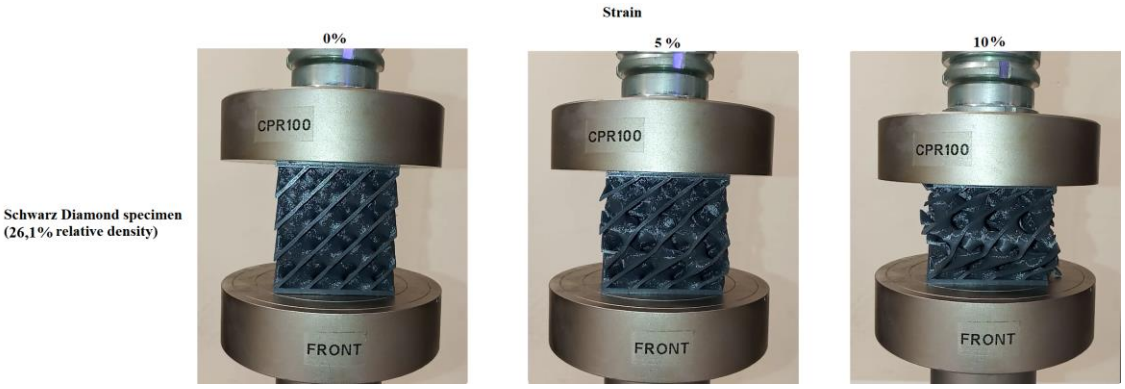

Fig. 51. Deformation of Schwarz Diamond specimen with 26,1% relative density.

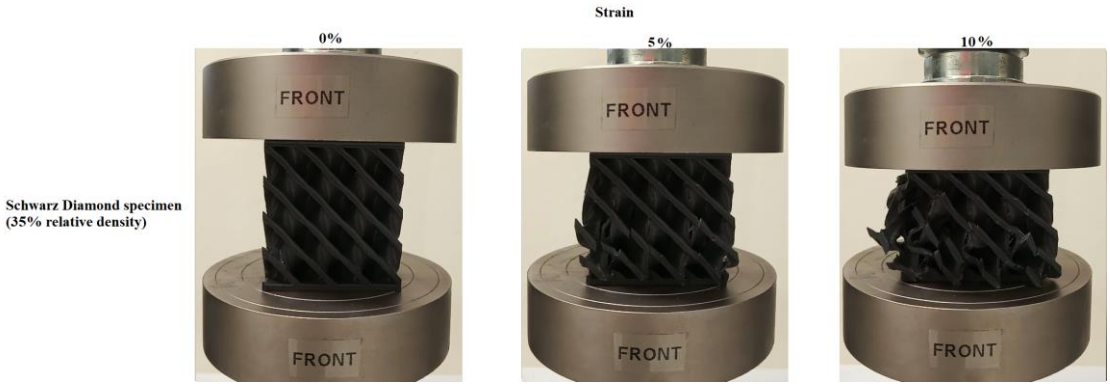

Fig. 52. Deformation of Schwarz Diamond specimen with 35% relative density.

The images above show the way in which the Schwarz Diamond structure receive the applied forces. The shear stresses in these structures are more intense than in Gyroid but are not capable of leading to immediate failure of the specimen. The failure of these specimens occurs when the columns of the structures are subjected to high bending stress due to the pressure, and eventually the fracture of the specimen begins.

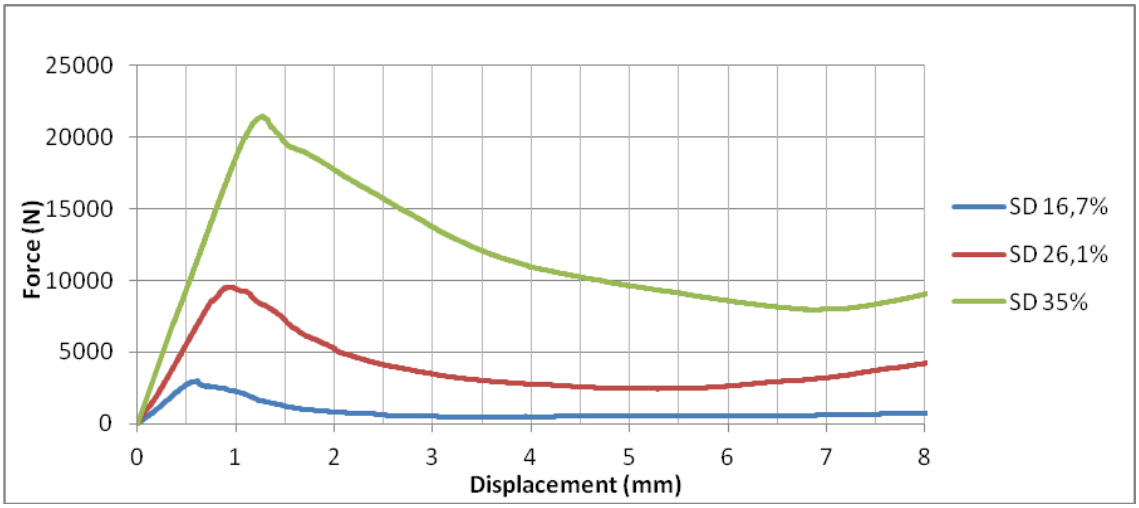

Fig. 53. Force to Displacement diagram for Schwarz Diamond specimens.

Table 7. Experimental Mechanical Properties of Schwarz Diamond specimens.

Experimental Results	*Relative Density*		
	16,7%	26,1%	35%
Effective Young Modulus	2624 MPa	2685 MPa	2896 MPa
Compressive Yield Strength	26,65 MPa	43,70 MPa	61,42 MPa
Max. Force	2981 N	9554 N	21504 N

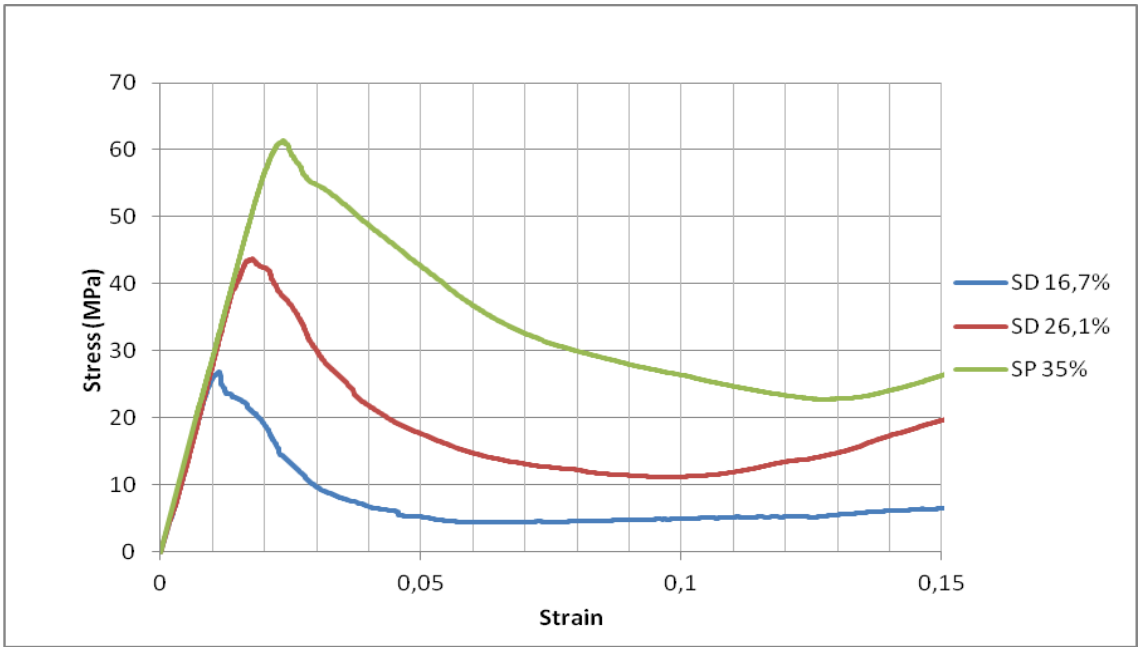

Fig. 54. Stress to Strain diagram for Schwarz Diamond specimens.

From the above results, it is concluded that the behavior of the specimens with Schwarz Diamond structure is similar to that of the specimens with Gyroid structure in both the elastic and plastic deformation branches. That is, very smooth elastic branch and post-softening effect after the yield point. However, these specimens can handle much larger forces, which means that the Schwarz Diamond structure provides more surface area for the applied force to diffuse.

3.3.3. Finite Element Analysis

The specimens with lattice structures, which were tested experimentally in the previous section, are examined in this section through a finite element analysis (FEA). It is worth noting that the analysis of finite elements for these specimens focuses mainly on the elastic branch of strees/strain diagram and the yield point.

In particular, ANSYS 19.2 Academic software was used for the analysis of finite element. As stated in a previous chapter, the 3D design of the geometry of the specimens was developed through the ANSYS's module called SpaceClaim. The Static Structural module was also used for the finite element analysis. The calculating mesh consists of a tetrahedrals for the lattice structure and a hexahedral for the upper and lower plates. As you can see in the pictures above,the structure of the mesh is fine enough.

The module Static Structural is a reliable tool for studying phenomena that do not result in rapid destruction of the specimens. For this reason, this study is used here to study mainly the elastic branches of the specimen's deformation and to identify the yield point. The model used to simulate printing material (PLA) is a combination of isotropic elasticity and bilinear isotropic hardening. This means that the plastic deformation branch is only simulated for the first small displacements from the yield point. The reason for this approach is that trying to simulate the whole plastic deformation branch would require a great amount of computational power and would be time consuming for this thesis. The following are the results of the specimens for each lattice structure extracted through finite element analysis.

Schwarz Primitive:

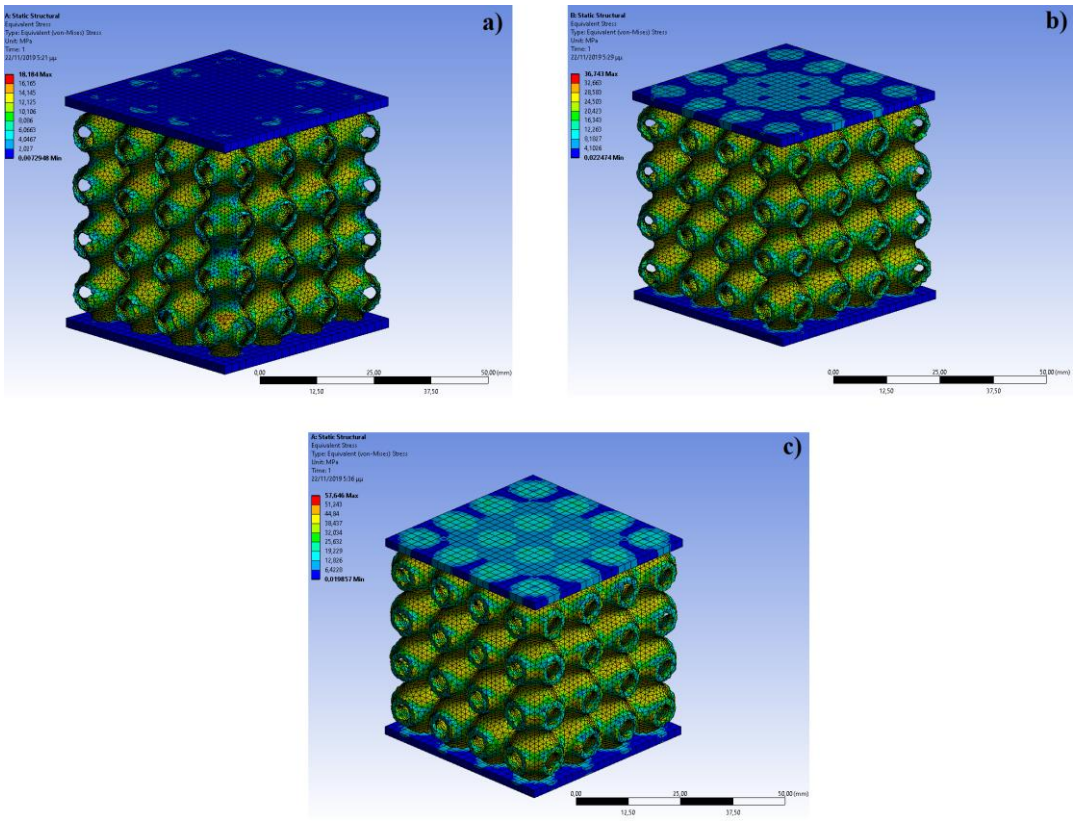

Fig. 55. Maximum Stresses for Schwarz Primitive specimens (a:16,7%, b:26,1%, c:35%)

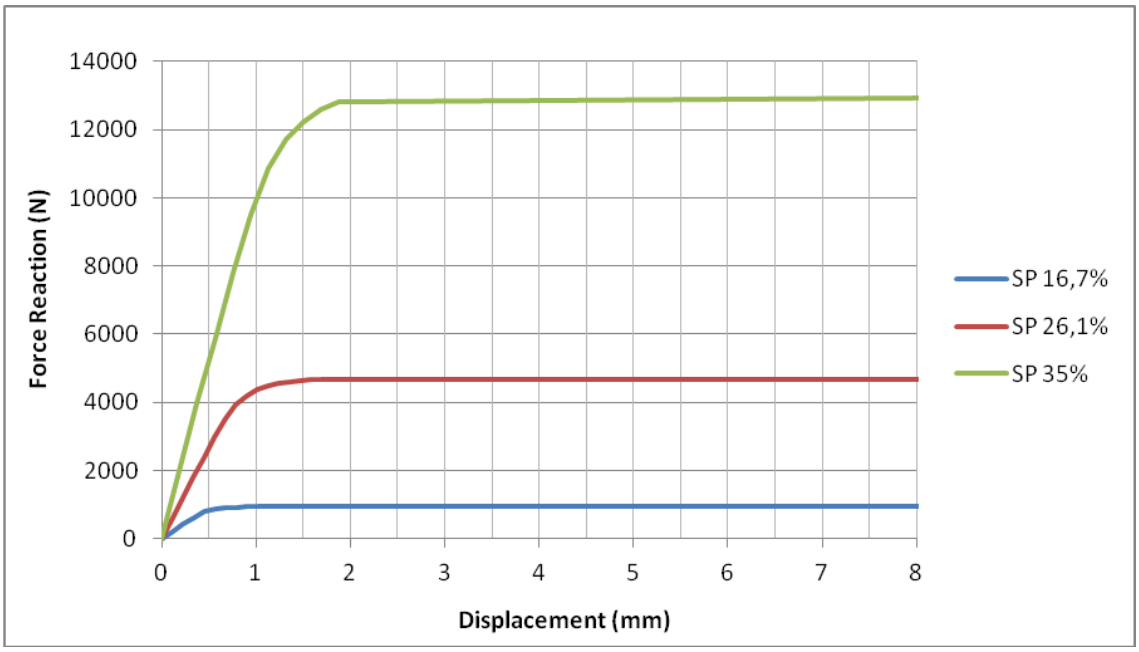

Fig. 56. Force Reaction to Displacement diagram for Schwarz Primitive specimens (FEA).

Table 8. FEA Mechanical Properties of Schwarz Primitive specimens.

FEA Results	*Relative Density*		
	16,7%	26,1%	35%
Compressive Yield Strength	18,18 MPa	36,74 MPa	57,65 MPa
Max. Force	940,5 N	4677 N	12577 N

The results of finite element analysis for Schwarz Primitive structures are presented above. As expected, the greater concentration of stresses occurs in the lattice structure, and in particular at points where there is maximum curvature of each unit cells of the structure. These points would be the region which fracture would begin.

Gyroid:

The results of the finite element analysis, which are listed below, show that the highest concentration of stresses is observed at the center of the specimen. Specifically, because Gyroid as a triply periodic minimal surface has highly curved surfaces especially at the boundary of each unit cell, these are the regions where stresses are concentrated and where Gyroid specimen's failure is expected to start.

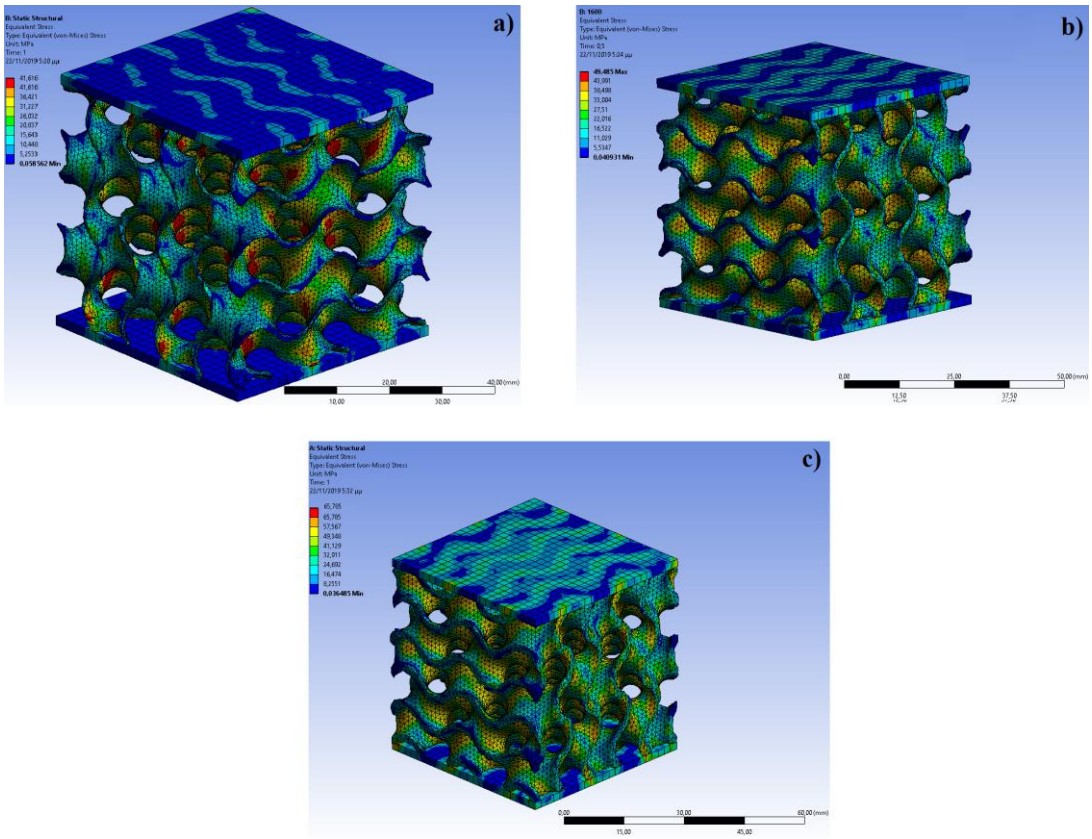

Fig. 57. Maximum Stresses for Gyroid specimens (a:16,7%, b:26,1%, c:35%).

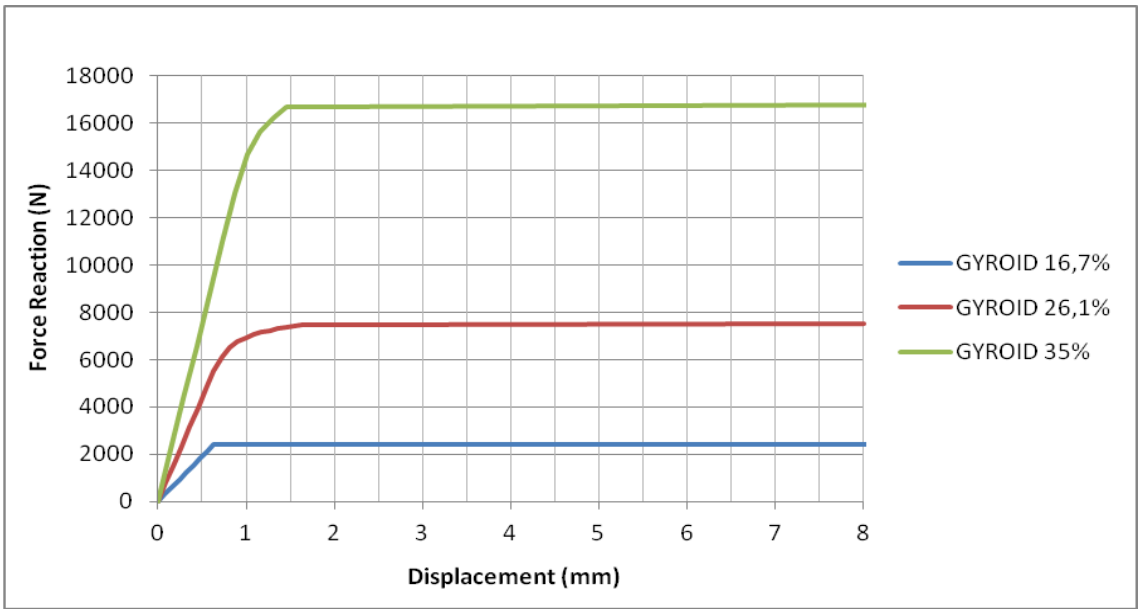

Fig. 58. Force Reaction to Displacement diagram for Gyroid specimens (FEA).

Table 9. FEA Mechanical Properties of Gyroid specimens.

FEA Results	*Relative Density*		
	16,7%	26,1%	35%
Compressive Yield Strength	36,42 MPa	43,99 MPa	65,79 MPa
Max. Force	2410 N	7450 N	16800 N

Schwarz Diamond:

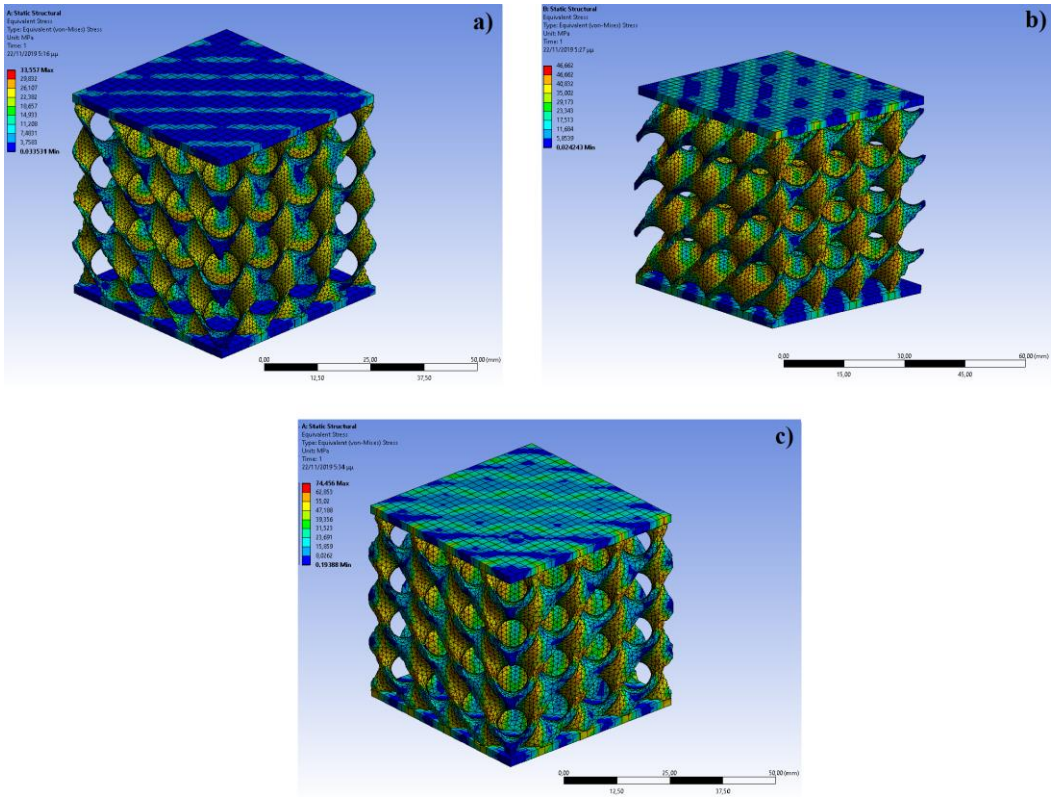

Fig. 59. Maximum Stresses for Schwarz Diamond specimens (a:16,7%, b:26,1%, c:35%).

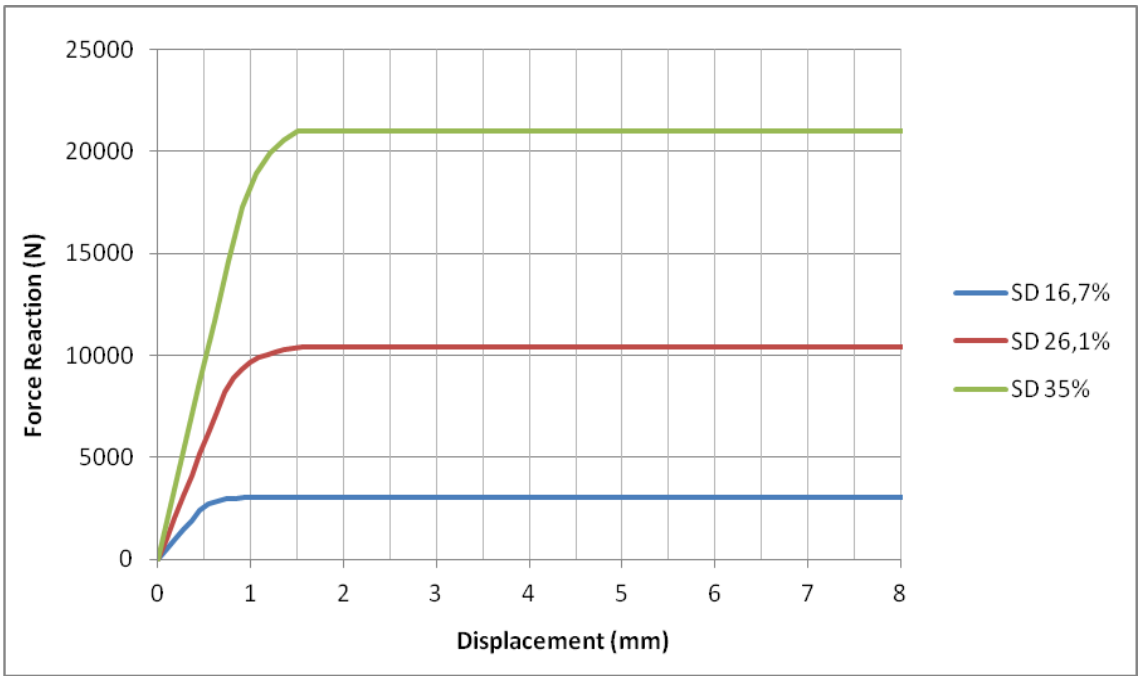

Fig. 60. Force Reaction to Displacement diagram for Schwarz Diamond specimens (FEA).

Table 10. FEA Mechanical Properties of Schwarz Diamond specimens.

FEA Results	*Relative Density*		
	16,7%	26,1%	35%
Compressive Yield Strength	29,83 MPa	46,66 MPa	62,85 MPa
Max. Force	3006 N	10400 N	21488 N

The above results of finite element analysis show that during the compressive loading of Schwarz Diamond specimens, columns are formed within the lattice structure that accumulates most of the stresses. It is these columns that give the structural strength to the specimens and they handle all the stresses that are received upon the specimens. Once these columns reach their yield points then the catastrophic failure of the specimens begins.

3.3.4. Comparison and Conclusions

In summary, the experimental results and the results from the finite element analysis would be compared and the main conclusions regarding the compressive loading of TPMS structures (Schwarz Primitive, Gyroid and Schwarz Diamond) would be extracted. Furthermore, lattice structures are compared in this section and with each other to determine which structure has better performance in compressive stresses.

Comparison

- For Gyroid lattice structure:

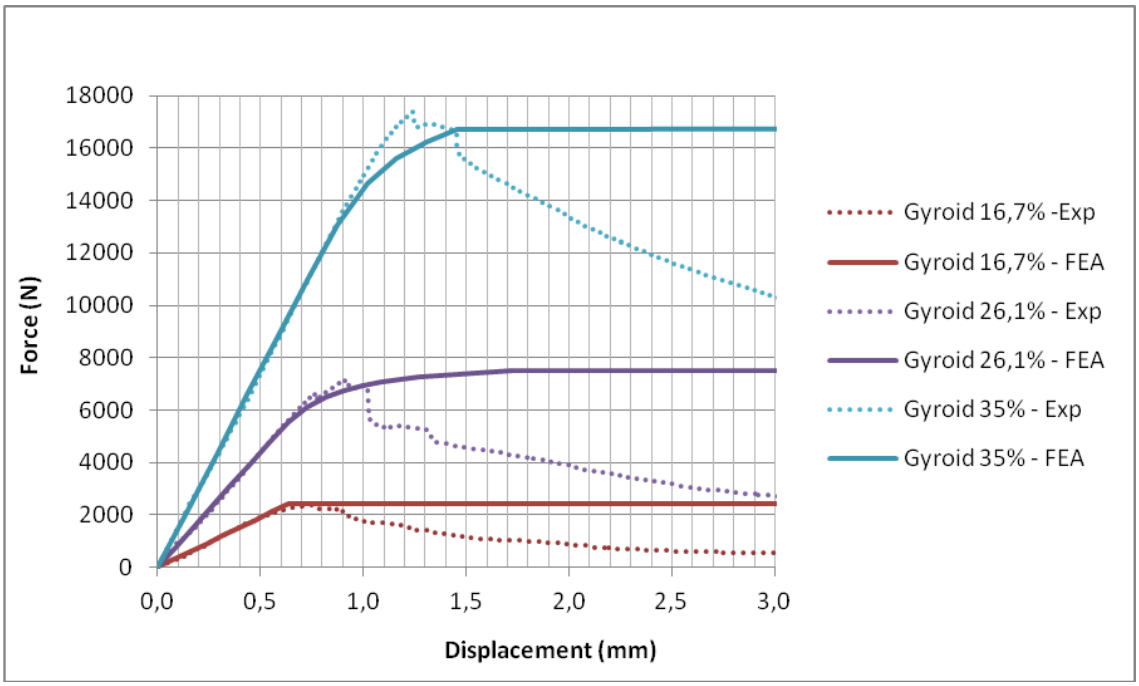

Fig. 61. Force Reaction to Displacement comparison diagram for Gyroid specimens.

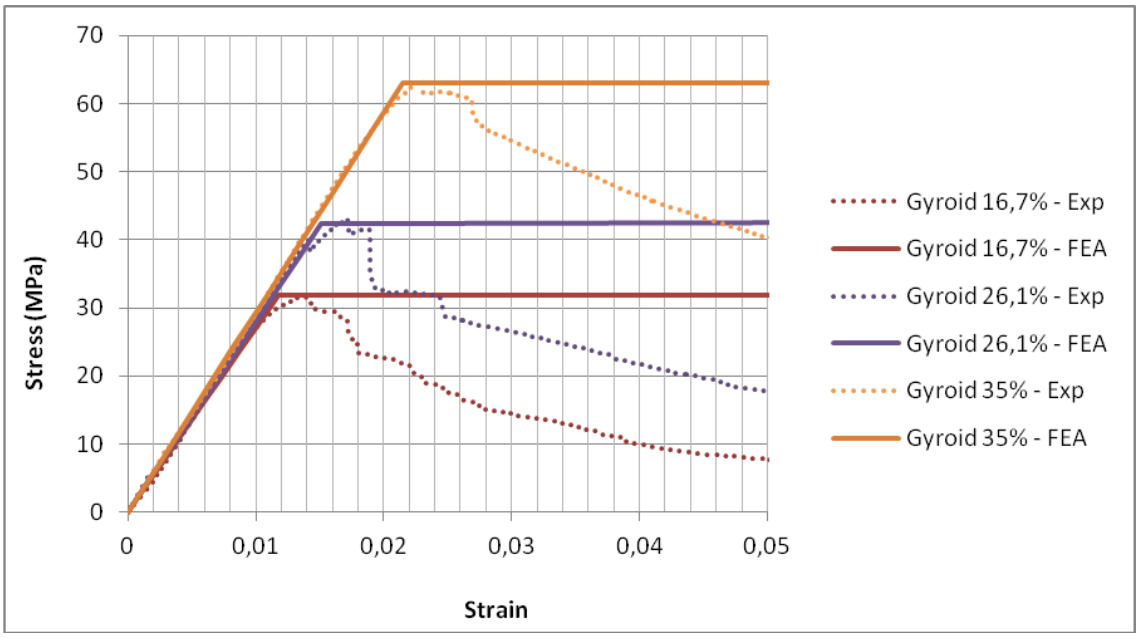

Fig. 62. Stress to Strain comparison diagram for Gyroid specimens.

The comparison of the above data shows that the theoretical approach (FEA) and the practical approach (Experiments) have a slight divergence in both force values and stress values. Obviously in the experimental specimen's plastic deformation occurs earlier and the mechanical strength is lower. This is most likely due to defects in the manufacturing of the specimens (3D Printing).

- For Schwarz Diamond lattice structure:

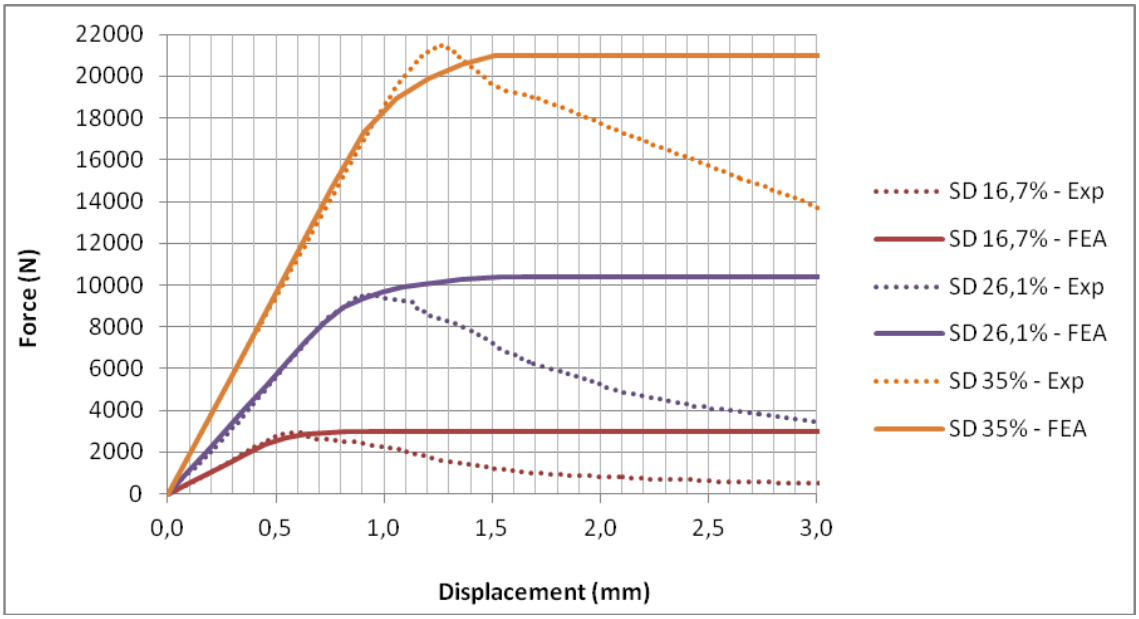

Fig. 63. Force Reaction to Displacement comparison diagram for Schwarz Diamond specimens.

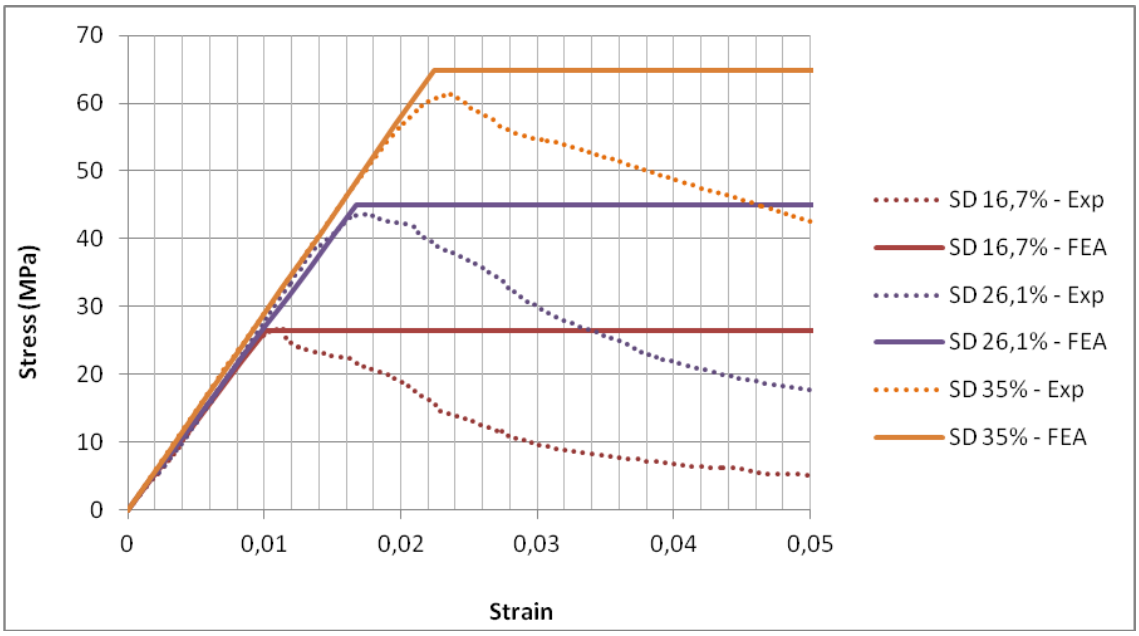

Fig. 64. Stress to Strain comparison diagram for Schwarz Diamond specimens.

The conclusions of comparing the results of the experiments and the finite elements analysis are similar to those of the Gyroid structure. The only difference is that the Schwarz Diamond structure has a slightly more intense difference between the experimental and the theoretical model. However, these deviations are relatively small.

- For Schwarz Primitive lattice structure:

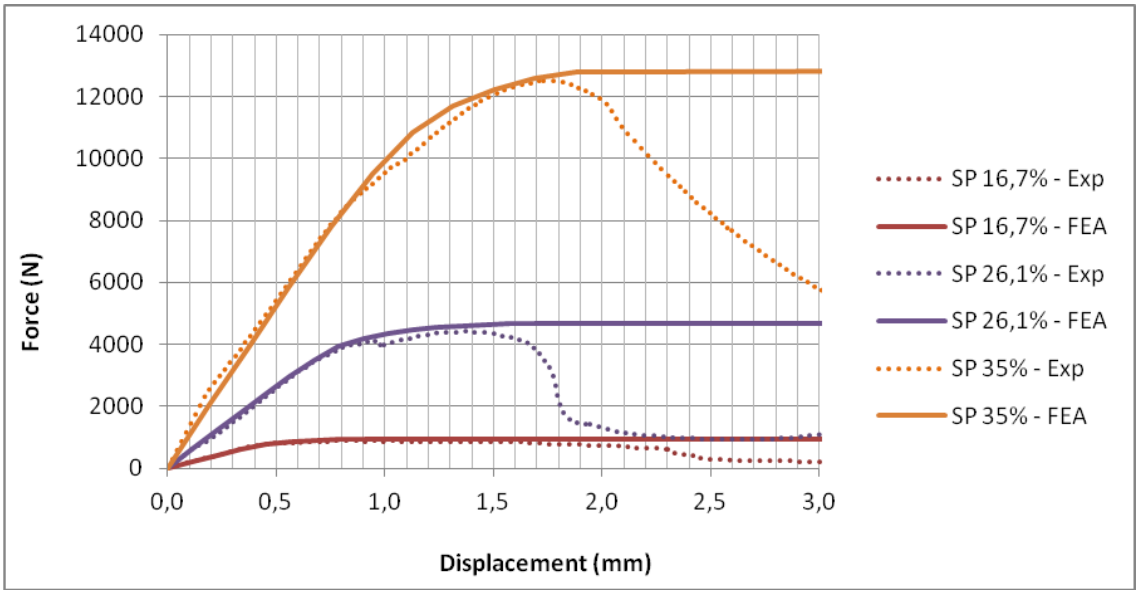

Fig. 65. Force Reaction to Displacement comparison diagram for Schwarz Primitive specimens.

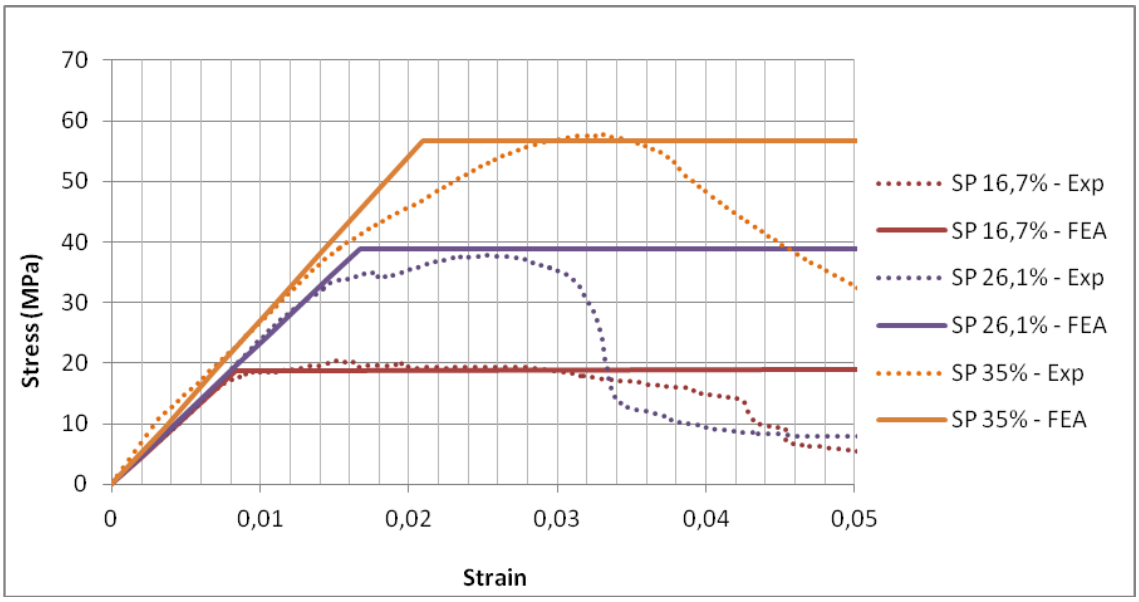

Fig. 66. Stress to Strain comparison diagram for Schwarz Primitive specimens.

Schwarz Primitive specimen's FEA results are similar to the results of experiments on the elastic branch stress-strain diagram. Moreover, because this particular lattice structure, during compressive loading and after passing the yield point, creates a plateua, the finite element analysis produces similar results to those of the experiments in the early stages of plastic deformation. Thus, up to 4% of the strain, the two results of the studies (experimental and FEA) almost coincide.

- Deviation of Mechanical Properties:

It is a fact that the mechanical properties of 3D printed parts are different from the mechanical properties [30] of the same pieces if were manufactured with a traditional way (e.g. injection molding). This difference is further increased when the part contains lattice structures. The lattice structures have a low relative density and the phenomenon of size effect becomes apparent which reduces the mechanical properties of the material.

First of all, as far as 3D printing is concerned, there is a plethora of literature that demonstrates through experiments the changes in mechanical properties depending on the printing parameters. The printing parameters that most affect the mechanical properties of the parts are the thickness of each layer, the printing orientation and the random defects of the printing process (in all manufacturing processes there some defects).

The other important factor affecting the mechanical properties of the produced part is the size effect. The size effect strongly reduces all the mechanical properties of a structure with an exponential relation to the relative density. Therefore, the lower the relative density of the structure is the weaker its mechanical properties (e.g. metal foams). Below is the equation through which the mechanical properties change relative to the relative density.

$$\Phi = C \cdot \Phi_s \cdot \rho_r^n$$

Where Φ is the property of interest (mechanical property of lattice), Φ_s is the same property of the solid material, ρ_r is the relative density of specimen (for ρ_r<0,3 the size effect become more intense) and C and n are the fitting parameters of size effect. The fitting parameters are influenced by the size, thickness, distribution and shape of the unit cells of each lattice structure. In summary, size effect is a phenomenon that adversely affects the integrity of a structure.

The mechanical properties of the structures studied in this thesis were influenced by both 3D printing and size effect. The first concern was to limit the size effect, so for the lattice structures, selected the size and thickness of the unit cells were large compared to the whole structure. Solid parts were also used in the structure to enhance the mechanical properties (upper and lower plates). In order to minimize the 3D printing affect in mechanical properties, the smallest available nozzle was used for 3D printing to achieve the minimum layer thickness. An attempt was also made to find the optimum print orientation, always keeping in mind the limitations of the FDM printing technique and the complexity of the TPMS surfaces.

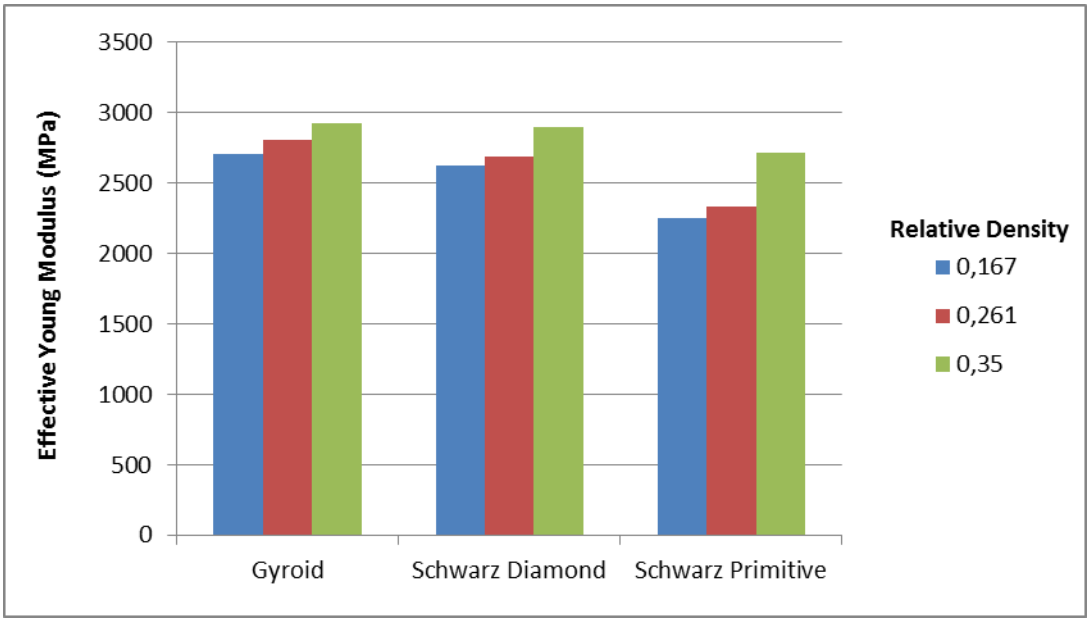

Fig. 67. Effective Young Modulus comparison diagram for each specimen.

However, as can be seen in the results, the mechanical properties, which were studied in this thesis (Effective Young Modulus and Compressive Yield Strength), are lower than the mechanical properties of the raw material, due to the reasons mentioned above. It is important to note that as the relative density decreases, so does the mechanical properties of the structure, which is caused by size effect. However, the influence of size effect on these structures is relatively small compared with literature.

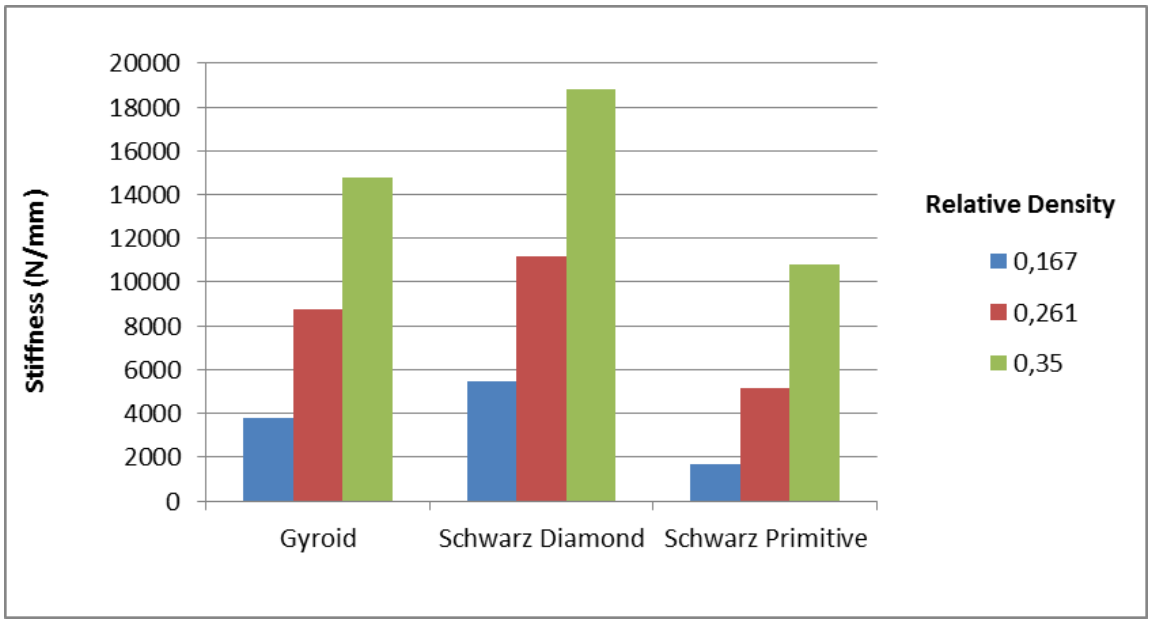

Fig. 68. Stiffness comparison diagram for each specimen.

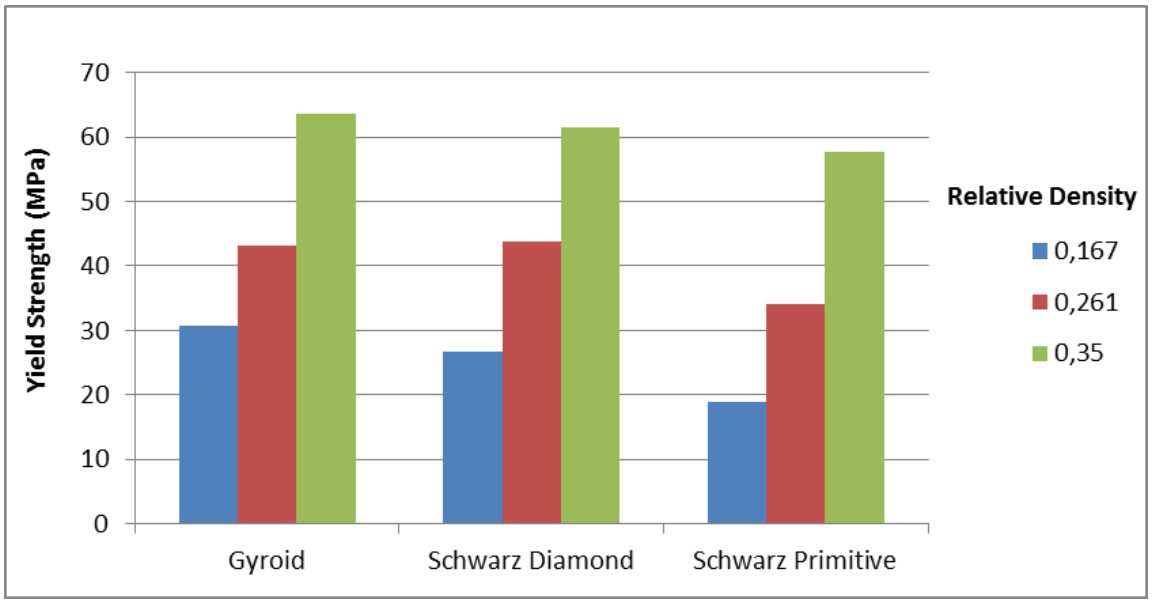

Fig. 69. Compressive Yield Strength comparison diagram for each specimen.

Conclusions

This thesis investigated the mechanical behavior of three lattice structures belonging to the family of triply periodic minimal surfaces, the Gyroid, the Schwarz Diamond and the Schwarz Primitive. The mechanical behavior of these structures was studied under the influence of compressive loads both through conducting experiments and through finite element analysis. Below, the conclusions are presented for each structure.

- *Schwarz Primitive:*

This is the lattice structure having the smallest structural strength of the 3. This is the lattice structure which is most affected by the size effect, which significantly reduces the strength of the material. This structure exhibits strong shear stresses resulting in diagonal failure of the specimens. Also, the maximum stress concentration appears in the maximum unit cell curvature. However, after the pass of the structure's yield point, it continues to withstand high loads due to the failure of individual unit cells and not the overall structure. This is also the most interesting element of this structure as it results in high energy absorption, which will be discussed in the next section.

- *Gyroid:*

The most widespread of TPMS geometries, with very good performance in both stiffness and structural strength is the Gyroid structure. The size effect in this structure is relatively small, so the integrity of the material is not greatly affected. Indicatively, it has the highest effective yield strength of the three structures that were studied. However, the particular structure in each unit cell has regions with a very large radius of curvature. These areas are located at the unit cell's boundaries or in the areas where unit cells join, and thus away from the support points. This makes, these areas very vulnerable as they accumulate high stresses, resulting in a total failure of the overall structure as soon as the loads exceed the yield point.

- *Schwarz Diamond:*

It is the structure that withstands the greatest compressive force of the three structures that were studied. Each unit cell of this structure is designed and positioned so that no stress concentration points can be created which can lead to failure. Also, the unique positioning of the unit cells creates columns that are full with material. The columns handle all the loads the construction receives and distribute them throughout the construction. This results in a better overall performance of the structure and greater strength. However, when these columns reach their yield points then all construction fails and leads to destruction.

In conclusion, the Schwarz Diamond lattice structure is the structure with the best mechanical behavior with a relatively small difference from Gyroid. This does not mean that the other two TPMS structures are not significant as the findings appear promising for their applications in various fields.

3.4. Energy Absorption

3.4.1. Introduction

In the previous chapters the elastic and plastic mechanical behavior of the three lattice structures was studied and analyzed. Furthermore, results were obtained for the structural strength of each structure and the mechanisms, by which each structure leads to fracture, were presented. This chapter analyzes the energy absorption capacity during compressive loading of these structures as the lattice structures are renowned for the high amounts of energy absorbed therefore are used in applications such as packaging.

The energy absorption study of a structure is very important parameter and directly affects the possible applications that each structure could use to. For this reason, it is important to calculate the energy absorption due to the structures rather than the size of the test specimens. Therefore, it is necessary to calculate values that are independent of the dimensions of the specimens.

Metal cellular materials have a standard way of calculating energy absorption through ISO 13314: 2011 (Mechanical testing of metals - Ductility testing - Compression test for porous and cellular metals) [31]. However, since there is no corresponding standardization for the absorption of energy in plastic cellular materials, the methodology for calculating the energy absorption as in ISO 13314: 2011 is used.

This means that the energy absorption per volume of each structure during a compressive load is calculated by the equation:

$$W_v = \int_0^{\varepsilon_0} \sigma d\varepsilon$$

Where, W_v is the amount of energy absorption per volume (MJ/m^3), ε_0 is the maximum strain limit (which should be above the 50% and for this study the maximum strain limit is 15%), σ is the compressive stress (MPa or N/mm^2) and ε is the strain.

$$W_v = \int_0^{\varepsilon_{15\%}} \sigma d\varepsilon$$

Moreover, with the appropriate treatment of the above equation could be calculated the energy absorption per mass of each structure or else the specific energy absorption (SEA) W_m (kJ/kg). The necessary transformation for this calculation is (where ρ is the density of the construction material):

$$W_m = \frac{W_v}{\rho}$$

3.4.2. Energy Absorption's Results

Based on the above equations, it is understood that the energy absorption of each structure is inextricably linked to the surface areas below the stress-strain curves for each structure extracted by compressive loading experiments. For this reason, it is necessary to present the following comparative stress to strain diagrams for each structure and relative density.

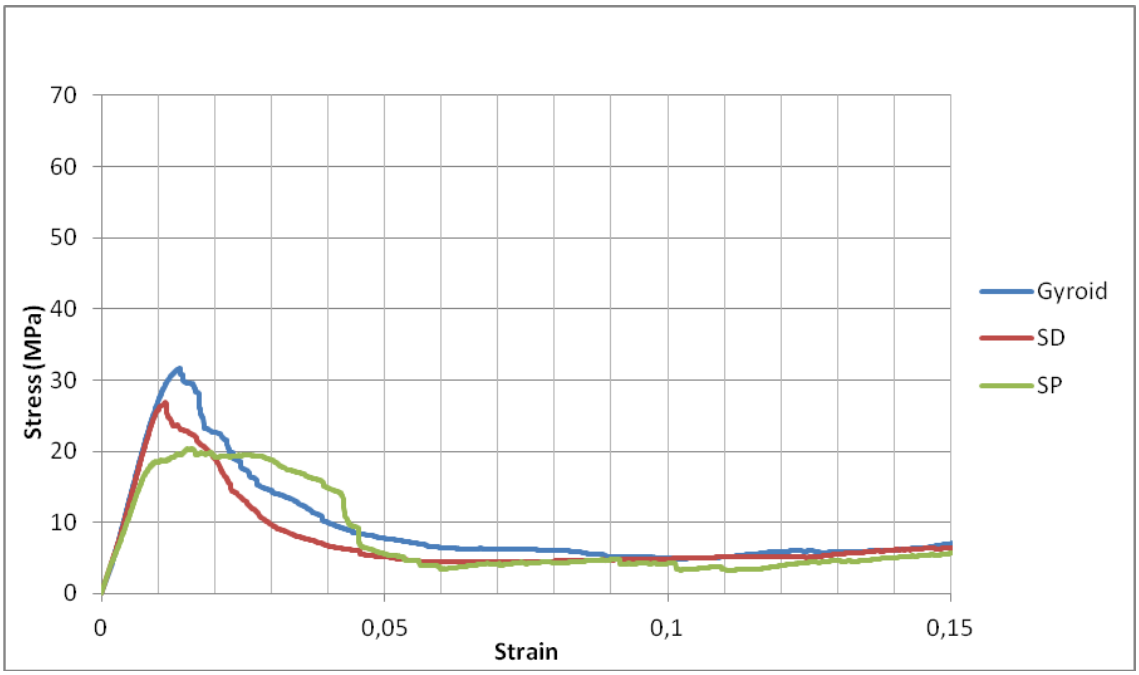

Fig. 70. Stress to Strain comparison diagram for all lattice Structure (ρ_r=16,7%).

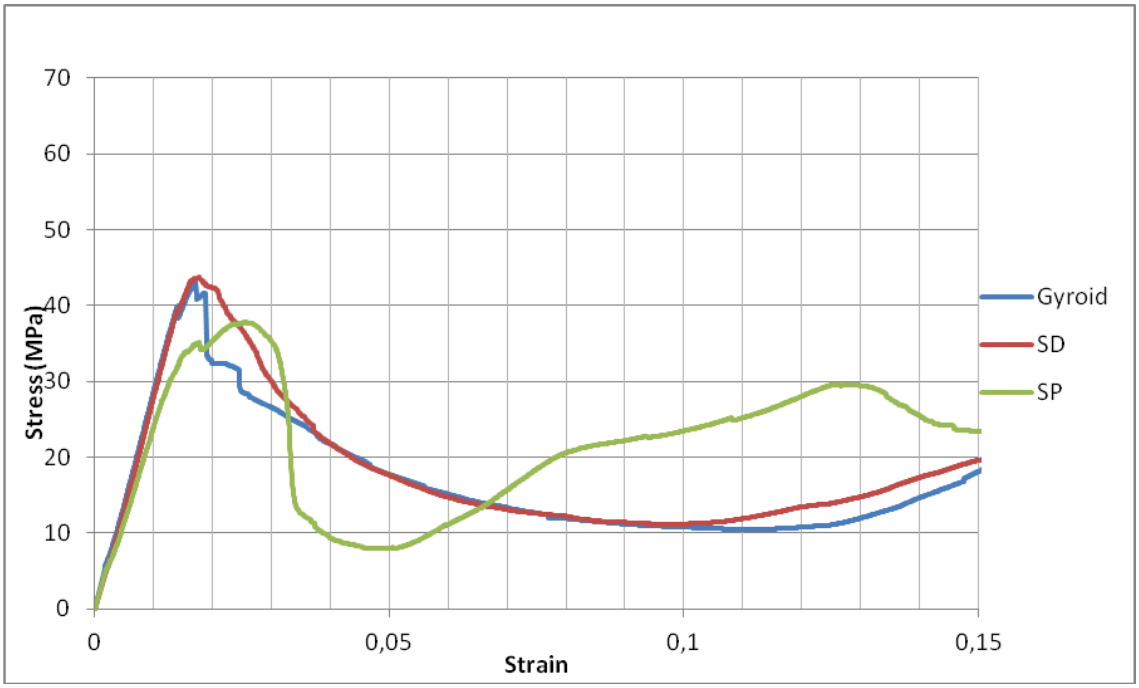

Fig. 71. Stress to Strain comparison diagram for all lattice Structure (ρ_r=26,1%).

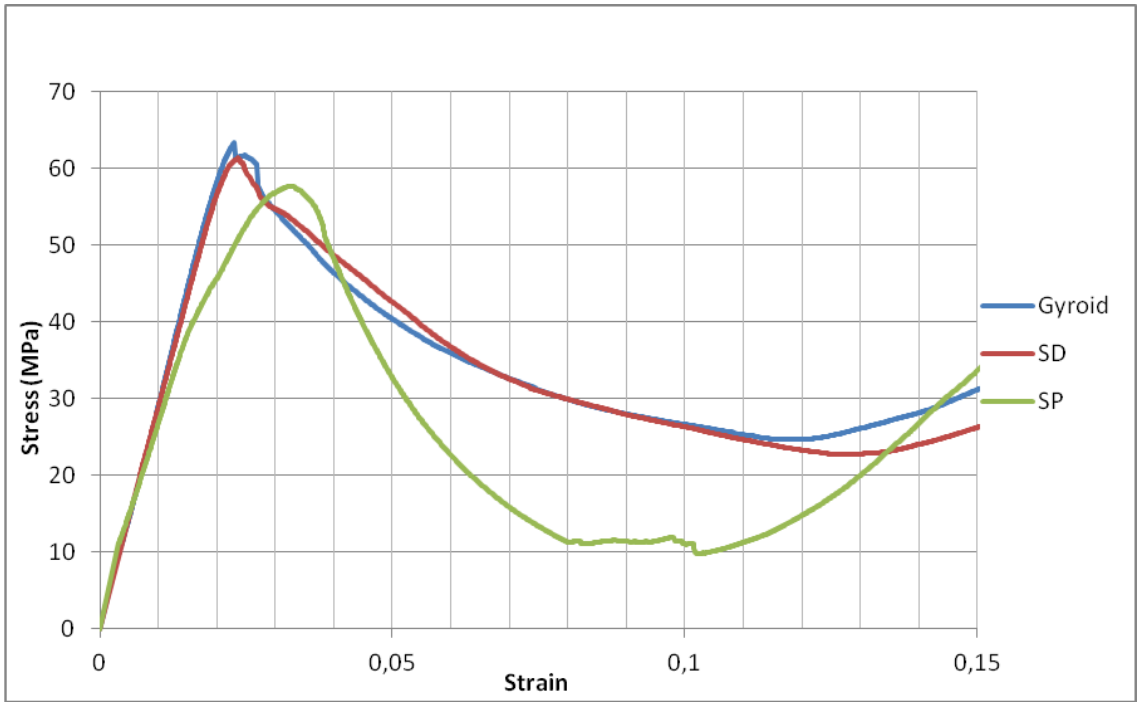

Fig. 72. Stress to Strain comparison diagram for all lattice Structure (ρ_r=35%).

Having the experimental stress-strain diagrams, the calculation of the energy absorption per volume for each lattice structure and for each relative density by numerically solving the equation for each structure is relatively easy.

The trapezoidal method was used for the numerical solution of the integral of the equations. More specifically, the following is a mathematical explanation of how the energy absorption value is calculated for each structure and relative density.

$$W_v = \int_0^{\varepsilon_{15\%}} \sigma d\varepsilon = \frac{1}{2}\left[\sigma(0) + 2\sigma(\varepsilon_1) + ... + \sigma(\varepsilon_{15\%})\right] \cdot \frac{1}{n}$$

Where, n is the number of experimental outputs which form the stress-strain chart. This number for the experiments that carried out in this study is around 3600, i.e. the 15% of the strain was given to the specimens in 3600 steps.

Comparative stress-strain diagrams show which lattice structures exhibit the highest energy absorption due to their surface area size. Nevertheless, the results of the numerical solution of the equations for energy absorption per unit volume and mass unit are shown below.

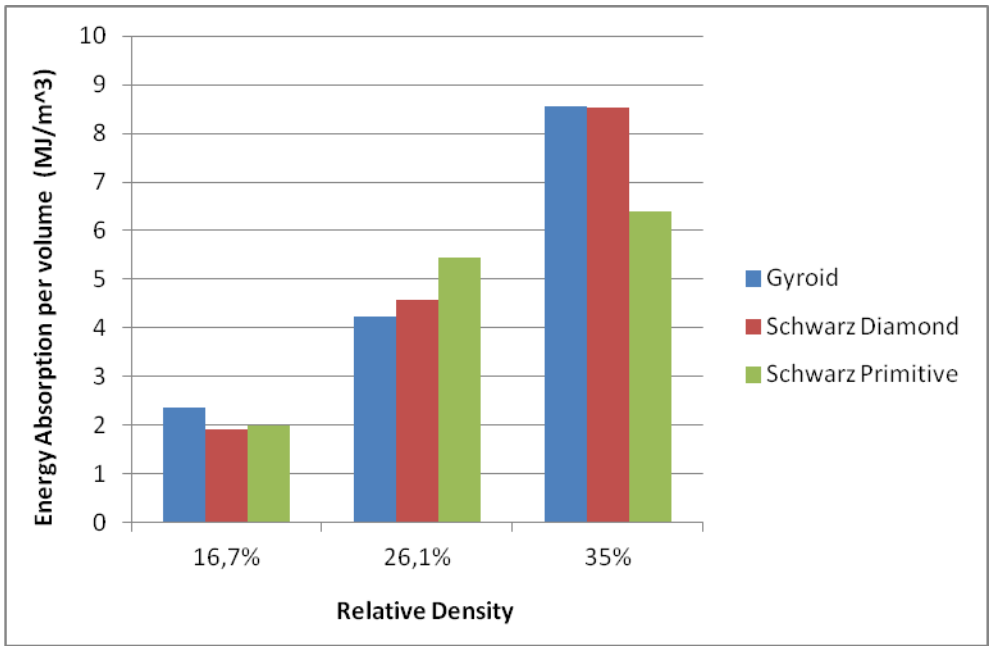

Fig. 73. Energy absorption per volume comparison between different lattice structures (up to 15% strain).

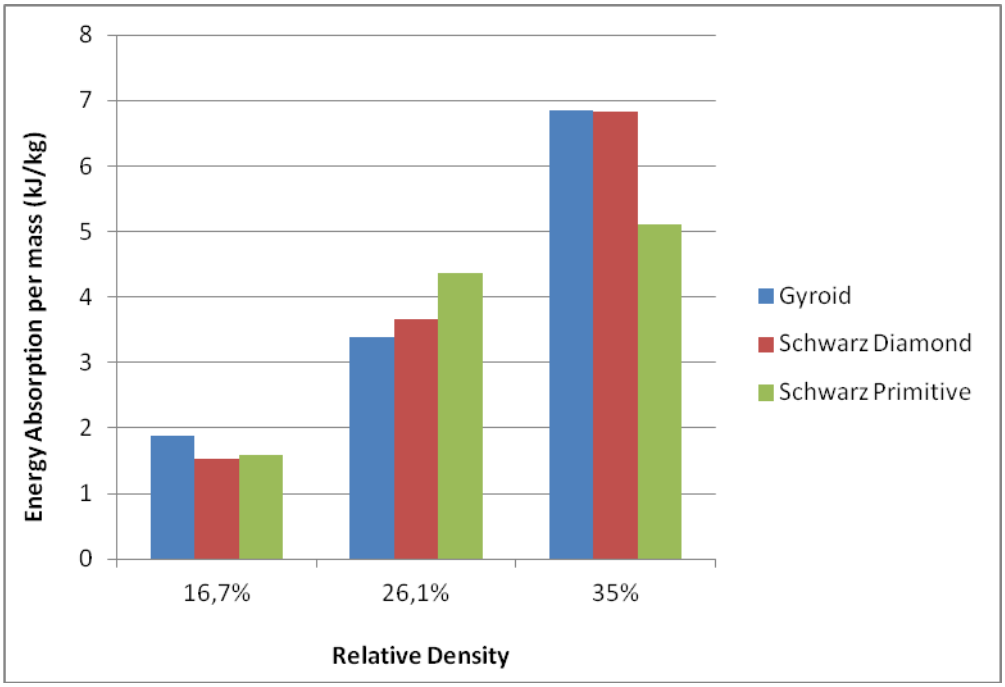

Fig. 74. Energy absorption per mass comparison between different lattice structures (up to 15% strain).

3.4.3. Conclusions

The numerical results for energy absorption per unit volume and per unit mass shown above and in combination with comparative stress to strain diagrams can be summarized into conclusions for each of the lattice structures. It is worth mentioning that energy absorption is measured up to 15% strain which means that the highest percentages of energy absorbed are from the elastic deformation branch.

- *Schwarz Diamond:*

This lattice structure has the best performance both in mechanical properties and in terms of energy absorption. It is worth noting that the specimens with Schwarz Diamond structure and relative density of 35% absorbs 8.53 MJ/m^3 for strain up to 15%. But also, in the other specimens with relative densities of 16.7% and 26.1% the energy absorption is in the same pattern with one difference due to the smaller loads on the specimens.

- *Gyroid:*

The lattice structure of Gyroid has the almost same results with the Schwarz Diamond structure for the largest amount of energy absorbed with 8.55 MJ/m^3 at a relative structure density of 35%. It also behaves similarly with the Schwarz Diamond structure in energy absorption pattern view, as most of the energy absorbed in both structures comes from the elastic branch and the height of the maximum loads.

- *Schwarz Primitive:*

The Schwarz Primitive structure exhibits interesting behaviour during energy absorption for two important reasons. The first reason is that it continues to absorb high amounts of energy after the yield point as it appears a plateau, as shown in the stress to strain chart. The second reason is that in the plastic deformation branch, and especially after 10% of the strain, the structure maintains its integrity due to the failure of specific unit cells and not of the whole structure, hence it continues to withstand high loads, in comparison with the maximum load , leading to high energy absorption. Thus, for this structure it claims that large amounts of energy are absorbed by the plastic deformation branch.

In conclusion, the Schwarz Diamond and Gyroid structures absorb the highest amount of energy. Moreover, they almost absorb the same amounts per unit volume and per unit mass mainly in the early stages of deformation (up to 5% of strain). However, the Schwarz Primitive structure can absorb smaller amounts of energy due to its lower strength, but there is a tendency to increase energy absorption during plastic deformation (after 10% of strain). This means that this structure can absorb much larger amounts of energy after the passing of its yield point. Hence, makes it suitable for use in applications where the destruction of part of the structure is certain, i.e. protection from impacts (high crashworthiness value).

CASE STUDY:
ADDITIVE MANUFACTURED SCAFFOLD WITH LATTICE INFILL

4.1. Introduction

In the context of this thesis, it was decided to study a possible application of the lattice structures, that where studied above, in order to achieve the optimal design of a product. The case study that was decided to be investigated is the design and fabrication of a customized additive manufactured scaffold for tissue engineering purposes.

First of all, it is necessary to explain what scaffolds are and how they are used in tissue engineering. Until now, when a human tissue (e.g. bone) was destroyed or in need of repair, artificial metal blades were positioned in such position the damaged tissue that it could regenerate and repair itself. In recent years, however, a technique called tissue engineering has been used in these cases. Tissue engineering technique works as follows; it is using a porous scaffold that acts as a template for regeneration of the bone's tissue. In addition to porous scaffolds, they must have enough structural strength as they maintain the continuity of the bone's tissue and receive all the loads that the bone receives. Still, scaffolds must be biocompatible with the human body so as not to lead to rejection [32-33].

This research proposes a combination of two techniques (tissue engineering and additive manufacturing) to design a customized additive manufactured scaffold with advanced lattice internal structure (TPMS structure). As a construction material, like in the experiments, the PLA was chosen, which is one of the most biocompatible plastics.

In particular, the case study examines the placement and function of customized scaffolds on the femur bone of the human body. The femur bone is selected as it is the longest bone of the human body and is one of the structural bones of the skeleton that manages the total weight of the human body. This makes it suitable for study and pilot application of customized additive manufactured scaffolds.

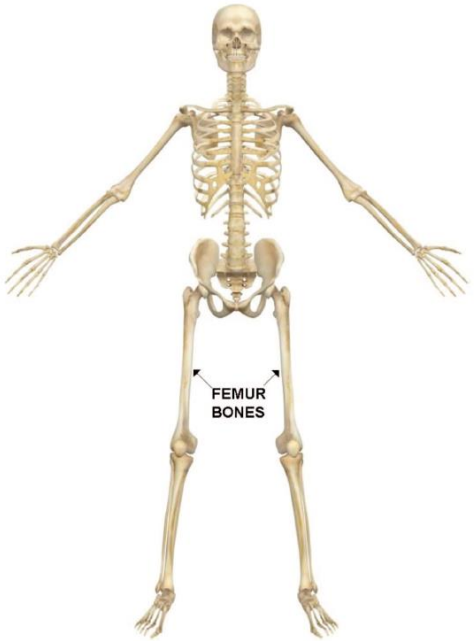

Fig. 75. Human Skeleton

4.2. Design and Fabrication of a Scaffold

The case study that is investigated is the placement of customized additive manufactured scaffold in order to replace and repair a damage or destruction at a specific region in the femur bone. The design and fabrication process are as follows.

First of all, the exact geometry of the bone to be repaired must be in a 3D CAD file. This can be done with modern scanning techniques such as CT scans and X-RAY scans. These scanning techniques are high-accuracy techniques, they can scan internal geometries and they do not require contact with the object (which is necessary for tissues within living organisms). For the purposes of this thesis, a 3D CAD of femur bone was selected from a 3D CAD library for which CT scans and Coordinate Measuring Machine techniques were used and belonged to an adult human with weight of 85kg (more details in Appendix IV).

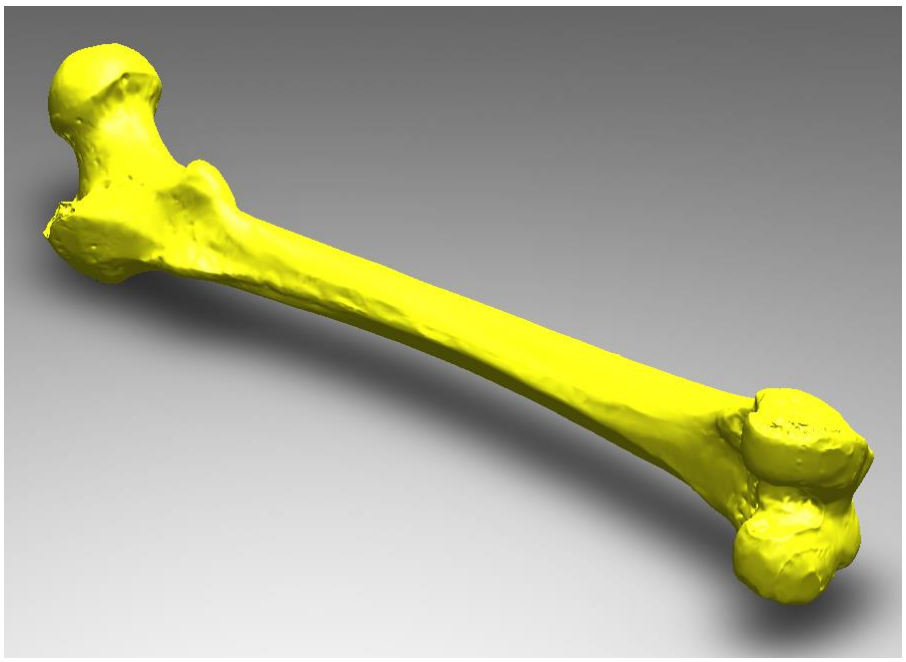

Fig. 76. 3D CAD of Femur bone.

Then, having the overall femur bone's geometry in a 3D CAD file, failure is detected (fracture). Immediately afterwards, it is done a straight cut and the area to be replaced is removed. The next step is to create a second solid body (except for the bone) where the gap will be filled and in essence this is the region where the scaffold will be placed. This created body combines many continuous cross sections of the bone's geometry with the loft command, so that the designed scaffold follows the geometry of the bone. Therefore, a different solid body is created that completes the bone.

Fig. 77. 3D CAD of Femur bone with the region where the scaffold would be placed.

After the extraction of the scaffold solid geometry, follows the creation of an internal structure with a lattice structure. In particular, following the results of the experiments in Chapter 3, it was decided to select the Schwarz Diamond structure with a relative density of 30% (for the lattice structure) as an internal lattice structure. This choice was made because the Schwarz Diamond structure exhibits the best performance in mechanical properties as well as in terms of energy absorption in the elastic region, that is, before the fracture (yield point).

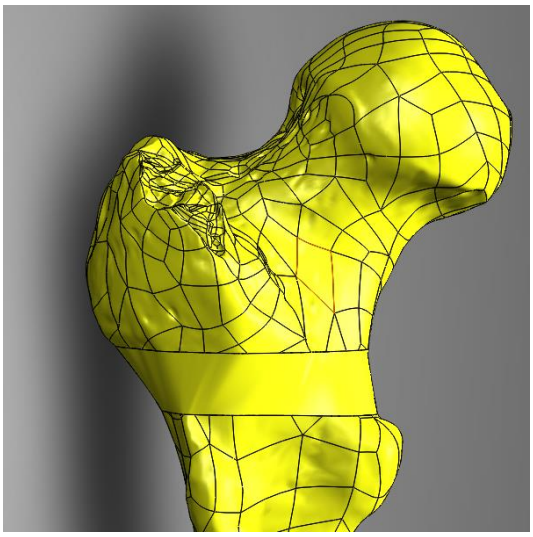

Fig. 78. Femur bone with the scaffold.

As in Chapter 3, the SpaceClaim software of the ANSYS platform was used to create the lattice structure. As control variables of geometry, length and thickness, 5.1mm and 2mm were chosen respectively, so as to be the relative density of the lattice structure 30%. Also, the scaffold's walls were selected in 2mm thickness so that the scaffold's material was evenly distributed.

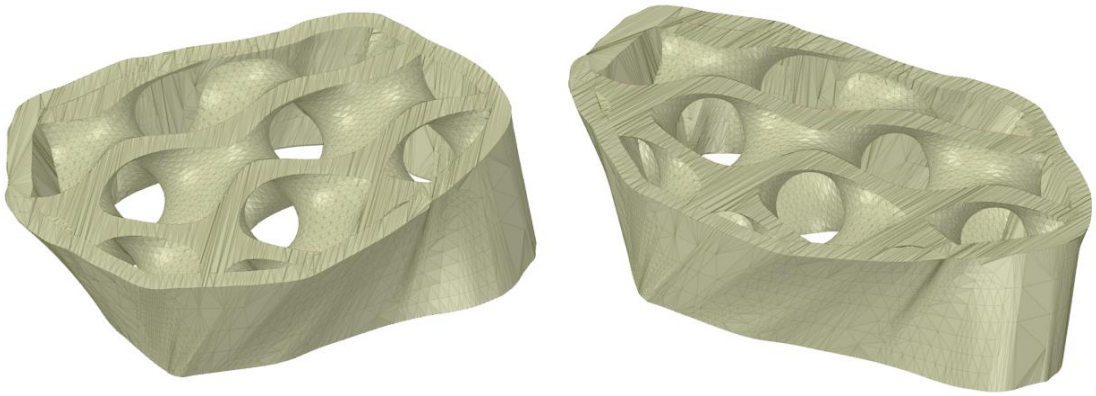

Fig. 79. Final 3D CAD geometry of scaffold with Schwarz Diamond structure.

Fig. 80. 3D printed PLA scaffold with FDM technique.

The same raw material (PLA filament) and 3D printer (FDM), used in Chapter 3, were used for scaffold's 3D printing. The print parameters are the same as the print parameters of the specimens and are listed in Table 1. The 3D printing, on a 1: 1 scale, of the scaffold took about 1 hour. The 3D printed scaffold had a weight of 8gr and a total relative density of ρ_r = 44.5%.

4.3. F.E.A. and Experimental Results

This section presents the results of finite element analysis as well as the experimental results on the amount of static loads this scaffold can handle. Subsequently, it is only through finite element analysis that the ability to withstand the product under normal operating conditions (in vivo) is examined.

- *Static load test:*

First of all, before testing the 3D printed scaffold on the application it must be verified, both through finite element analysis and experimentation, that it will have similar mechanical behavior to the corresponding structure in Chapter 3.

Thus, a static finite element analysis is first performed having as mechanical parameters of the structure the results obtained for the equivalent structure in chapter 3 (Young Modulus, Compressive Yield Strength etc). As in Chapter 3, finite element analysis is also performed in two branches, isotropic elasticity and bilinear isotropic hardening.

After extracting the results from the finite element analysis, a compression experiment is performed for the 3D printed scaffold shown above. The experimental setup is similar to the experiments in Chapter 3. While the experiment was conducted at a speed of 5mm / min. A force displacement chart was extracted during the experiment. This diagram was then compared to the corresponding diagram obtained from the finite element analysis and are displayed in figure below.

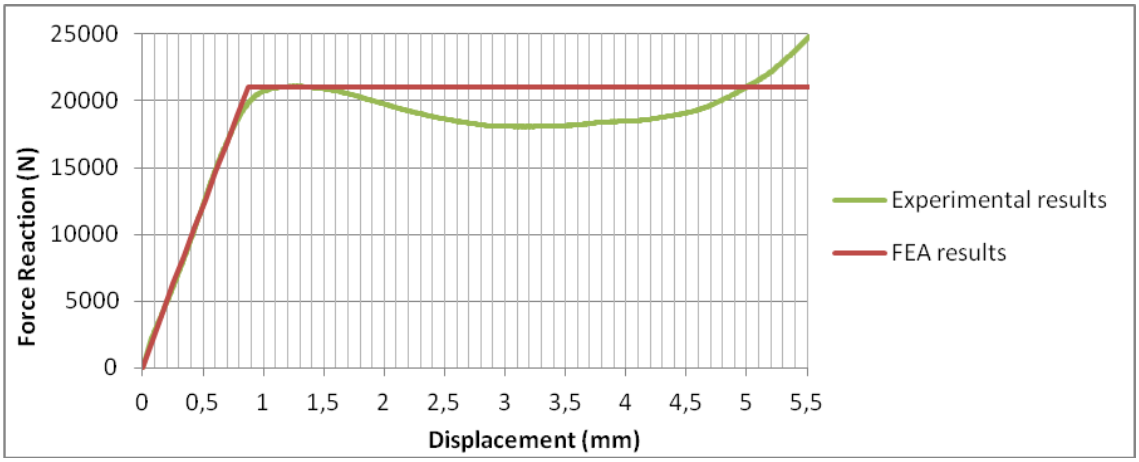

Fig. 81. Force displacement comparison chart for scaffold.

As shown in Figure 81, the results of the finite element analysis are very close to the experimental results, mainly for the elastic deformation branch but also for a significant portion of the plastic deformation branch. This fact confirms that the mechanical behavior of the structures can be reliably predicted. Furthermore, noteworthy is the mechanical strength of the scaffold in compression, which can handle force reaching 21.000N. In summary, since finite element analysis can produce reliable results and the scaffold appears to withstand large compressive loads (i.e., the type of loads that femur bone handles) it is necessary to perform finite element analysis to study and predict the actual mechanical behavior in application of 3D printed scaffold.

- *Real application test:*

In order to simulate the mechanical behavior of scaffold in real conditions, the entire femur bone in the simulation must be studied as well as examined under the influence of real loads both at nominal values and points of application.

First of all, some rational assumptions and simplifications have to be made in order to simplify the complex layout of the human body in that region. All assumptions come from the existing literature. Therefore, the femur bone is considered to have a fixed support in the knee joint for static loading. It also claims that all loads on this bone apply to the hip joint. The direction of the loads is usually the same as the weight as it will be seen below that all the loads are directly related to the weight of the patient.

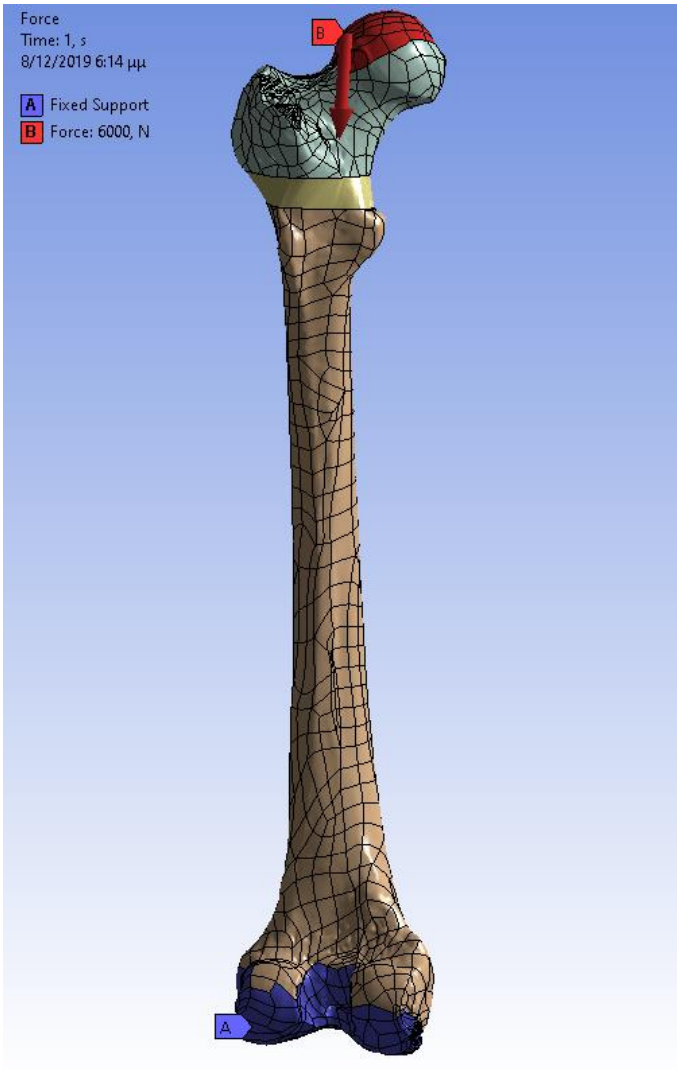

Fig. 82. Position of fixed support and force application on femur bone.

Once the assumptions and the boundary conditions of the simulations have been determined, the next step is to determine the nominal values of the loads that the hip joint accepts. These values are determined by the experimental results of Bergman et al. and are presented in the table below. It is worth remembering that the bone comes from a male person weighing 85kg [34-35-36].

Table 11. Loading for femur bone in different activities

Activity	Maximum load (% of body weight)	Maximum force (N)
Slow walking in flat surface	282	2350
Climbing upstairs	356	2970
Tripping	720	6000
Climbing downstairs	387	3230

Having shown the points of application of the force as well as the value of the maximum loads exerted on the femur bone, remains one last step before performing the finite element analysis. This step is to identify the mechanical properties of the bone in the existing literature. So according to the literature the femur bone has the mechanical properties shown in Table 11 [37].

Table 12. Mechanical Properties of femur bone.

Mechanical Properties	
Compressive Yield Strength	170 MPa
Young Modulus	17,6 GPa
Poisson Ratio	0,3
Density	2000 kg/m^3

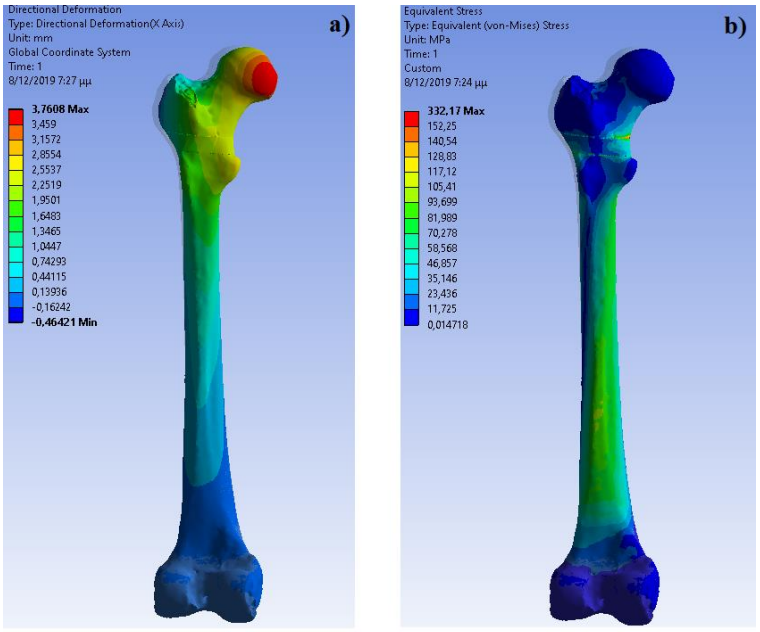

Fig. 83. Contour of (a) Directional Deformation and (b) Max. Equivalent Stress.

Table 13. Summary of Maximum overall Stress for Bone and Scaffold,

Loading (N)	Maximum Stress in femur bone (MPa)	Maximum Stress in scaffold (MPa)
1200	33,217	16,701
2400	66,434	33,402
3600	99,651	50,103
4800	132,87	66,804
6000	166,08	83,505

4.4. Conclusions

In this chapter a realistic application of lattice structures was studied. This application was the creation and installation of 3D printed scaffold for tissue engineering purposes. Consequently, a scaffold for femur bone made of PLA material was designed, manufactured and tested for the capability to handle compressive loads.

The first conclusion that can be drawn from the whole process is that with great ease and relatively little time it is possible, if there is the bone 3D geometry, to extract a customized scaffold via FDM printing technology. It is, thus possible to design and manufacture a customized scaffold for any patient in need at a low cost.

Another important conclusion from this case study is that through this particular lattice structure and the proper combination with a solid structure a scaffold can be extracted which is capable of withstanding loads much greater than the weight of the human body. This fact combined with the high biocompatibility and the porosity of the material makes it a capable and very promising candidate for the replacement of costly and time-consuming metal blades and scaffolds.

Finally, this chapter demonstrates the utility of lattice structures in a biomechanical application. However, these structures are suitable for a number of uses due to their high porosity, lightweight structure and the ability to not greatly affect the integrity of the mechanical properties of the material.

CONCLUSIONS

This dissertation explored the possibility of topology optimization of the design of a product using lattice structures and more specifically with structures belonging to the TPMS family (Gyroid, Schwarz Diamond and Schwarz Primitive). Moreover, with tools as the finite element analysis and the experiments, for additive manufactured structures, examined the mechanical behavior of each structure. The mechanical properties, that were studied, were the effective Young Modulus, the compressive yield strength and the amount of energy absorption. The conclusions for each structure are presented below.

- *Schwarz Primitive:*

The Schwarz Primitive structure which is most affected by the size effect, which significantly reduces the performance of mechanical behavior. Also, this structure exhibits strong shear stresses resulting in diagonal failure of the specimens. However, after the pass of the structure's yield point, it continues to withstand high loads due to the failure of individual unit cells and not the overall structure. Thus, the Schwarz Primitive structure exhibits interesting behavior in energy absorption terms. These reasons lead to large amount of absorbed energy in plastic deformation branch, which make this structure suitable for application such as protection from impacts.

- *Gyroid:*

The Gyroid structure has very good performance in both stiffness and structural strength. The integrity of the structure is not great affected by the size effect. The areas that are located at the unit cell's boundaries are the most vulnerable region of the structure. Hence, in that region is where the failure starts and leads in the destruction of whole structure. However, the Gyroid structure has very good mechanical behavior in energy absorption terms due to its high yield point. The majority of absorbed energy's amount comes from elastic deformation branch.

- *Schwarz Diamond:*

The Schwarz Diamond structure has the best performance both in mechanical properties and in terms of energy absorption. It is not great affected from size effect, like Gyroid structure. Nevertheless, due to the material distribution in the structure, Schwarz Diamond structure can handle bigger forces. In addition, this structure has large amount of absorbed energy because of the high yield strength and its elastic deformation branch.

Hence, the Gyroid and Schwarz Diamond structures are not so much affected by the size effect, which allows the integrity of the mechanical properties of the material to be maintained in high level. However, the Schwarz Diamond structure has better material distribution within the space and therefore distributes the loads more effective. In conclusion, the Schwarz Diamond structure is most suitable for use in applications where the main loads are compressive forces.

One such case is the femur bone of the human body. Thus, case study for this thesis is a customized additive manufactured scaffold with Schwarz Diamond structure. The results show that not only the mechanical behavior of the designed scaffold can be predicted but it is also capable of handling compressive loads much greater than the weight of human body. This makes it a very promising candidate for metal implant substitute, as they have lower cost and are easier to manufacture.

Future studies proposes:

The field of research of lattice structures, specifically of TPMS, and the 3D printing techniques of extracting complex geometries are at a very early stage and there are many aspects that can be explored. Below, there are listed some suggestions for future research that will help to better apply of lattice structures as well as optimize design and 3D printing.

- Research for possible interference with the 3D printing process in order to optimize the printing parameters for complex geometries construction (orientations, layer thickness, defects on the procedure etc).

- Research on the creation and use of lattice structures, through 3D printing, with more advanced materials. For example, metals alloys, biomaterials, smart materials (4D applications).

- There is also a need for research into the mechanical behavior of TPMS structures in other types of loading. For example, tensile stress, bending, fatigue, etc.

- Another interesting finding of this study is the high energy absorption of these structures. Therefore, it is necessary to study the crashworthiness of each structure through impact tests. The goal is the applications in shielding objects from impacts (International Space Station shield etc).

- Finally, it is necessary to perform further analyzes of these structures such as thermal analysis and computational fluid dynamics analysis. The reason is that because these structures have a large surface-to-volume ratio, it makes them suitable for use in applications such as catalysts, filters and heat exchangers.

BIBLIOGRAPHY

1. Michell, A. G. M. (1904). "The limits of economy of material in frame-structures". Philosophical Magazine, Vol. 8(47), p. 589-597.

2. U. Kirsch, "Structural Optimization Fundamentals and Applications", Berlin (1993), Springer.

3. M. Ehrgott, "Multicriteria Optimization", Berlin (2005), Springer.

4. A W Gebisa, H G Lemu. "A case study on topology optimized design for additive Manufacturing". IOP Conf. Ser.: Mater. Sci. Eng, 2017.

5. Bendsøe, M. P., & Sigmund, O. "Topology optimization: theory, methods, and applications". Springer, 2003.

6. Larsen, S.D., Sigmund, O. & Groen, J.P. "Optimal truss and frame design from projected homogenization-based topology optimization". Structural Multidiscipline Optimization 57, 1461–1474, 2018.

7. Evangelos Tyflopoulos, David Tollnes Flem, Martin Steinert, Anna Olsen. "State of the art of generative design and topology optimization and potential research needs". Conference: Nord Design 2018, Sweden.

8. L. J. Gibson, M. F. Ashby, "Cellular solids. Structure and properties", Cambridge (1997), Cambridge University Press.

9. Feng Zhu, Guoxing Lu, Dong Ruan, Zhihua Wang. "Plastic Deformation, Failure and Energy Absorption of Sandwich Structures with Metallic Cellular Cores". International Journal of Protective Structures, 2010.

10. Oraib Al-Ketana, Reza Rowshan, Rashid K. Abu Al-Ruba. "Topology-Mechanical Property Relationship of 3D Printed Strut, Skeletal, and Sheet Based Periodic Metallic Cellular Materials". Journal of Additive Manufacturing, 2018.

11. Schoen, Alan H. "Infinite periodic minimal surfaces without self-intersections" NASA, 1970.

12. Lord, Eric A. and Mackay, Alan L. (2003) "Periodic minimal surfaces of cubic symmetry". Current Science 85 (3), pp. 346-362.

13. Kamran A. Khan1 and Rashid K. Abu Al-Rub, M. Asce. "Modeling Time and Frequency Domain Viscoelastic Behavior of Architectured Foams". Journal of Engineering Mechanics, 2018.

14. F. Fraternali, G. Carpentieri, R. Montuori, A. Amendola, and G. Benzoni. "On the use of mechanical metamaterials for innovative seismic isolations systems". 5 th ECCOMAS Thematic Conference on Computational Methods in Structural Dynamics and Earthquake Engineering, 2015.

15. Mike Jetzer. "S-II Insulation. The Apollo Flight Journal". NASA, 2010.

16. Nandyala, Varun Reddy. (2016). "Development of a high-performance catalyst structure under the consideration of thermal and mechanical properties".

17. Mohammad Sadeq Saleha, Jie Lib, Jonghyun Parkb, Rahul Panata. "3D printed hierarchically-porous microlattice electrode materials for exceptionally high specific capacity and areal capacity lithium ion batteries". Journal of Additive Manufacturing, 2018.

18. Carmen M. González-Henríqueza, Mauricio A. Sarabia-Vallejosc, Juan Rodriguez-Hernandeze. "Polymers for additive manufacturing and 4D-printing: Materials, methodologies, and biomedical applications". Journal of Polymer Science, 2019.

19. Merum Sireesha, Jeremy Lee, A. Sandeep Kranthi Kiran, Veluru Jagadeesh Babu, Bernard B. T. Kee and Seeram Ramakrishn. "A review on additive manufacturing and its way into the oil and gas industry". Journal of RSC Advances, 2018.

20. Manpreet Kaur, Tae Gwang Yun, Seung Min Han, Edwin L. Thomas, Woo Soo Kim. "3D printed stretching-dominated micro-trusses". Journal of Materials and Design, 2017.

21. Dawei Li, Wenhe Liao, Ning Dai and Yi Min Xie. "Comparison of Mechanical Properties and Energy Absorption of Sheet-Based and Strut-Based Gyroid Cellular Structures with Graded Densities". Journal of Materials, 2019.

22. Jens Bauer, Lucas R. Meza, Tobias A. Schaedler, Ruth Schwaiger, Xiaoyu Zheng and Lorenzo Valdevit. Nanolattices: "An Emerging Class of Mechanical Metamaterials". Journal of Advanced Materials, 2017.

23. Miao Zhao, Fei Liu, Guang Fu, David Z. Zhang, Tao Zhang and Hailun Zhou. "Improved Mechanical Properties and Energy Absorption of BCC Lattice Structures with Triply Periodic Minimal Surfaces Fabricated by SLM". Journal of Materials, 2019.

24. Oraib Al-Ketan, Rachid Rezgui, Reza Rowshan, Huifeng Du, Nicholas X. Fang, and Rashid K. Abu Al-Rub. "Microarchitected Stretching-Dominated Mechanical Metamaterials with Minimal Surface Topologies". Journal of Advanced Engineering Materials, 2018.

25. Diab W. Abueidda, Mohamed Elhebeary, Cheng-Shen (Andrew) Shiang, Siyuan Pang, Rashid K. Abu Al-Rub, Iwona M. Jasiuk. "Mechanical properties of 3D printed polymeric Gyroid cellular structures: Experimental and finite element study". Journal of Materials and Design, 2019.

26. I. Maskery, L. Sturm, A.O. Aremu, A. Panesar, C.B. Williams, C.J. Tuck, R.D. Wildman, I.A. Ashcroft, R.J.M. Hague. "Insights into the mechanical properties of several triply periodic minimal surface lattice structures made by polymer additive manufacturing". Journal of Polymer, 2017.

27. Xiaoyang Zheng, Zhibing Fu, Kai Du, Chaoyang Wang, and Yong Yi. "Minimal surface designs for porous materials: from microstructures to mechanical properties". Journal of Materials Science, 2018.

28. M.M. Sychov, L.A. Lebedev, S.V. Dyachenko, L.A. Nefedova. "Mechanical properties of energy-absorbing structures with triply periodic minimal surface topology". Journal of Acta Astronautica, 2017.

29. D. Barba, E. Alabort, R.C. Reed. "Synthetic bone: Design by additive manufacturing". Journal of Acta Biomaterialia 2019.

30. C.K. Chua, W.Y. Yeong, M.J. Tan, E.J. Liu and S.B. Tor. "Study of the influence of 3D printing parameters on the mechanical properties of PLA". 3rd International Conference on Progress in Additive Manufacturing (Pro-AM 2018).

31. ISO 13314. "Mechanical testing of metals -Ductility testing- Compression test for porous and cellular metals". First edition, 2011.

32. Jessica M. Williams, Adebisi Adewunmi, Rachel M. Scheka, Colleen L. Flanagan, Paul H. Krebsbacha, Stephen E. Feinberg, Scott J. Hollister, Suman Das, " Bone tissue engineering using polycaprolactone scaffolds fabricated via selective laser sintering ". Journal of Biomaterials, 2005.

33. Uzair N. Mughal, Hassan A. Khawaja and M. Moatamedi. "Finite element analysis of human femur bone". The International Journal of Multiphysics, 2015.

34. Bergmann et al., "Clinical Biomechanics" (1993) 969-990.

35. S Karuppudaiyan1, D Kingsly Jeba Singh and Vora Mani Santosh. "Finite element analysis of scaffold for large defect in femur bone". 2nd International conference on Advances in Mechanical Engineering, ICAME, 2018.

36. Katarina Colica, Aleksandar Sedmak, Aleksandar Grbovic, Uros Tatic, Simon Sedmak, Branislav Djordjevic. "Finite element modeling of hip implant static loading". International Conference on Manufacturing Engineering and Materials, ICMEM, 2016.

37. Min Yang, Changhe Li, Yanbin Zhang, Dongzhou Jia, Xianpeng Zhang, Yali Hou, Bin Shen & Runze Li. "Microscale bone grinding temperature by dynamic heat flux in nanoparticle jet mist cooling with different particle sizes". Journal of Materials and Manufacturing, 2017.

Appendix I

Specifications of 3D FDM printer: BCN3D SIGMA R17

PHYSICAL DIMENSIONS

Overall dimensions
465mm x 440mm x 680mm
(including cables)

Weight: **15kg**
(without filament spools)

Shipping box dimensions
550mm x 550mm x 630mm

Shipping weight: **21kg**

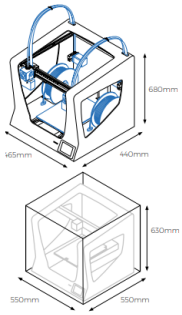

PRINTER PROPERTIES

Architecture
Independent Dual Extruder
(IDEX)

Technology
Fused Filament Fabrication (FFF)

Build Volume
210mm x 297mm x 210mm

Extruders: **2**

Nozzle diameter
0,3mm / 0,4mm (Standard) /
0,6mm / 0,8mm / 1,0mm

Heated bed
PCB

Screen
Full Color Capacitive TouchPAD

Electronics
BCN3D Electronics v1.0
Independent Stepper Drivers

Firmware
BCN3D Sigma - Marlin

Supported files
gcode

Operating Sound
58 dB(A)

Certifications
CE / FCC

Connectivity
SD Card (autonomous)
USB

PRINTING PROPERTIES

Layer height
0,05 - 0,5mm
(depending on the nozzle diameter)

Positioning resolution (X/Y/Z)
1,25µm / 1,25µm / 1µm

Operating temperature
15°C - 35°C

Extruder maximum temperature
290°C

Extruder maximum printing temperature
280°C

Heated bed maximum temperature
100°C

Support Material
PVA for PLA // HIPS for ABS

SOFTWARE

File preparation software
Cura-BCN3D, Simplify3D, Slic3r

Operative Systems
Windows, Mac, Linux

Supported files
STL, OBJ, AMF

ELECTRIC PROPERTIES

Input
AC 84-240V, AC 3,6-1,3A, 50-60Hz

Output
24V DC, 13A

Power Consumption
240W

MATERIALS

Filament diameter
2,85 ± 0,05 mm

Compatible Materials
PLA
ABS
PVA
Co-polyesters
Nylon
TPU
HIPS
Specials

Appendix II

Specifications of SHIMADZU DUH-211S

Model		DUH-211	DUH-211S
Loading Unit	Loading Method	Electromagnetic coil	
	Test Force Range	Full scale of 0.1 to 1,961 mN	
	Test Force Accuracy	±19.6 μN or ±1% of displayed test force, whichever is greater	
	Minimum Measurement Increment	0.196 μN (for a test force not exceeding 1.96 mN)	
Displacement Measurement Unit	Measurement Method	Differential transformer	
	Measurement Range	0 to 10 μm	
	Minimum Measurement Increment	0.0001 μm	
	Linearity	±2% of full scale (20 μm)	
Indenter	Type	Triangular pyramid indenter with tip angle of 115° (Vickers indenter and Knoop indenter are available as options.)	
	Tip Radius	0.1 μm max.	
Optical Monitor	Total Magnification (microscope)	×500	
	Objective Lens	×50 (Up to 2 lenses can be attached.)	
	Eyepiece	×10	
	Lighting Method	Reflected illumination	
	Light Source (lamp)	LED: 3 W, 3 V	
	Light-Path Switching	Observation or photograph (selectable)	
Micrometer	Collimation Method	Direct connection between encoder and control handle; synchronized movement of two indexes	
	Detector	Optical encoder	
	Effective Measurement Range	200 μm (with ×50 objective lens)	
	Minimum Measurement Increment	0.01 μm/pulse	
Specimen Stage	Vertical Distance	Approx. 60 mm	
	Area	Approx. 125 (W) × 125 (L) mm	
	Stage Movement Range	25 mm in both X and Y directions	
	Specimen Holder	Specimen dimensions (i.e., 8 (thickness) × 30 (width) mm) when thin-type attachment (type 3) is used	
Test Modes	Load–Hold Test	○	○
	Load–Unload Test	○	○
	Cyclic Test	○	○
	Depth Setting Test	—	○
	Depth Setting Load–Unload Test	—	○
	Step Load Test	—	○
	Step Load-Unload Test	—	○
Required PC Specifications	OS	Windows® 7 (32/64 bit edition)	
	CPU	1 GHz min.	
	Disk Drives	CD-ROM drive	
	Display Resolution	1024 × 768 min.	
	Expansion Bus	PCI Express ×1, 2 slots min. more than one ×1 slot is required (or slot size ×2 or more)	
Utilities	Power Supply	Single phase, AC 100–115 V ± 10%, AC 230 V ± 10% (Ground resistance 100 Ω max.)	
	Power Consumption	Approx. 100 W (not including power consumption of PC)	
	Grounding	The ground terminal on 3-prong connectors must be properly grounded with grounding resistance at 100 Ω or less.	
	Temperature	Recommended temperature: 23±1°C Allowable range: 10°C to 35°C	
	Vibration	Horizontal vibration: 0.017 Gal max. (at 10 Hz or more) 0.01 μm max. (at less than 10 Hz) Vertical vibration: 0.010 Gal max. (at 10 Hz or more) 0.005 μm max. (at less than 10 Hz)	
	Humidity	80% max. (no condensation)	
Dimensions and Weight	External Dimensions	Tester: Approx. 355 (W) × 405 (D) × 530 (H) mm Control unit: Approx. 315 (W) × 375 (D) × 110 (H) mm	
	Weight	Tester: Approx. 60 kg Control unit: Approx. 5 kg	

*Windows 7 is registered trademark of Microsoft Corporation in the US and other countries.

Standard Configuration

Name		Quantity
Hardness Tester (main unit)		1
Objective Lens (×50)	P/N 344-89964-40	1
Triangular Pyramid Indenter (tip angle: 115°)	P/N 340-47013	1
Specimen Stage (XY stage)	P/N 347-24205-41	1
Micrometer Head		2
Specimen Holder	P/N 344-17737-40	1
Control Unit		1
Accessories (Cords, AC adapters, tools, instruction manual, installation disk)		1 set

PC and Printer are not included.

External Dimensions

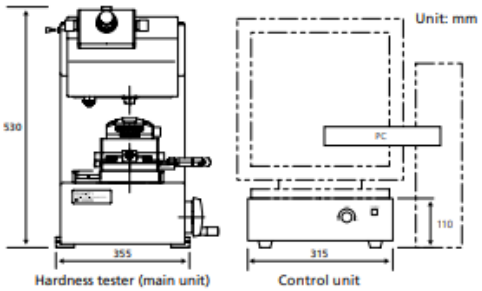

Appendix III

Specifications of Testometric-M500-50AT

Range kN	50	Data sampling rate	Maximum 12kHz with up to 200Hz data frames.
Accuracy	+/- 0.5% of reading down to 1/1000th of load cell capacity.	Overall dimensions W x D x H	762 x 505 x 1585
Vertical space mm	1180	Weight kg	245
Crosshead travel/resolution mm	980 by 0.001	Electrical supply	Universal input. (de-rate max speed at 115V)
Throat mm	420	Operating temp degree C	-10 to +40
Frame stiffness kN/mm	200	Operating humidity	+10 to +90% non-condensing
Speed range mm/min	0.001 to 1000	Machine Configuration	Table top, base cabinet available
Speed accuracy	+/- 0.1% under stable conditions.	Number of Columns	2
Crosshead guidance	Linear slides integral within column	Available load cells	5N, 10N, 20N, 100N, 250N, 500N 1kN, 2.5kN, 3kN, 5kN, 10kN, 20kN, 25kN, 30kN, 50kN Maximum of four load cells up to capacity of machine.
Max force at full speed kN	50	Spigot Ø mm	30
Max speed at full load mm/min	600	Power kW	1

Appendix IV

Details about femur bone and scanning procedure

"Prepared by Digital Imaging (DI) (CMM Optical) and CT Scan (CT Imaging) Human specimen's properties for this Femur bone are: Male, Left leg, Age 44, Death 2016, Weigh 85 (kg), Height 185 (cm) (original scale)

Femur bone was created in 3D using Digital Imaging (DI) (CMM Optical 2015, Made by GOM Co., Germany). Digitized model was first modelled as Shell and cloud points, i.e. STEP format, in CATIA V5/R21 and then was surfaced as a Solid. The inner area of the Femur (the central cavity and inner layer) cannot be modelled and surfaced using this method. So, to model this section (which is one of the most important parts in FE model), Computed Tomography (CT) scan method is used (Only the Cortical bone tissue is modelled using this approach and Trabecular tissue is not modelled). In this way, the bone is completely and precisely modelled. In this type of imaging, first, all the bone is scanned and then sections with a space of 10mm of each other and with an exact coordinate from the top of Femur bone (Proximal region) to the end part (Distal region) of the bone is created using the related software. All sections are stored in two-dimensional and with Digital Imaging and Communication in Medicine (DICOM) format (Using Marco PACS and SECTRA PACS or Sonic PACS software and DICOM files, all the sections, i.e. 25 sections in diaphysis region with a distance of 10mm and almost 45 sections in throughout of bone), the output format of CT scanner, and visualized in Photoshop CC. Finally, the three-dimensional model of the original bone along with 2D images of cross sections of CT scan separately with the desired scaling transferred into Solid Works 2013 and each cross section corresponded to the outer boundaries of the same cross section in 3D models so that its central hole were determined in separate plans as sketched. Similarly, all the cross sections were modelled and, in the end, using the lofted cut modules (removed) option all the sketches emptied from the original bone volume. This method is accurate to 0.01mm."

From 3D CAD library: https://grabcad.com/library/femur-bone-2